Synthesis of integrated chemical processes for the production of single enantiomers

Dissertation
zur Erlangung des akademischen Grades
Doktoringenieur
(Dr.-Ing.)

von Dipl.-Ing. Javier García Palacios

geb. am 13. Mai 1982 in Gijón (Spanien)

genehmigt durch die Fakultät Elektrotechnik und Informationstechnik der Otto-von-Guericke-Universität Magdeburg

Gutachter:

<div align="center">

Prof. Dr.-Ing. Achim Kienle
Prof. Dr.-Ing. Andreas Seidel-Morgenstern

</div>

Promotionskolloquium am 10. November 2011

to my best friend
Alejandro Castillo Martínez
(1982-2006)

Acknowledgements

This research project would not have been possible without the support of many people.

I want to express my gratitude to my supervisors, Prof. Dr.-Ing. A. Kienle and Dr.-Ing. M. Kaspereit, who gave me the opportunity to be where I am today. I want to thank them for their patience and their understanding, especially in the most complicated moments.

Special thanks also to Prof. Dr.-Ing. A. Seidel-Morgenstern who has been an endless source of motivation since the first day I entered the Max Planck Institute.

I would also like to convey thanks to many people who offered me their guidance and helped me grow up intellectually as well as personally. Thanks to Dr.-Ing. M. Mangold, who always kept his door opened and made me feel welcomed to ask him any question I had. Thanks to Prof. Dr. D. Flockerzi, whose passion for the mathematics ended up being contagious. Thanks to B. Kramer, with whom I had the luck to spend many months in the laboratory whilst we both could learn from each other.

I would like to extend my gratitude to many other colleagues at the Max Planck Institute, whose names I cannot list here. They provided me everyday with the support I needed to keep going.

Last but not least, I want to thank my family and friends. Without them I could not be here, because I would not be myself.

Magdeburg, December 3, 2011   Javier García Palacios

Contents

List of Symbols

Latin symbols

b	isotherm parameter	[l/g]
c	liquid phase concentration	[g/l]
d_c	column diameter	[dm]
Da	Damköhler number	[-]
L	column length	[mm]
F	phase ratio	[-]
K_{eq}	equilibrium constant	[-]
k	kinetic constant forward reaction	[min^{-1}]
k_b	kinetic constant backwards reaction	[min^{-1}]
m	dimensionless flow rate	[-]
OF	objective function	[-]
Pr	productivity	[g/min]
Pu	purity	[%]
Q	liquid phase volumetric flow rate	[l/min]
Q_s	solid phase volumetric flow rate	[l/min]
q	solid phase concentration	[g/l]
q_s	saturation capacity	[g/l]
r	reaction rate	[g/l/min]
R	decision variable (reaction)	[-]

t	time	[min]
T	temperature	[°C]
v	liquid phase velocity	[cm/min]
V	stage volume	[l]
V_c	column volume	[l]
V_r	reactor volume	[l]
X	conversion	[%]
Y	yield	[%]
z	spatial coordinate	[cm]

Greek symbols

α	separation factor	[-]
λ	propagation velocity	[cm/min]
ε	porosity	[-]
υ	stoichiometric coefficient	[-]

Subscripts and superscripts

CTD	chlorthalidone
i	component
k	stage
n	column
z	zone
out	outlet
D	desorbent
F	feed
R	raffinate
E	extract
Re	regeneration
SP	side product

Abstract

Enantiomers are non superimposable isomers structured like mirror images. They exhibit similar physical and chemical properties in an achiral environment but behave differently towards chiral molecules. In particular, they can produce different physiological effects in pharmaceutical applications. Often only one enantiomer has the desired physiological effect, while the other might be ineffective, have a lower positive effect or be even harmful. Thus, the production of the pure desired enantiomeric form plays an important role, especially for the pharmaceutical industry.

Often selective chemical synthesis is infeasible or expensive and, therefore, nonselective chemical synthesis is applied. This leads to a mixture of both enantiomeric forms in equal amounts and requires a separation process to isolate the desired enantiomer with high purity. Possible separation processes which are usually applied in this field comprise chromatography, crystallization or kinetic resolution. However, the overall yield of such a process is limited to a maximum of 50 %. This is a major economical problem because enantiomers are often very expensive.

To further increase the yield, subsequent chemical conversion of the undesired to the desired enantiomer can be applied by racemization. The yield of racemization reactions is also limited to a maximum of 50 % requiring further separation, which can be achieved for example by recycling to the separation unit. Alternatively, the racemization reaction can be integrated into the separation unit. It is known from other fields of application that integrated processes that combine reaction and separation in the same unit can be a very powerful. This thesis aims at a detailed investigation of the benefits that the integration of racemization within a continuous chromatographic setup can bring for the production of single enantiomers.

A three step approach is devised. First, the performance of selected process alternatives is compared using model-based optimization for true moving bed (TMB) systems.

Several degrees of integration are considered: flowsheet integration, partial integration using side reactors and total integration. The completely integrated alternatives achieve the best performance results for the cases studied. This indicates that the integration of the reaction within the separation device can improve process performance. However, a spatial distribution of the reaction within the chromatographic unit is required to achieve pure products. It is shown, that the racemization is optimally placed within the regeneration zones to support the regeneration of the TMB unit and thereby to improve the overall performance. This effect is denoted as reaction-assisted regeneration. It is analyzed in detail on the basis of an equilibrium model. Analytical solutions are derived to explain and quantify this effect.

In view of practical implementation, the analysis is extended in a second step to more realistic simulated moving bed (SMB) processes. Superstructures of SMB-based systems are defined that reflect the three different levels of integration mentioned above. Process candidates are generated by simultaneously optimizing process structure and operating conditions. The complex mixed integer nonlinear problems are solved by the use of evolutionary algorithms.

The comparison among the process alternatives supports the findings of the conceptual investigation based on TMB models. Both approaches indicate that process performance can profit from the integration of the reaction within the separation unit. Additional effects arising from finite switching in the SMB setting are analyzed in detail.

Based on the SMB optimization studies, a 3-zone SMB system with internal distribution of the racemization reaction is suggested as an attractive process alternative for the production of pure enantiomers. It combines good performance with a rather simple setup. Theoretically, this process can deliver single enantiomer with 100% purity, recovery yield, and conversion.

In the last part of the thesis, the new process idea is validated experimentally. A semi-preparative scale SMB unit is designed to produce a single enantiomer of the chlorthalidone enantiomeric model system. The experimental investigation supports the theoretical findings, demonstrating that the new process can deliver purified single enantiomers with almost 100% yield and conversion.

Zusammenfassung

Enantiomere sind spiegelbildlich aufgebaute, nicht zur Deckung zu bringende Isomere. Sie weisen in einer achiralen Umgebung gleiche physikalische und chemische Eigenschaften auf, währenddessen sie sich gegenüber chiralen Molekülen unterschiedlich verhalten. Besonders in pharmazeutischen Anwendungen können sie unterschiedliche physiologische Auswirkungen hervorrufen. Häufig zeigt nur eines der beiden Enantiomere die gewünschte physiologische Wirkung, während das andere ineffektiv, weniger stark wirksam oder sogar schädlich sein kann. Deshalb spielt, besonders für die pharmazeutische Industrie, die Herstellung der reinen gewüschten Enantiomerenform eine bedeutende Rolle.

In vielen Fällen wird die nicht-selektive chemische Synthese angewandt, da sich die selektive chemische Synthese als undurchführbar oder kostspielig erweist. Dies führt zur Entstehung einer Mischung, bestehend aus beiden Enantiomerenformen in gleicher Anzahl und erfordert einen Trennprozess zur Isolierung des gewünschten Enantiomers in hoher Reinheit. Die in diesen Fällen üblicherweise angewandten Trenntechniken umfassen Chromatographie, Kristallisation oder kinetische Racematspaltung. Allerdings ist die Gesamtausbeute solcher Prozesse auf maximal 50% begrenzt. Dies stellt aufgrund der hohen Preise für Enantiomere ein bedeutendes wirtschaftliches Problem dar.

Um die Ausbeute weiter zu erhöhen, kann im Anschluss die chemische Umwandlung des ungewünschten zum erwünschten Enantiomer mittels Racemisierung erfolgen. Die Ausbeute von Racemisierungsreaktionen wiederum ist auch auf 50% begrenzt und erfordert eine nachfolgende Trennung, die zum Beispiel durch eine Rückführung zur Separationsanlage erreicht werden kann. Alternativ kann die Racemisierungsreaktion in die Trennanlage integriert werden. Von anderen Anwendungsgebieten ist bekannt, dass integrierte Prozesse, die Reaktion und Trennung in einer Anlage kombinieren, sehr leistungsfähig sein können. Die vorliegende Arbeit hat eine detaillierte Untersuchung der Vorteile, die die Integration von Racemisierung in einem kontinuierlichen chromtographischen Aufbau für die Produktion von

Einzel-Enantiomeren bewirken kann, zum Ziel.

Es wird ein dreistufiger Ansatz verfolgt. Zu Beginn wird die Leistungsfähigkeit ausgewählter Prozessalternativen verglichen, indem eine modell-basierte Optimierung fuer True Moving Bed (TMB) Systeme angewandt wird. Mehrere Stufen der Integration werden betrachtet: Die Prozessfließbild-Integration, die partielle Integration durch Benutzung von Seitenreaktoren und die vollständige Integration. Die vollständig integrierten Varianten erzielen für die untersuchten Fälle die beste Leistung. Das weist darauf hin, dass die Integration der Reaktion in der Trenneinheit die Prozessleistung verbessern kann. Allerdings ist fuer die Herstellung reiner Produkte eine räumliche Verteilung der Reaktion in der chromatographischen Einheit notwendig. Es wird gezeigt, dass die Racemisierung am besten in der Regenerationszone platziert wird, um auf diesem Wege die Regeneration der TMB-Einheit zu unterstützen und letzlich das gesamte Leistungsvermögen zu verbessern. Dieser Effekt wird als reaktionsunterstützte Regeneration (engl. reaction-assisted regeneration) bezeichnet. Er wird basierend auf einem Gleichgewichtsmodell detailliert untersucht. Analytische Lösungen werden hergeleitet, um diesen Effekt zu erklären und zu quantifizieren.

In Hinsicht auf die praktische Umsetzung wird in einem zweiten Schritt die Analyse auf realistischere Simulated Moving Bed (SMB) Prozesse ausgeweitet. Es werden Überstrukturen von SMB-basierten Systemen definiert, die die drei vorherig erwähnten Stufen der Integration widergeben. Mit Hilfe gleichzeitiger Optimierung von Prozessstruktur und Betriebsbedingungen werden geeignete Prozesskandidaten erzeugt. Die komplexen, gemischtganzzahligen, nichtlinearen Probleme werden mit Hilfe von Evolutionären Algorithmen gelöst.

Der Vergleich zwischen den Prozessvarianten unterstützt die Ergebnisse der auf TMB-Modellen basierenden konzeptuellen Untersuchung. Beide Ansätze zeigen, dass die Prozessleistung von der Integration der Reaktion in der Trenneinheit profitieren kann. Die zusätzlich durch diskrete Schaltung im SMB-Aufbau aufkommenden Effekte sind detailliert analysiert.

Basierend auf den Studien der SMB-Optimierung wird ein Drei-Zonen SMB-System mit interner Verteilung der Racemisierungsreaktion als attraktive Prozessvariante für die Produktion reiner Enantiomere vorgeschlagen. Es vereint eine gute Leistungsfähigkeit mit einem recht einfachen Aufbau. Theoretisch kann dieser Prozess Einzel-Enantiomere mit jeweils 100% Reinheit, Ausbeute und Umsatz zur Verfügung stellen.

Im Letzten Abschnitt dieser Arbeit wird die neue Prozess-Idee experimentell bestätigt. Um Einzel-Enantiomere des Enantiomer-Modellsystems Chlorthalidon herzustellen, wird eine semi-präparative SMB-Anlage entworfen. Indem gezeigt wird, dass der neu entworfene Prozess gereinigte Einzel-Enantiomere mit nahezu 100% Ausbeute und Umsatz bereitstellen kann, bestätigt die experimentelle Untersuchung die theoretischen Ergebnisse.

CHAPTER *1*

Introduction

The first part of this chapter introduces briefly the basic characteristics of enantiomers. Special attention is paid to the most relevant aspects regarding the production of single enantiomeric compounds. In this frame, as an interesting separation technology able to resolve chiral mixtures, continuous chromatographic operation is introduced. Later, the combination of reaction and continuous chromatography is addressed with special attention on the idea of process integration. Here, the most significant contributions in the literature are reviewed. In the second part of this chapter, the problem approach is presented. At the end, a short outline of the thesis is given.

⚚ · ⚚

1.1. Enantiomers and their production

Isomers are compounds which have identical stoichiometry meanwhile they show different molecular structures. As a particular case of isomers, stereoisomers are three dimensional structures in which their spatial orientation determines its attributes and reaction behavior [23, 40].

A challenging example in this context are enantiomers. These stereoisomers are of great importance for the production of pharmaceuticals, agrochemicals, and fine chemicals [23]. Enantiomers are structured like mirror images but they are non superimposable. This

property is called chirality, from the greek word for hand $\chi\varepsilon\iota\varrho$ (cheir). They have no symmetry centre or symmetry plane. They are optically active and rotate linear polarized light in similar amounts but opposite ways. If they turn the light rightwards they are marked by *(+)*. If they turn it leftwards their are denoted with *(-)* [97]. If enantiomers show up in a mixture in the same amount, this is called racemate. They still have their optical activity, but due to the oppositional rotation the total angle is zero. Further, not corresponding to the optical rotation, but according to the CIP system, they can be named referring to their absolute configuration with *R* and *S* [23]. In Fig. 1.1 this can be observed in a simplified example. Another classification, often used for amino acids and sugars, is the discrimination between *D*- and *L*-enantiomers [25].
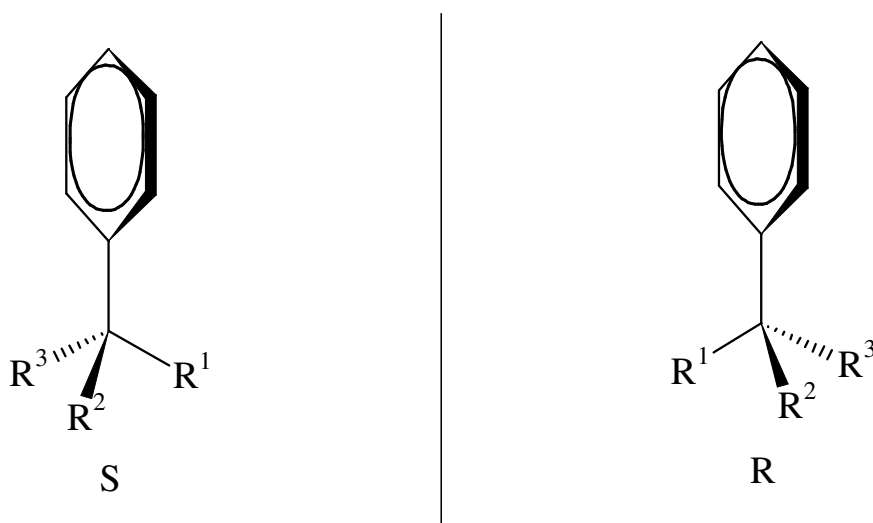

Figure 1.1. – R- and S-enantiomer of a central coordinated carbon atom with four substituents at its mirror plane. The valence of the substituents is set as $R^1 > R^2 > R^3 >$ aromatic hydrocarbon.

From a macroscopic perspective, the reaction which transforms in an irreversible manner a purified enantiomeric form into a racemate is called racemization [96]. Racemization reactions occur due to breakage of chemical bonds next to the chiral center of the molecule or due to rotation or stretching of the atoms around this bond [97]. In general, the chemical mechanism of racemization contains an achiral planar intermediate which can be a carbocation or an excited state. The necessary energy to form this intermediate state can be thermal, electrochemical, or triggered by a basic or acidic enviroment [18]. The probability for the formation of the two enantiomeric forms from the intermediate state is identical leading to the 50/50 racemic mixture.

In contrast to racemization, enantiomerization describes a microscopic process of reversible interconversion of one enantiomer into the other, by passsing through a transition state or an intermediate product [72]. For the sake of simplicity, only the term racemization

will be used throughout the work, referring to the equilibrium reaction established between the two enantiomeric forms.

In pharmaceutical applications often only one enantiomer has the desired physiological effect, while the other might be ineffective, have a lower positive effect or be even harmful [4, 23]. Therefore, a pure enantiomeric form is often required.

One of the most relevant examples resembling the importance of obtaining purified single enantiomers is that of the drug Contergan. Based on the enantiomeric active molecule thalidomide, the drug was prescribed to pregnant women between the years 1957 and 1961 as a sedative. However, only one enantiomer provided the desired sedative effect while the other was responsible for tragic deformations of human embryos [91]. The increasing relevance of chirality in the recent pharmaceutical industry is resembled by the fact that nine of the top ten drugs contain a chiral active ingredient [75].

Also in other sectors, the demands for enantiomerically pure chiral compounds is progressively rising. For example, in the field of flavors, it is well known that the R-enantiomer of carvone smells of spearmint while the S-enantiomer smells of caraway. Another well known example is the different flavour obtained from the limonen enantiomers. While the R-form smells like oranges, for the S-enantiomer a more citric lemon-like flavor can be obtained. Nowadays, fragrance companies have also started to commercialize stereoisomerically enriched synthetic fragrances. Several trademarks such as Kharismal®, or Paradisone® are a good example in this direction.

There are two major approaches to produce single enantiomers. The chiral pathway and the racemic pathway.

The first alternative requires a selective synthesis by means of catalysis, building blocks or the use of chiral auxiliaries. This synthetic pathway is a unique research field of great importance. However, selective synthesis is often infeasible or too expensive which limits its indutrial applicability.

The racemic pathway uses conventional chemical synthesis producing the 50/50 mixture of both enantiomers. This necessitates a subsequent separation step in order to resolve the racemate. Classical resolution techniques are based on converting the enantiomers into diastereomers enabling a simpler separation between both species. As an alternative, other techniques such as chromatography using chiral stationary phases can successfully perform enantioseparations [80]. Further, crystallization techniques [34] or kinetic resolution [1] offer a large spectrum of methods allowing for enantioseparations.

In this work, continuous chromatographic processes are considered for the resolution of enantiomeric mixtures.

1.1.1. Continuous chromatography

Chromatography is a separation technique in which a liquid solvent containing the components to be separated moves through a column packed with a solid formation, the stationary phase. Due to thermodynamic interactions, the compounds exhibit different distribution equilibria between the stationary phase and the solvent. This causes that the components propagate through the chromatographic column at different velocities. Thus, the species leave the column separated at different points in time.

Resolution of enantiomers by chromatography is predominantly performed by using specific chiral stationary phases (CSP). The commercially available CSPs contain chiral selectors such as proteins, polysaccharides, antibiotics, brush-type molecules, ionic exchangers, crown ethers, cyclodextrines, and multiple polymers [57]. The challenge is to find adequate CSPs to resolve racemic mixtures for large scale production processes.

Batch chromatography is a discontinuous process where limited amount of the sample is injected as a pulse in the chromatographic column. A mobile phase, the eluent, carries the components through the column until they leave the system at different points in time. This type of operation usually entails high eluent consumption. As an alternative to overcome the weak points of such discontinuous separation, continuous chromatographic processes were developed.

The True Moving Bed (TMB) concept performs a countercurrent continuous separation of binary mixtures as shown in Fig. 1.2. Two inlet and two outlet ports divide the system into four different zones, I to IV in Fig. 1.2. A liquid stream entering zone I moves countercurrently to a solid flow introduced in zone IV. The feed enters the unit between zones II and III. In these zones the separation takes place while zones I and IV are responsible for the regeneration of the solid and the liquid phases, respectively. By adjusting the flows of the two phases in each zone, the most retained component can be withdrawn in the extract while the less retained can leave the unit via the raffinate stream.

The TMB concept is lacking practical implementation, due to severe technical problems of particle abrasion of the solid phase and back-mixing effects of the liquid phase. Therefore, in the 1960s the Simulated Moving Bed (SMB) process was developed [19], providing separations for the petrochemical industry.

In Fig. 1.3 the scheme of an SMB process is illustrated. The SMB unit is divided analogously to the TMB into four zones, delimited by the four inlet and outlet ports. In the example in Fig. 1.3, eight identical chromatographic columns are connected in series, two in each zone of the unit. The columns in this setup are shifted periodically in opposite direction to the liquid flow. This switching mimics the countercurrent solid flow allowing for continuous separation and overcoming the limitations of TMB systems, discussed above.
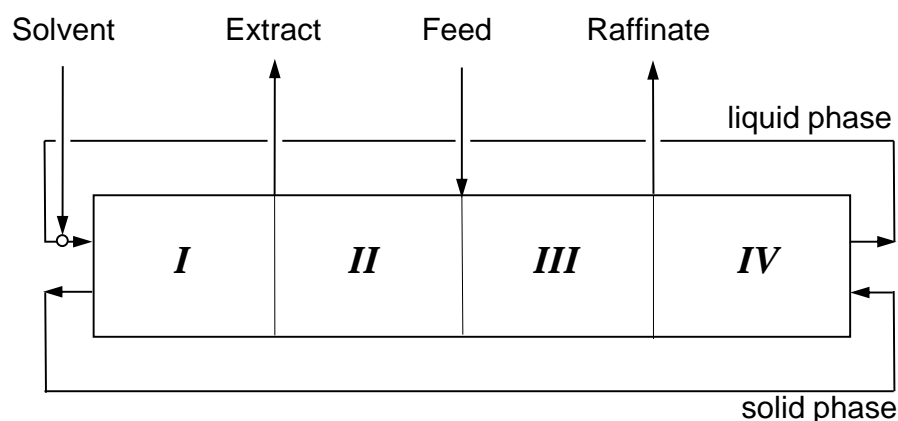
Figure 1.2. – General concept of a true moving bed (TMB) unit.

New fields of application such as pharmaceuticals, agrochemicals and fine chemistry have contributed to raise interest in simulated moving bed chromatography during the last 20 years. Current investigations of SMB processes involve variations of the operating conditions, for example regulation of feed concentration (ModiCon) [81, 82], zone length (VariCol) [56, 101] and flowrates (PowerFeed) [100] as well as solvent gradients (MCSGP) [6]. Several studies also investigated its applicability for ternary mixture separations through coupling of two SMB units [66] and pseudo-SMB processes [60].
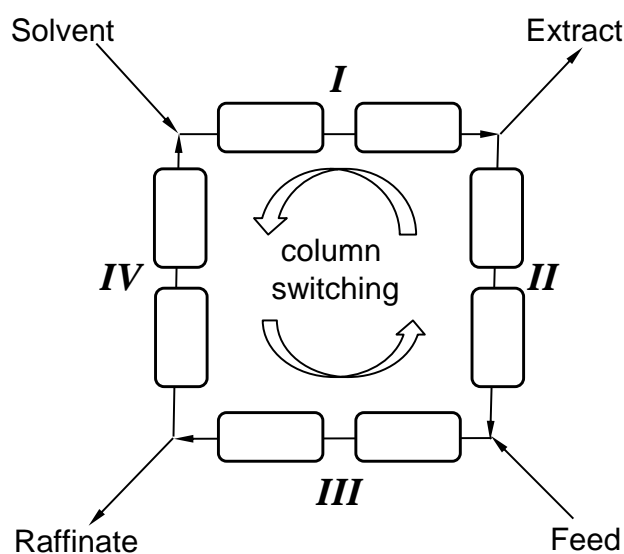

Figure 1.3. – General concept of a simulated moving bed (SMB) unit.

Many studies investigated the production of pure enantiomers by resolving the racemic mixture by means of SMB chromatography (e.g., [35, 43, 45]). However, as already mentioned,

the achievable yield by this approach is inherently limited to 50%. This is a major problem since enantiomers are frequently expensive. The recovery and reconversion of the undesired enantiomer is required to produce single enantiomers with purity, yield and conversion close to 100%. Thus, suitable combinations of racemization and separation are required.

1.1.2. Process integration

Integrated processes that combine chemical reaction and separation are an attractive approach to improve yield, selectivity, or productivity of chemical productions. They are especially useful for equilibrium-limited reactions such as esterification and ester hydrolysis reactions. Conversion can be increased shifting the reaction equilibrium by continuous removal of reaction products from the reaction zone. This can help to reduce overall costs and can be relevant for sustainable development due to a lower consumption of resources. Reactive distillation, reactive absorption, membrane reactors and reactive extraction, to name some, have been the focus of several investigations in the last decade [30, 90].
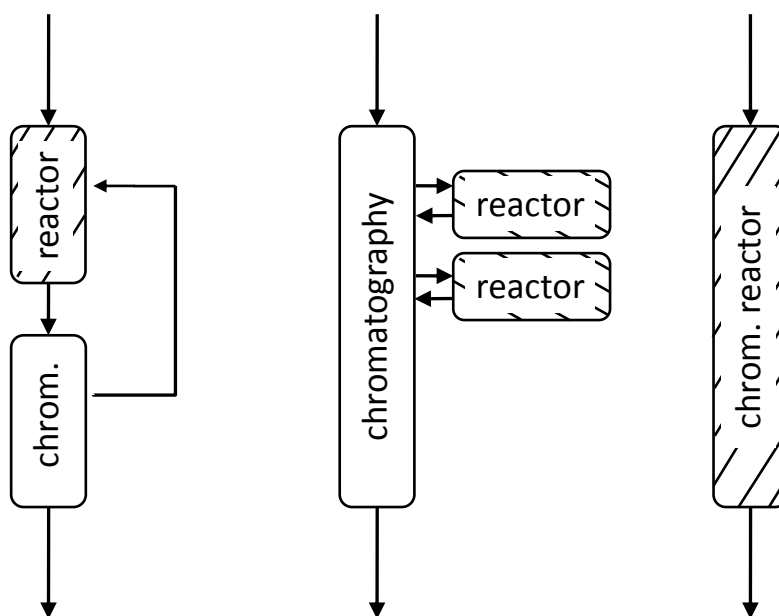
Figure 1.4. – General concepts with different degree of process integration. Left – flowsheet-integrated process (reactor-separator-recycle). Center – semi-integrated process with side reactors. Right – fully integrated process (reactive separator).

One possible option among the different variants are combinations of reaction and continuous chromatographic separations. These are particularly useful if the separation of the components

is very difficult, or if products are sensitive to harsh conditions [90].

In the literature, discontinuous chromatographic reactors have been considered mainly to enhance equilibrium-limited conversion for reversible reactions with a stoichiometry $A \leftrightarrow B + C$ or $A + B \leftrightarrow C + D$ [90]. These hold for the well-studied esterifications and ester hydrolyses (e.g., [31, 79, 98]), and the synthesis of acetals [29].

In this work, the focus is on integrated processes using continuous chromatography. General process concepts that combine continuous chromatography and reaction fall mainly into three general categories, as illustrated in Fig. 1.4:

- The first approach (Fig. 1.4, left) is a conventional flowsheet integration where reaction and separation are performed in different units. The unconverted educts are recycled back after the separation to an external reactor where the desired compound is produced again.
- The second option (Fig. 1.4, center) is a system with side reactors distributed spatially along the chromatographic unit. Reaction and separation tasks take place sequentially in this type of semi-integrated process scheme. The spatial distribution of the reactors
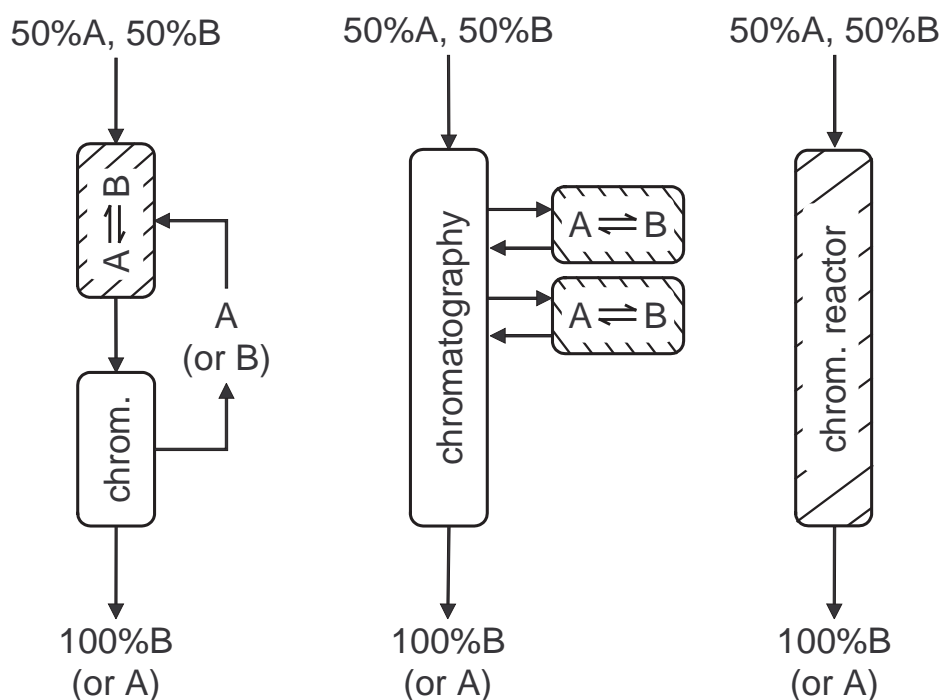

Figure 1.5. – General concepts for producing a single enantiomer by chromatography and racemization reactions. Left – flowsheet-integrated process (reactor-separator-recycle). Center – semi-integrated process with side reactors. Right – fully integrated process (reactive separator).

aims at confining the reaction to positions where it is not affecting product purity.

- The last option (Fig. 1.4, right) is a fully integrated separator-reactor where reaction and separation occur simultaneously throughout the unit.

Application to racemization reactions of the type $A \leftrightarrow B$ starting from the racemate is completely analogous and is illustrated in Fig. 1.5. In the first case (Fig. 1.5, left) the undesired isomer can be reconverted to the desired form inside of the reactor and fed back into the chromatographic unit. So far, this type of scheme has been studied only for few enantiomeric systems. These combine an enzymatic or thermal racemization with simulated moving bed (SMB) chromatography [9, 15, 46].

Also, the second approach (Fig. 1.5, center) has been most frequently considered for the production of isomers combining SMB chromatography and isomerization reactions. This concept was suggested by Hashimoto *et al.* [38]. Most investigations were devoted to the isomerization of glucose to fructose [15, 16, 38, 39, 99]. It should be noted that the investigated examples share several very specific properties. Typically, the desired component is the strong adsorbed isomer, and one or both components exhibit a peculiar adsorption behavior characterized by so-called unfavorable isotherms. Also, the product is obtained in these cases only at limited purity and/or conversion. The only enantiomeric system considered so far with these partially integrated systems is the thermal racemization of Tröger's base [15].

The completely integrated approach (see Fig. 1.5, right) was applied, for example, to esterifications [50, 77, 88, 89] and different enzymatic reactions [7, 48, 49]. For isomerization reactions, theoretical studies on integrating isomerization reactions into a chromatographic unit were reported in [21, 68, 73, 78]. They provided mathematical evidence that the desired isomer can be produced with high purity for specific ratios between adsorption and reaction kinetics. However, these theoretical findings have not found experimental support in later years. Theoretical studies and practical implementations with simultaneous reaction and separation were limited to reduced product purities [14, 92]. For the specific case of enantiomers, the production of pure single enantiomeric form by using such completely integrated chromatographic process has not been reported.

In addition to the concepts discussed above, more sophisticated continuous schemes were also suggested with alternating reactive and non reactive columns [12, 69, 70]. However, these schemes include purge and vent streams which limit conversion and yield.

Only few studies attempt a comparison of the existing process alternatives. Borren [15, 16] evaluated several processes for the two mentioned examples, glucose/fructose and Tröger's base, and suggested more complex extensions of the Hashimoto concept. His investigations indicated that completely integrated processes are not a good alternative to produce isomers at high purity requirements. Also, a partial integration showed benefits for performance only for purities lower than 95% compared to a flowsheet integrated scheme.

Tylko [95] discussed spatially distributed functionalities in view of the Hashimoto concept. Fricke [28] investigated theoretically the role of different reaction rates in the zones of a continuous reactive chromatographic process under linear conditions. However, for the realization he suggested only the Hashimoto concept.

In summary, the concepts developed so far were designed mostly for very specific cases. For the production of single isomers, the typical application is characterized by limited product purity, the stronger adsorbing component being the target component, and specific types of adsorption equilibria. Furthermore, the theoretical comparisons among the different process alternatives was done for selected fixed process schemes based on established technology.

1.2. Problem statement & approach

Against this background, this work aims here at a more detailed investigation of the different options to implemet integrated processes for the production of single isomers. In order to achieve this, a three step approach is devised:

- **Conceptual design**: In a first part, a fundamental investigation is presented of the possibility to integrate continuous chromatography and racemization reactions in order to deliver single enantiomers with purity, yield and conversion values close to 100%. For this purpose, existing and new process options will be investigated on a conceptual level in order to evaluate their potentials and limits. The investigation is focused on the production of single isomers but paying especially attention to the very relevant case of enantiomers. Such conceptual design can provide a clear and unbiased understanding of the effects that the integration of the reaction provokes in a continuous chromatographic unit.

  The theoretical study is based on mathematical optimization. For that purpose, in a first step the simplified true moving bed (TMB) model is applied. The resulting nonlinear optimization problems are solved with standard software using gradient based methods. Besides the numerical optimization also analytical results based on equilibrium theory [73] are presented. These analytical results provide simple explanation and quantification of the effects found in the numerical optimization study.

- **Process synthesis**: In a second study, in view of practical implementation, the investigations are extended to simulated moving bed systems. Based on the findings of the

previous study on true moving bed models, certain process candidates were identified and are considered here. To deal with the very large number of different possible process structures a process synthesis investigation is performed based on superstructures. The complex mixed integer non linear problem is solved using dynamic simulations and evolutionary algorithms.

By this approach, an attractive candidate in terms of high process performance and low complexity is indentified. Further, this process is analyzed in detail to determine its capabilities and define its possible field of application.

- **Experimental validation**: Finally, the new concept is validated experimentally for the separation of a model compound. The experimental proof of principle for the innovative process supports that the production of single enantiomers is feasible with almost 100% purity, yield, and conversion.

1.3. Thesis outline

According to the points mentioned above, the thesis is organized in three main chapters as follows:

Chapter 2 contains a theoretical investigation of different process options combining true moving bed chromatographic separations and isomerization reactions.
In section 2.1 different processes – including new approaches – are defined based on the three general options shown in Fig. 1.5. Subsequently, in section 2.2, the mathematical model is explained. The optimization problem is introduced and the tools are described. In section 2.3, the optimization results are summarized. The performance of the processes is optimized under various conditions that reflect typical practical aspects. Two cases are analyzed simultaneously, situations where the strongly adsorbed component is the target and cases where the weakly adsorbed component is the desired product. While the challenging production of a single enantiomer will serve as a reference case, the results are readily applicable to other isomerization problems.
In section 2.3.2, the effects found with the numerical optimization are discussed based on equilibrium theory. In section 2.3.4, the role of relevant aspects is investigated: section 2.3.4.1 describes the effect of the separation factor on the performance of the different processes; section 2.3.4.2 studies the influence of the reaction equilibrium constant on the performance of the processes, extending the reference case of enantiomers to the more general case of isomerization reactions.

In chapter 3, a large number of process alternatives combining simulated moving bed

chromatography and racemization reactions is evaluated and compared in terms of performance and complexity. In section 3.1 possible structures are introduced, and summarized to superstructures. In section 3.2 the mathematical model, the optimization problem and the necessary tools are explained. The results are shown in section 3.3. In section 3.3.1, the results of the process synthesis and optimization study are discussed for two different scenarios: moderate purity requirements in section 3.3.1.1, and high purity requirements in section 3.3.1.2. In these sections, the comparison between the large number of process structures facilitates the identification of an innovative integrated process as an attractive alternative. In section 3.3.2, focus is on the comparison of partial integration with side reactors with the new integrated process mentioned above. Finally, in section 3.3.3 the new integrated process is analyzed in some more detail to clarify its potential and define its possible field of application.

Chapter 4 describes the experimental validation of the new process alternative for the production of single enantiomers using chlorthalidone as a model compound. In section 4.2, the mathematical model introduced in chapter 3 is extended to the experimental setup suggested here. Section 4.3 summarizes the chemicals, the instrumentation and the experimental conditions. The results are discussed in section 4.4. First, in section 4.4.1, the model parameters necessary to describe the integrated scheme are determined experimentally. Reaction and adsorption behavior need to be determined for a large range of operating conditions. In section 4.4.1.1 the racemization kinetics of the model compound are investigated for different temperatures and pH values. Suitable mathematical relations are suggested to describe the kinetic constant of the racemization reaction as a function of these parameters. In section 4.4.1.2, the adsorption behaviour is studied for different pH values under reactive and non reactive conditions by the use of an inverse method. Finally, in section 4.4.2 the results of the experiments carried out in the semi-preparative SMB unit are discussed and compared with the theoretical predictions.

Finally, in chapter 5 conclusions and future directions are sumarized.

CHAPTER 2

Conceptual Design of Integrated TMB Processes

*In this chapter a fundamental investigation is performed for integrated pro-
cesses that combine continuous chromatography and isomerization reactions to
produce a single (stereo-)isomer. Focus is on the conceptual design of different
process concepts and their theoretical analysis. The general concepts introduced
in the previous chapter are investigated. They include reactor-separator-reactor
systems, schemes with side reactors, and chromatographic reactors. As a new
option, continuous chromatographic reactors with internally distributed function-
alities are suggested. Using parameters of a model system, the performance of the
processes is compared based on optimization of the corresponding models. The
results reveal the potential and the limits of the different approaches under var-
ious conditions. It is found that the suggested new option can enhance process
performance significantly.*

 formula · formula

2.1. Investigated processes

Based on the three general options shown in the previous section in Fig. 1.5, the five different
process concepts shown in Fig. 2.1 were selected for detailed investigations. In a first step,
a true moving bed (TMB) model is applied assuming countercurrent movement between the
solid and the liquid phase. In contrast to most of the existing literature, the processes in
Fig. 2.1 are designed to obtain the weaker adsorbing component B as product. Setups for the

stronger adsorbing solute A are obtained easily by "inverting" these schemes as illustrated in Fig. 2.2. Since one goal of this work is to maximize conversion and yield, the schemes shown have only a single product outlet and no waste streams.
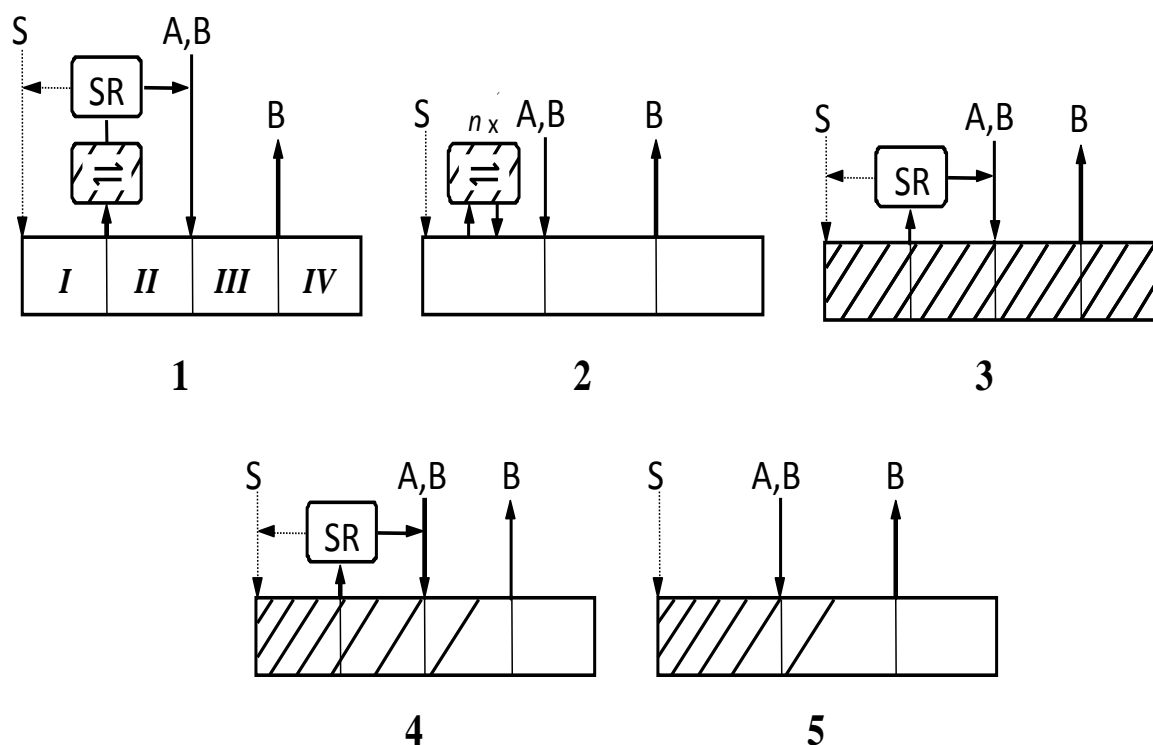

Figure 2.1. – Investigated processes for the production of the weakly adsorbed component B. 1 – classical flowsheet-integrated process with a separation by TMB chromatography, isomerization reactor, recycle, and intermediate solvent removal (SR). 2 – 3-zone TMB process with n side reactors ("Hashimoto concept"). 3 – 4-zone TMB reactor with recycle and solvent removal. 4 – 4-zone TMB reactor with *internally distributed* reaction, recycle, and solvent removal. 5 – 3-zone TMB reactor with internally distributed reaction.

The first option (process 1) is a classical reactor-separator-recycle system with a 4-zone TMB process. The weaker adsorbing product B is obtained at the so-called raffinate port, while the unconverted educt A is transported towards the reactor. As also applied in [15], an intermediate removal of excess solvent (SR) is included to counter-balance the continuous feeding of solvent to zone I. The removed solvent can be re-used. The next processes correspond to the previously mentioned Hashimoto concept (2) and a fully integrated TMB reactor (3), respectively. The latter also has a solvent removal. The last two processes are new suggestions. They combine the spatial distribution attempted by the Hashimoto approach and

the reduced flowsheet-complexity of a fully integrated process. In both schemes it is assumed that the reaction rate can be "distributed" optimally within the unit. The 4-zone version (4) contains a recycle and solvent removal. In contrast, the simple 3-zone system (5) requires no external devices.
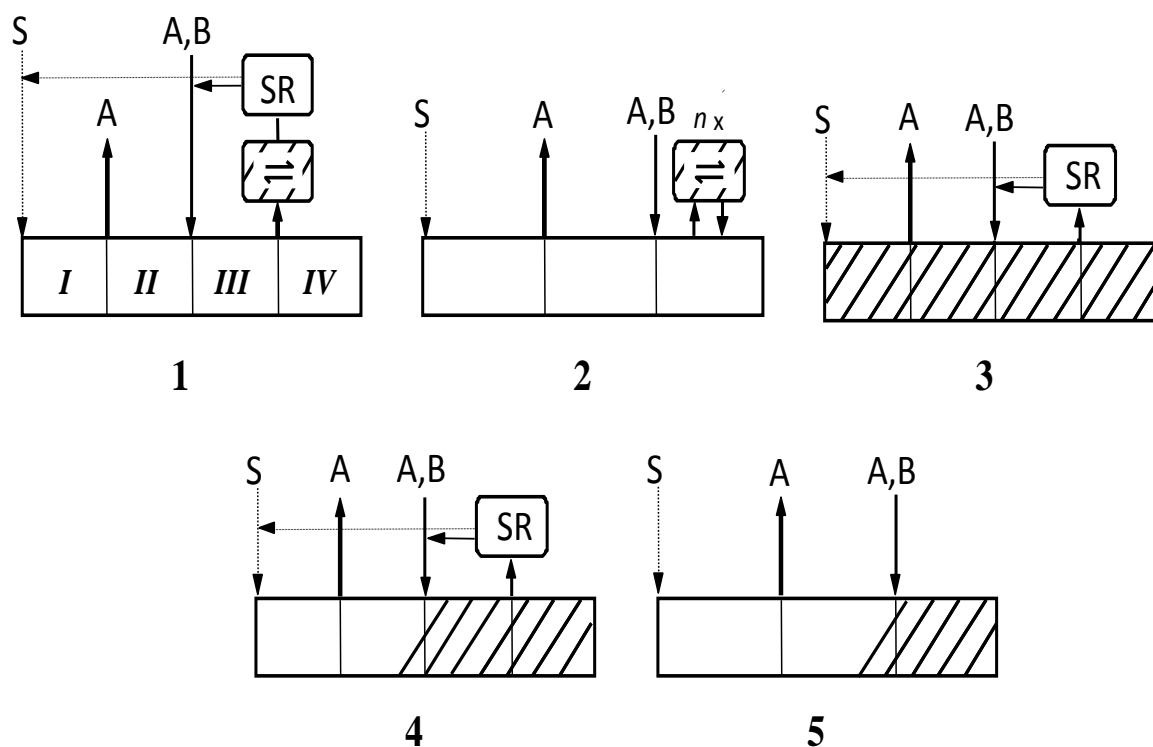
Figure 2.2. – Investigated processes for the production of the strongly adsorbed component A. 1 – classical flowsheet-integrated process with a separation by TMB chromatography, isomerization reactor, recycle, and intermediate solvent removal (SR). 2 – 3-zone TMB process with n side reactors ("Hashimoto concept"). 3 – 4-zone TMB reactor with recycle and solvent removal. 4 – 4-zone TMB reactor with *internally distributed* reaction, recycle, and solvent removal. 5 – 3-zone TMB reactor with internally distributed reaction.

It is emphasized that it is beyond the scope of this section to suggest detailed practical implementations for the schemes in Figs. 2.1 and 2.2. Since it is more or less impossible to realize a TMB process in practice, such integrated process will rely on the simulated moving bed (SMB) concept. Therefore, the issues related to the practical implementation will be treated in detail in the next chapter.

2.2. Mathematical model and optimization

The large number of optimizations carried out in this work requires a flexible and numerically efficient model. Here we use an equilibrium stage model for the TMB process, which consists of the mass balances for the two components in the fluid and solid phases within each stage

$$\epsilon V \frac{\mathrm{d}c_i^{k,z}}{\mathrm{d}t} + (1 - \epsilon)\, V \frac{\mathrm{d}q_i^{k,z}}{\mathrm{d}t} = Q^z \left(c_i^{k-1,z} - c_i^{k,z} \right) + Q_s \left(q_i^{k+1,z} - q_i^{k,z} \right) + \epsilon V \nu_i\, r^{k,z} \quad (2.1)$$

where the indices $i = A, B$ denote the component, $k = 1 \ldots N_s$ the stage, and $z = 1 \ldots N_z$ the zone of the TMB process (see Figs. 2.1 and 2.2), respectively. c_i and q_i are the liquid and solid phase concentrations, V is the volume of a stage and ϵ the porosity. Q and Q_s are the volumetric flow rates of the fluid and the solid phase, respectively. The axial dispersion is adjusted by the number of stages, N_s [37].

The last term in Eq. (2.1) describes the chemical reaction with ν_i as the stoichiometric coefficient and r as the reaction rate. In this work, we consider a reversible (i.e., equilibrium-limited) isomerization $A \leftrightarrow B$. Unless otherwise stated, the reaction is assumed to occur in the fluid phase. Thus, the reaction equilibrium constant is given by

$$K_{eq} = \frac{c_B}{c_A} = \frac{k}{k_b} \quad (2.2)$$

with k and k_b as rate constants of the forward and backward reaction, respectively. In cases where the reaction takes place in the solid phase an analogous definition holds

$$K'_{eq} = \frac{q_B}{q_A} \quad (2.3)$$

According to Eq. (2.2) the rate expression for an isomerization reaction in the liquid phase is given by

$$r^{k,z} = k \left(c_A^{k,z} - \frac{c_B^{k,z}}{K_{eq}} \right) \quad (2.4)$$

The design variables to be optimized in this work are the dimensionless zone flow rate ratios, m^z, and the Damköhler number, Da^z, for each zone z:

$$m^z = \frac{Q^z}{Q_s} \quad (2.5)$$

$$Da^z = \epsilon\, \tau_s\, k^z \quad (2.6)$$

where $\tau_s = V/Q_s$ is the residence time of the solid within a single stage. Using these defini-

tions and Eq. (2.4), we can rewrite Eq. (2.1) for the reactive TMB process as

$$\epsilon \, \tau_s \left(\frac{\mathrm{d}c_i}{\mathrm{d}t}^{k,z} + F \frac{\mathrm{d}q_i}{\mathrm{d}t}^{k,z} \right) = m^z \left(c_i^{k-1,z} - c_i^{k,z} \right) + q_i^{k+1,z} - q_i^{k,z} + \nu_i \, Da^z \left(c_A^{k,z} - \frac{c_B^{k,z}}{K_{eq}} \right) \quad (2.7)$$

with $i = A, B$, $k = 1 \ldots N_s$, and $z = 1 \ldots N_z$ and where $F = (1 - \epsilon)/\epsilon$ is the phase ratio. Using corresponding values for Da^z, Eq. (2.7) allows for a simple modelling of both non reactive chromatographic processes (i.e., $Da^z = 0$ for all z), as well as of reactive processes with or without spatial distribution of the reaction within the unit (i.e., $Da^z \neq 0$ for selected z).

The relation between the solid and the liquid phase concentrations in Eq. (2.7) is given by the adsorption equilibrium. Often, the Langmuir isotherm model is used to describe multicomponent adsorption behavior in preparative chromatography

$$q_i = \frac{q_S \, b_i c_i}{1 + b_A c_A + b_B c_B} \quad , \quad i = (A, \, B) \quad (2.8)$$

Here, bi-Langmuir adsorption isotherms are applied, which are most frequently used for enantiomeric systems

$$q_i = \frac{q_{S,1} \, b_{i,1} c_i}{1 + b_{A,1} c_A + b_{B,1} c_B} + \frac{q_{S,2} \, b_{i,2} c_i}{1 + b_{A,2} c_A + b_{B,2} c_B} \quad , \quad i = (A, \, B) \quad (2.9)$$

Eq. (2.9) describes competitive adsorption of the two solutes (A, B) on two different types of adsorption sites of the solid (1, 2); $q_{S,1}$ and $q_{S,2}$ are the corresponding saturation capacities related to the Henry coefficient as follows

$$H_i = q_S \, b_i \quad , \quad i = (A, \, B) \quad (2.10)$$

For Langmuir isotherms, a separation factor (valid for infinite dilution) can be defined as

$$\alpha = \left. \frac{q_S \, b_A}{q_S \, b_B} \right|_{c_A = c_B = 0} \quad (2.11)$$

while for the bi-Langmuir model the separation factor is defined as

$$\alpha = \left. \frac{q_{S,1} \, b_{A,1} + q_{S,2} \, b_{A,2}}{q_{S,1} \, b_{B,1} + q_{S,2} \, b_{B,2}} \right|_{c_A = c_B = 0} \quad (2.12)$$

The external devices connected to TMB units shown in Figs. 2.1 and 2.1 were modeled as follows. The reactors in processes (1) and (2) are described as continuously stirred tank reactors (CSTRs) with an infinite reaction rate and negligible volume. The devices for solvent removal (SR) were assumed to instantaneously adjust the mixture concen-

trations such that the higher concentrated component has the same concentration as in the feed.

The following objective function was applied in the optimization to evaluate the different process schemes

$$OF = \frac{Q^S}{Q^{out} c_i^{out}} = \frac{Q^S}{Pr} = \text{Performance}^{-1} \tag{2.13}$$

where Q^S and Q^{out} are the flow rates of the solvent and product ($out = R$ for raffinate, $out = E$ for extract port), respectively. c_i^{out} is the concentration of the desired component in this stream. The term $Pr = Q^{out} c_i^{out}$ is the productivity of the process. Note that for calculating Q^S, a possible re-use of the removed solvent (as indicated in Figs. 2.1 and 2.2) was not considered. Eq. (2.13) is the most frequently used objective function for continuous chromatography, since it simultaneously minimizes solvent consumption and maximimizes productivity. The optimization problem can be summarized as

$$\begin{aligned} &OF(m^z, Da^z) \longrightarrow min \\ &s.t. \\ &Pu^{out} = \frac{c_i^{out}}{c_A^{out} + c_B^{out}} \geq Pu_{min} \end{aligned} \tag{2.14}$$

where Pu^{out} denotes the product purity. Note that no additional constraint for the conversion is required because the processes in Figs. 2.1 and 2.2 have only a single outlet. It can be shown that, for such processes, the following relation between purity and conversion holds

$$X_j = \frac{Pu^F + Pu^{out} - 1}{Pu^F} \tag{2.15}$$

where the purity of the feed is defined with respect to component j. If the weaker adsorbing component B is the target product, for the indices in Eqs. (2.13) to (2.15) we have $i = B$, $j = A$, and $out = R$. Correspondingly, if the stronger adsorbing component A is desired, $i = A$, $j = B$, and $out = E$.

The simulation and optimization in this work was performed using the Fortran based DIVA 3.9 dynamic simulation environment [51, 58]. The integration of the system of ordinary differential equations shown in Eq. (2.7) was performed with the integrator "INT80", constituting a LIMEXS version 4.2B1 extrapolation method with variable order and stepsize. They proved to integrate much faster than other available integrators in DIVA like "INT10" and "INT60" based on Backward Differentiation Formula (BDF-Method) which are recommended for nonlinear problems with rather smooth solutions.

The solver for nonlinear algebraic equations "SOL2" in DIVA was used which is a modified Levenberg-Marquardt method.

All optimizations were performed using "OPT20", a sequential quadratic programming (SQP) algorithm available in DIVA. This algorithm is based on the SQP-method implemented

in E04UCF of the NAG-Library [51]. It is suitable for function minimization with bounds on the variables and nonlinear constraints.

2.3. Results

2.3.1. Optimization of the reference case

In order to provide a basis for further discussions, we optimize the performance of the processes shown in Figs. 2.1 and 2.2 for a reference case. The optimized parameters are the flow rate ratios m^z, Eq. (2.5), and – where applicable – the Damköhler numbers Da^z, Eq. (2.6). The enantiomers of chlorthalidone are considered as a model system. For this substance, experimental parameters are available in [46]. For enantiomeric systems, the reaction equilibrium constant in Eq. (2.2) is $K_{eq} = 1$. The feed is considered to be racemic (i.e., $c_A^F = c_B^F$). Table 2.1 summarizes the parameter values and conditions used for the reference case.

Table 2.1. – Properties of the model system as taken from [46] and parameters of the reference case.

Parameter	Symbol		Values	
bi-Langmuir adsorption isotherms,	$q_{S,1}$	[g/l]	94.175	
Eq. (2.9)	$q_{S,2}$	[g/l]	0.244	
	$b_{i,1}$	[l/g]	0.207	0.141
	$b_{i,2}$	[l/g]	6.395	3.192
porosity	ϵ	[−]	0.796	
stage volume	V	[ml]	1.0	
number of stages per zone	N_s	[−]	50	
Reference parameters				
feed concentration	c_i^F	[g/l]	0.2	
equilibrium constant	K_{eq}	[−]	1.0	
separation factor	α	[−]	1.496	
purity requirement	Pu_{min}	[%]	90	

Firstly we apply moderate purity requirements of $Pu_{min} = 90\%$, which correspond to a conversion of $X = 80\%$ (see Eq. (2.15)). Table 2.2 contains the optimization results for the case that the weakly adsorbed component B is the desired product. The table lists the optimized parameters, the values of the objective function, and the performance indicators productivity, Pr, and the desorbent stream, Q^S (see Eq. (2.14)). The purity of the recycle stream Pu^{rec}, if present, is also indicated.

Table 2.2. – Optimization results for the processes shown in Fig. 2.1 for the reference case. The target product is the weakly adsorbed component B, which is obtained at the raffinate port at a purity requirement of $Pu^R \geq 90\%$. Note that the purity of the recycle stream, Pu^{rec}, is (if present) defined with respect to component A. Note that process 2* represents the specific case of process 2 in Fig. 2.1 using a total of 5 side reactors.

Process	OF	Pr	Q^S	Pu^{rec}	m^I Da^I	m^{II} Da^{II}	m^{III} Da^{III}	m^{IV} Da^{IV}
1	5.30	1.12	5.94	78.44	19.466 –	11.182 –	18.669 –	13.530 –
2*	5.98	0.67	4.02	–	17.275 –	19.140 –	13.259 –	– –
3	24.79	0.40	9.93	77.93	21.839 $3 \cdot 10^{-2}$	0.534 $3 \cdot 10^{-2}$	19.039 $3 \cdot 10^{-2}$	11.410 $3 \cdot 10^{-2}$
4	2.88	1.14	3.29	50.02	16.369 10^2	11.311 10^{-4}	18.468 10^{-8}	13.078 10^{-8}
5	4.37	0.81	3.56	–	16.630 10^2	18.892 10^{-8}	13.072 10^{-8}	– –

Obviously, all processes are capable of delivering the product at the required purity of 90%. The conventional reactor-separator-recycle scheme (process 1 in Fig. 2.1) achieves an average performance. An interesting aspect is that the recycle stream (i.e. the extract) has a purity of $Pu^{rec} \approx 78\%$. This indicates that, under optimal conditions, a complete separation of the components is not required. It should be mentioned that a simple design method exists for continuous chromatography for such a scenario [47], which could be applied directly to design process 1 for adsorption isotherms of the Langmuir-type.

The performance of a partially integrated process with five side reactors (process 2 in Fig. 2.1) is slightly worse than for process 1. While the productivity is about 40% lower, this is partially compensated by a 32% lower desorbent flow rate Q^S. The latter is due to the lower optimal m^I value, which indicates an easier regeneration of zone I. It is emphasized that the performance of process 2 depends strongly on the number of side reactors. This will be discussed in more detail below.

The fully integrated process 3 affords only an inferior performance (OF is about 5 times higher than for process 1). This is due to the "omnipresence" of the forward and backward reaction throughout the unit. As a consequence, the purity requirement can only

be achieved by having a low Damköhler number. In turn, this requires a very high recycle ratio through the reactor, as indicated by the low value of m^{II}. Interestingly, the purity of the recycle stream is very similar to the value found for process 1.

The 4-zone process with an internally distributed reaction (process 4 in Fig. 2.1) achieves the best performance of all concepts. As expected, the optimizer determines a high optimal reaction rate in zone I (i.e., Da^I), which is the only zone that is not adjacent to the product port. In the other zones, very low Da values are found, which cause basically no conversion (note that Da^{III} and Da^{IV} are equal to the lower limits allowed in the optimization). The favorable value for OF (almost 50% lower than for process 1) is mainly due to a significantly lower solvent requirement. Q^S reduces strongly due to lower m^I values. Obviously, the high reaction rate in zone I facilitates an easier desorption of the components within this zone. This effect is denoted as *reaction-assisted regeneration* and will be analyzed in the subsequent section.

Finally, the performance of the simple 3-zone scheme with an internally distributed reaction (process 5) ranks second for the given purity requirement. This is also caused by reaction-assisted regeneration in zone I. This is an encouraging finding, because this simple process requires no additional unit operation like a solvent removal (see Fig. 2.1).

As mentioned above, the performance of the Hashimoto process (process 2 in Fig. 2.1) will obviously depend on the number of side reactors. This is further quantified in Fig. 2.3 and compared to the 3-zone process with internally distributed reaction (process 5 in Fig. 2.1) for the present case study. It is shown in Fig. 2.3 that the performance of process 5 is always better than that of process 2. The difference is monotonically decreasing for an increasing number of side reactors. It can be concluded that a rather high number of side reactors for the Hashimoto process is required to obtain similar performance like for process 5.

The optimization was repeated for the stronger adsorbing component A as the target product (see structures in Fig. 2.2). Table 2.3 summarizes the results. The performance of most schemes is rather similar in comparison to the case that the weaker adsorbing B is desired (see Table 2.2). Exceptions are processes 2 and 4, which require higher desorbent flow rates. This is due to the reaction-assisted regeneration now taking place in zone IV, where it is less effective for the type of adsorption isotherms used here, as will be also discussed in the next section.

The purity requirement of 90% used so far might be sufficient in certain cases. For many applications, for example, in the production of a single, pharmaceutically active enantiomer, more restrictive demands hold with respect to product purity and conversion. To address this aspect, the calculations were repeated for a purity of $Pu_{min} = 99.9\%$ (corresponding to $X = 99.8\%$).

Out of the five schemes, only processes 1 and 4 are capable of delivering this required purity.
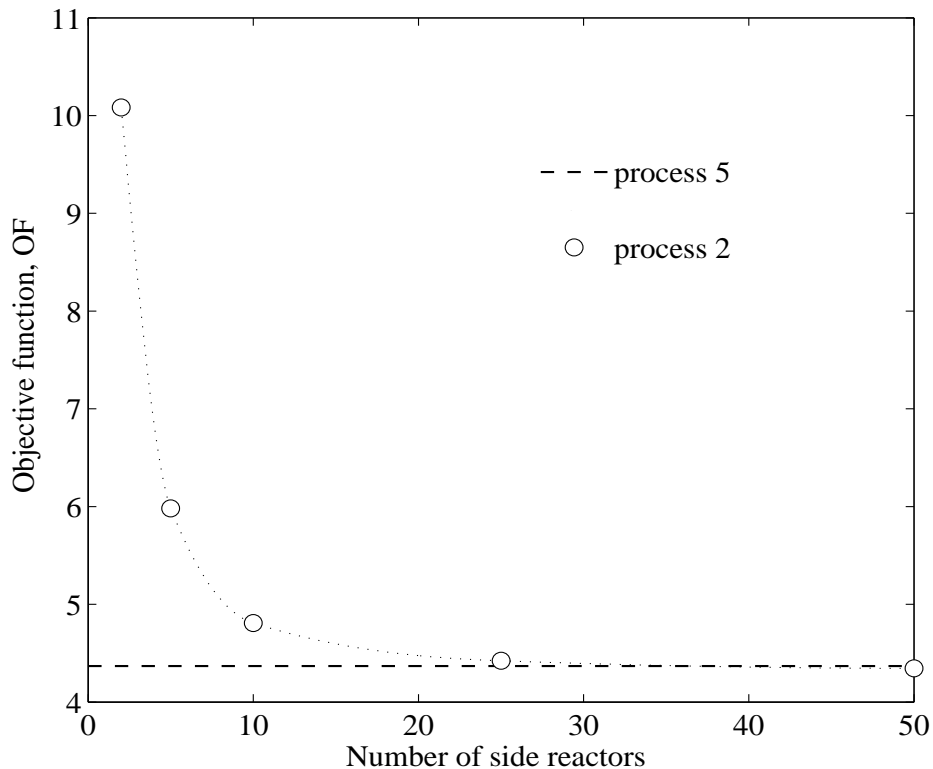
Figure 2.3. – Comparison of the performance of the three-zone setup with a distributed reaction (process 5, dashed line) and the Hashimoto concept (process 2, circles) with different numbers of side reactors. The target product is the weaker adsorbing component B. $K_{eq} = 1.0$, $Pu_{min} = 90\%$.

Table 2.4 lists the optimization results for the two schemes that are capable of performing this task. Process 1 achieves an acceptable performance despite the comparably low number of theoretical stages used (50 per zone). The new process 4 again outperforms this for the production of the weakly adsorbed B (upper part of Table 2.4), but not for the production of the stronger adsorbing A (lower part of the table). Process 4 in both cases profits from the reaction-assisted regeneration, as is indicated by the lower m^I or the higher m^{IV} when producing B or A, respectively. However, in the second case the positive effect on m^{IV} is outbalanced by a higher value of m^I. In process 1 a partial breakthrough of component A from zone I to zone IV enhances performance. This is similar to earlier observations for non reactive systems [47]. In contrast, such breakthrough is detrimental in process 4. The reason for this appears to be that any component A entering zone IV decreases the driving force of the isomerization within this zone. The conversion would be reduced by this, which would require more restrictive internal flowrates. This is also supported by independent calculations which indicate that this can be overcome by suppressing the reaction in the rightmost parts of zone IV.

Table 2.3. – Optimization results for the reference case for corresponding processes that deliver the stronger adsorbing component A (see Fig. 2.2) with a purity of $Pu^E \geq 90\%$. The purity of the recycle stream, Pu^{rec}, is (if present) defined with respect to component B. Note that process 2* represents the specific case of process 2 in Fig. 2.1 using a total of 5 side reactors.

Process	OF	Pr	Q^S	Pu^{rec}	m^I Da^I	m^{II} Da^{II}	m^{III} Da^{III}	m^{IV} Da^{IV}
1	5.01	0.96	4.82	72.77	18.022 $-$	12.573 $-$	19.943 $-$	13.199 $-$
2*	7.75	0.96	7.44	$-$	20.849 $-$	12.740 $-$	13.408 $-$	$-$ $-$
3	24.16	0.41	9.81	89.36	23.370 $4.3 \cdot 10^{-2}$	14.069 $4.3 \cdot 10^{-2}$	17.600 $4.3 \cdot 10^{-2}$	13.588 $4.3 \cdot 10^{-2}$
4	3.62	1.04	3.75	50.07	19.291 10^{-8}	13.041 10^{-8}	20.560 10^{-8}	15.541 10^{2}
5	4.15	1.02	4.22	$-$	19.905 10^{-8}	12.852 10^{-8}	15.682 10^{2}	$-$ $-$

Table 2.4. – Optimization results for process 1 and 4 shown in Figs. 2.1 and 2.1 and $Pu^{out} = 99.9\%$. The target products are the weakly adsorbed component B (upper part of the table) and the strongly adsorbed component A (lower part).

Process	OF	Pr	Q^S	Pu^{rec}	m^I Da^I	m^{II} Da^{II}	m^{III} Da^{III}	m^{IV} Da^{IV}
1	11.69	0.87	10.22	79.24	23.458 $-$	11.427 $-$	17.344 $-$	13.224 $-$
4	8.56	0.87	7.44	50.06	19.699 10^{2}	11.690 10^{-4}	17.239 10^{-8}	12.260 10^{-8}
1	9.66	0.74	7.11	73.67	19.345 $-$	14.712 $-$	20.435 $-$	12.236 $-$
4	10.37	0.81	8.41	50.53	23.382 10^{-8}	14.958 10^{-8}	20.750 10^{-3}	14.971 10^{2}

The other process schemes (2, 3, 5) are not capable of obtaining a product with 99.9% purity for the number of stages used. Obviously, process 3 would require an extremely high stage number to resolve this task. In contrast, doubling the stage number for process 5 already leads to a similar performance as achieved here by process 1. The effect of the stage number on the performance will be exhaustively discussed in the next chapter for the more realistic scenario of a simulated moving bed system.

2.3.2. Analysis of reaction-assisted regeneration

In the previous section, the superior performance of processes with an internally distributed reaction was explained by an effect denoted as reaction-assisted regeneration. Here this effect is analyzed.
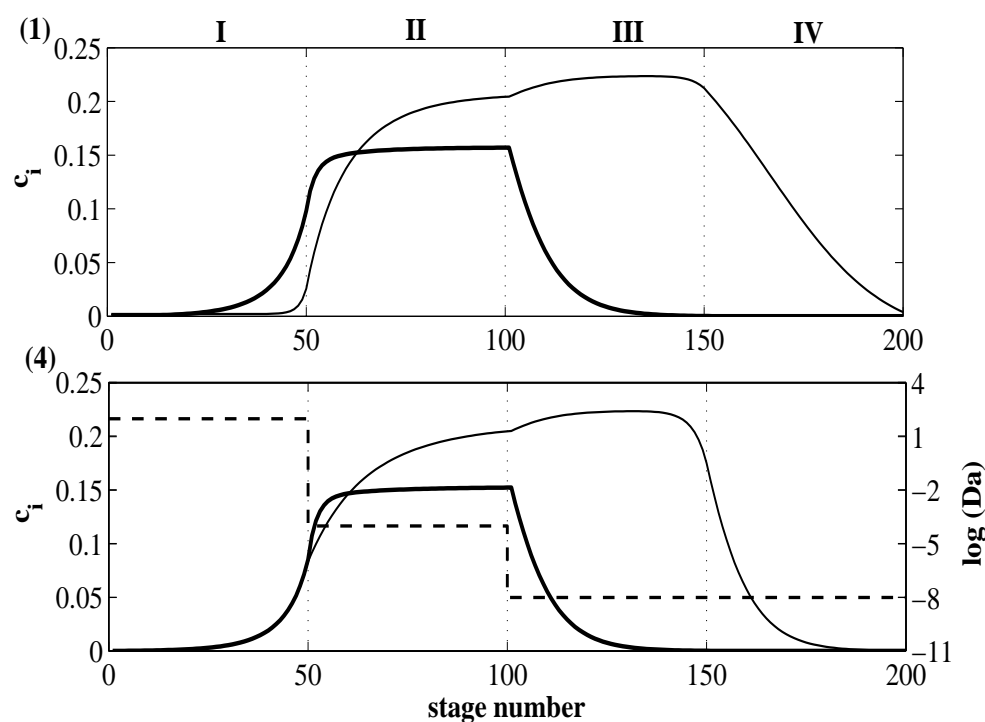

Figure 2.4. – Steady-state concentration profiles for the 4-zone processes 1 (top) and 4 (bottom) under optimized conditions. Operating parameters corresponding to the optimization shown in Table 2.4, top. The target product is the weaker adsorbing component B. $K_{eq} = 1.0$, $Pu_{min} = 99.9\%$. Lines: components A (thick) and B (thin), Damköhler number, Da (dashed). Reaction-assisted regeneration taking place in zone I.

First of all, the optimized internal concentration profiles at steady state are compared for the four-zone processes 1 and 4 in Fig. 2.1. These are shown for the production of the less retained enantiomer B in Figure 2.4. In the non reactive process 1 (Fig. 2.4, top) the concentration fronts of the two components in zone I are located at different positions. In contrast, for process 4 (bottom), the fast reversible isomerization leads to a common concentration front for both components. As already indicated, a lower flow rate (i.e. m^I) suffices to stabilize this front. This can be explained when considering that the reaction converts strongly adsorbed molecules into weakly adsorbed ones. These, in turn, are desorbed more easily and will migrate with the liquid before being converted again. An analogous effect is observed in zone IV if the stronger adsorbed solute A is desired, although here the benefits observed are slightly lower. Similar obervations were made using SMB reactors with reactive desorbents in [32].

This effect can be quantified using equilibrium theory, i.e. by assuming an instantaneous reaction and adsorption equilibrium throughout the process. In this case, it is possible to estimate the necessary flow rate ratio to achieve complete regeneration of a reactive zone I, m^I_{min}, for the production of the less retained component B. Also, analytical expressions can be obtained to estimate the necessary value of the flow rate ratio in a reactive last zone, $m^{N_z}_{max}$, when producing the more retained component A. For this second scenario, the expressions are no longer explicit, but a function of the plateau concentrations. These values are a priori unknown, and require to solve the global material balance around the unit. However, here the implicit solutions suffice to explain and support the observed effects caused by the isomerization reactions taking place within the regeneration zones.

Such analysis was performed for homogeneous and heterogeneous reactions and for the two most frequently used adsorption isotherm models: Langmuir and bi-Langmuir. The mathematical derivations are summarized in the Appendix A.

The expressions obtained for m^I and m^{N_z} are given in Table 2.5 for Langmuir isotherms. These expresions represent the minimum m^I and the maximum m^{N_z} values necessary to fully regenerate zones I and N_z, respectively. Three cases are shown: non reactive separation, homogeneous reaction, and heterogeneous reaction. The expressions can be used for basic design purposes. Furthermore, they allow to quantify the required regeneration efforts in each particular case.

As an example, Fig. 2.5 shows the flowrates required for the complete regeneration of zone I for the three cases mentioned above. The values in the figure were scaled with respect to the non reactive separation. The abscissa is the separation factor α, which is defined for the Langmuir adsorption isotherm by $\alpha = \frac{b_A}{b_B}$, respectively $\alpha = \frac{H_A}{H_B}$. For racemization reactions

Table 2.5. – Minimum m^I and maximum m^{N_z} for complete regeneration of the corresponding zones. Values hold for Langmuir adorption isotherms and infinite reaction and adsorption rates.

	m^I_{min}	$m^{N_z}_{max}$
Non reactive	H_A	$\dfrac{H_B}{1 + b_B c_B^{N_z}}$
Homogeneous reaction	$\dfrac{H_A + H_B K_{eq}}{1 + K_{eq}}$	$\dfrac{H_A + H_B K_{eq}}{1 + K_{eq} + b_A C^{N_z} + b_B K_{eq} C^{N_z}}$
Heterogeneous reaction	$\dfrac{H_A(1 + K'_{eq})}{1 + K'_{eq}\dfrac{H_A}{H_B}}$	$\dfrac{H_A\left(1 + K'_{eq}\right)}{\left(1 + \dfrac{H_A}{H_B}K'_{eq}\right)\left(1 + b_B\, c_B^{N_z}\left(\dfrac{K'_{eq} + 1}{K'_{eq}}\right)\right)}$

K_{eq} and K'_{eq} are equal to unity and we find from Table 2.5:

$$
\frac{m^I}{m^I_{\text{nonreactive}}} =
\begin{cases}
1 & : \text{no reaction} \\[2ex]
\frac{\alpha+1}{2\alpha} & : \text{homogeneous reaction} \\[2ex]
\frac{2}{\alpha+1} & : \text{heterogeneous reaction}
\end{cases}
\tag{2.16}
$$

The figure underlines that the effect of a reaction-assisted regeneration alleviates the separation especially for high separation factors. This holds in particular for a heterogeneous reaction. For example, for $\alpha = 3$, the flow rate in zone I could be reduced by 30% or 50%, depending on whether the reaction is homogeneous or heterogeneous. These numbers translate directly into a reduced solvent requirement.

The results for the bi-Langmuir isotherm model are summarized in Table 2.6. Note that the expressions for m^{N_z} are not explicit and depend on concentration values which a priori are unknown. The details regarding the derivation of this mathematical expression are discussed in Appendix A.

In order to validate the analytical solutions derived from equilibrium theory, several optimization runs are performed for process 4 in Fig. 2.1 for different α values. To force complete
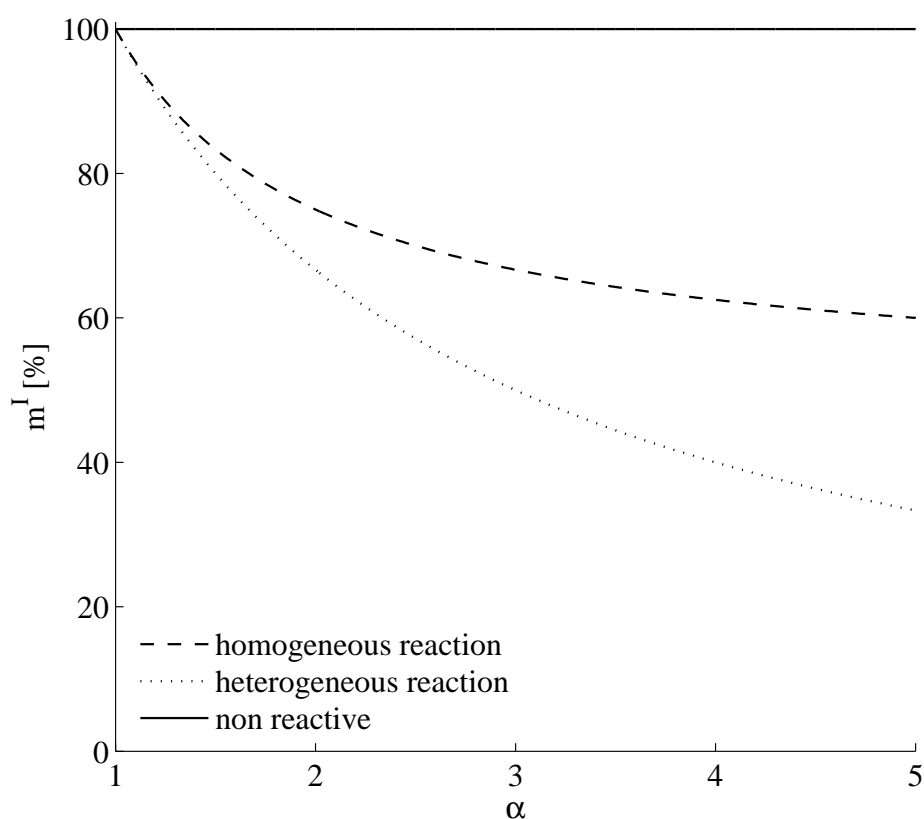
Figure 2.5. – Flow rates required for the regeneration of zone I as a function of the separation factor. Calculated for Langmuir isotherms using the expressions given in Table 2.5 ($K_{eq} = 1$). Values are scaled with respect to the non reactive case.

regeneration of zone I, the purity requirement is set to $Pu_{min} = 99.9\%$. Figure 2.6 depicts the m^I values obtained from the optimizations as a function of the separation factor α for the bi-Langmuir model, when producing the weaker adsorbed B (process 4 in Fig. 2.1). The same three cases as before are considered: non reactive separation, homogeneous reaction, and heterogeneous reaction. It can be observed that the optimization results (symbols) follow the trends given by the analytical solutions in Table 2.6 (lines). As expected, the differences decrease with decreasing dispersion (e.g. when using a total stage number of 400 instead of 200). Furthermore, in the reactive cases a lower m^I value than in the non reactive case suffices for regeneration, which translates into a lower desorbent consumption. The benefit increases with increasing α and is more pronounced for a heterogeneous reaction. The reason for this is the interplay of reaction and adsorption. For a heterogeneous reaction, more of the stronger adsorbing component A is adsorbed. Consequently, more A is converted into B. Upon desorption, this causes $c_B > c_A$. This excess of B leads to an overall easier desorption.
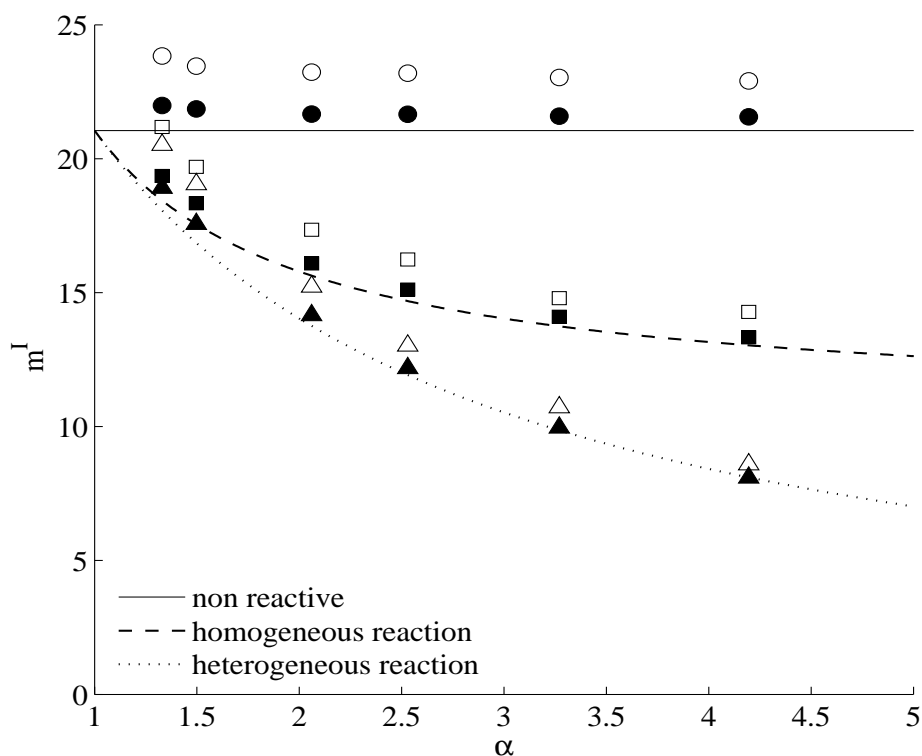
Figure 2.6. – m^I required for complete regeneration as a function of the separation factor, α, for the production of component B. Considered cases: non reactive separation (solid line, circles; see Fig. 2.1, process 1), homogeneous reaction (dashed line, squares; Fig. 2.1, process 4), and heterogeneous reaction (dotted line, triangles; Fig. 2.1, process 4). Lines correspond to the analytical expressions in Table 2.6. Symbols denote optimization results. Open symbols – 200 theoretical stages; filled symbols – 400 theoretical stages. The data hold for enantiomeric systems ($K_{eq} = K'_{eq} = 1$) and adsorption isotherms as given in Table 2.1.

Analogously, several optimization runs are performed for process 4 in Fig. 2.2 for different feed concentrations at $Pu_{min} = 99.9\%$. Figure 2.7 shows the m^{IV} values required to regenerate the liquid phase in zone IV for the production of the strongly adsorbed compound A. The abscissa is the total concentration in the liquid phase C. It is readily observed that in all cases the optimal m^{IV} decreases with increasing C. Simultaneously, the differences between the analytical solutions and the optimization results decrease. Both findings are related to the fact that the shock within this zone becomes faster and sharper with increasing C (cf. Eqs. (A-5) and (A-11)). Again, the two reactive cases will have a lower desorbent consumption because m^{IV} is higher than in a non reactive separation. Note that in this case an excess of B is detrimental. Thus, the benefit is more pronounced for a homogeneous reaction.
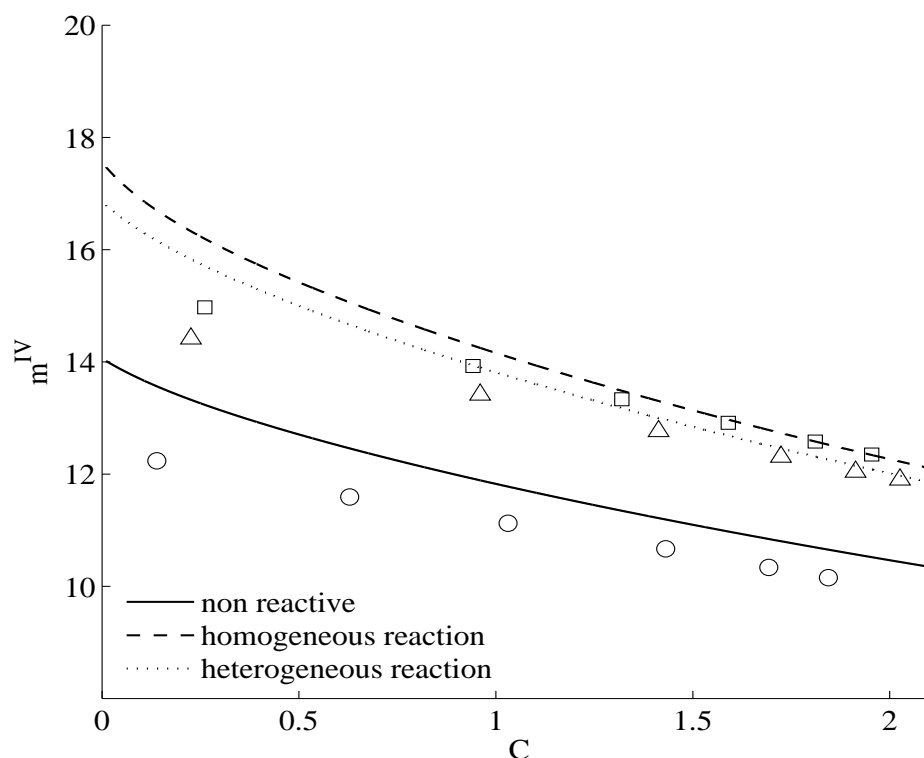
Figure 2.7. $- m^{IV}$ required for complete regeneration as a function of the total concentration in the liquid phase C in zone IV. For notation and parameters, see Fig. 2.6.

This analysis holds under the assumption of complete regeneration of the corresponding first and last zones in a TMB unit. For reduced purity demands and incomplete regeneration, the analytical expressions are not suitable and numerical solutions are required. Analogously to Fig. 2.4, Fig. 2.8 compares the steady-state concentration profiles for processes 1 (top) and 4 (bottom) for the production of the less retained component B. In this case, moderate purity requirements of 90% are considered, accordingly to the optimization results in Table 2.2. As in Fig. 2.4, the single front observed in zone I for process 4 indicates that reaction-assisted regeneration takes place within that zone. However, under reduced purity requirements, the purity of the raffinate is determined by concentration fronts originating from zones III and I. This indicates that it is not necessary to fully regenerate zone I, as already observed in the optimization results in Table 2.2. A breakthrough of components from zone I to zone IV can can be beneficial for the overall peformance as discussed for non reactive cases in [47].

Table 2.6. – Optimal m^I and m^{N_z} for complete regeneration of the corresponding zones. Values hold for bi-Langmuir adorption isotherms and infinite reaction and adsorption rates. *$q_i := q_i(c_A, c_B)$ with $c_A = \Psi(C), c_B = C - \Psi(C)$ as in Eq. (A-20).

	m^I_{min}	$m^{N_z}_{max}$
Non reactive	$H_{A,1} + H_{A,2}$	$\dfrac{H_{B,1}}{1 + b_{B,1}c_B} + \dfrac{H_{B,2}}{1 + b_{B,2}c_B}$
Homogeneous reaction	$\dfrac{H_{A,1} + H_{A,2} + (H_{B,1} + H_{B,2})K_{eq}}{1 + K_{eq}}$	$\dfrac{H_{A,1} + H_{B,1}K_{eq}}{1 + K_{eq} + (b_{A,1} + b_{B,1}K_{eq})C} + {}$ $+\dfrac{H_{A,2} + H_{B,2}K_{eq}}{1 + K_{eq} + (b_{A,2} + b_{B,2}K_{eq})C}$
Heterogeneous reaction	$\dfrac{(1 + K'_{eq})(H_{A,1} + H_{A,2})(H_{B,1} + H_{B,2})}{K'_{eq}(H_{A,1} + H_{A,2}) + (H_{B,1} + H_{B,2})}$	$\dfrac{1 + K'_{eq}}{2K'_{eq}C}\left[K'_{eq}\,q_A + q_B \right]^*$

2.3.3. Design considerations

Theoretically, the reaction-assisted regeneration effect allows for the production of pure enantiomer with a 3-zone TMB setup like process 5 in Figs. 2.1 and 2.2. To illustrate the effect, the so-called triangle theory is used in this section. For simplicity, focus is here on linear adsorption isotherms.

Triangle theory is used as a powerful design tool in the non reactive cases [61, 86]. Based on this method, a region of complete separation can be plotted on the m^{II}–m^{III} plane for standard 4-zone TMB systems. Analogously, such complete separation region can be shown for the integrated 3-zone TMB. In this case, the corresponding region is defined in the parameter space m^I–m^{II} for the raffinate setup. Analogously, the complete separation region can be defined in the parameter space m^{II}–m^{III} for the extract case.

Figure 2.9 shows these two different scenarios for the 3-zone TMB process. A homogeneous racemization reaction is considered to take place in zones I and III for the raffinate and the extract setups, respectively. On top, the theoretical profiles inside the TMB unit to achieve complete separation and regeneration are sketched for the production of B (left) and A (right). According to the explanation given in the Appendix A, the position of these fronts depends on their propagation velocities. Thus, only under certain constraints on the flow rate ratios in the different zones of the TMB complete separation can be achieved.

For the production of B (left), complete regeneration of zone I is required. According
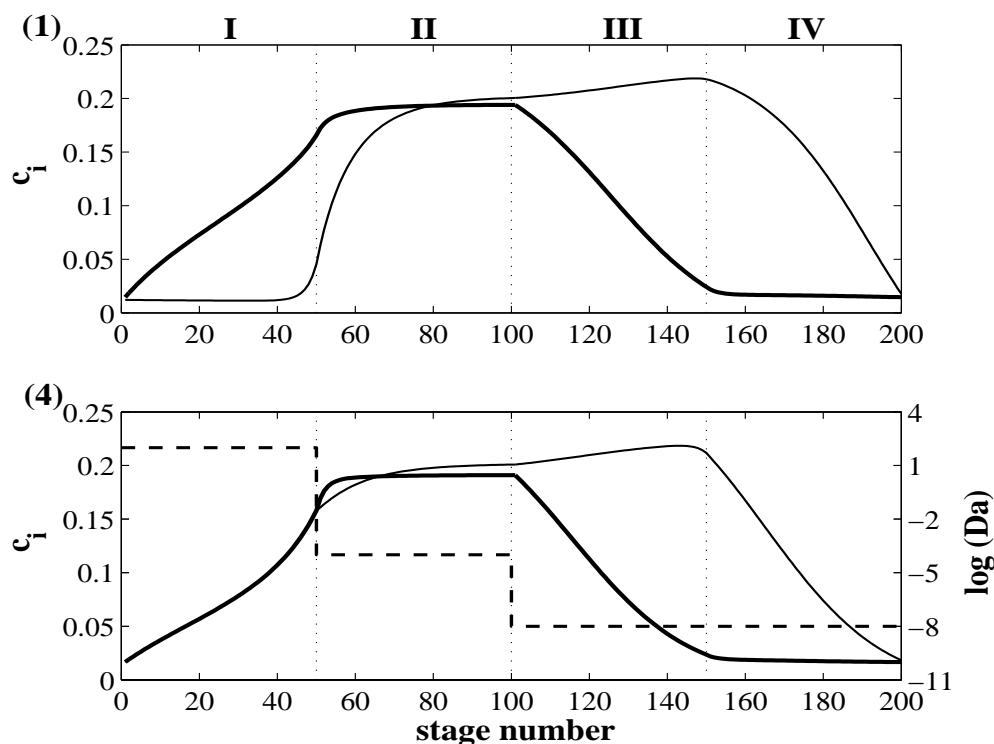
Figure 2.8. – Steady-state concentration profiles for the four-zone processes 1 (top) and 4 (bottom) under optimized conditions. Operating parameters corresponding to the optimization shown in Table 2.2. The target product is the weaker adsorbing component B. $K_{eq} = 1.0$, $Pu_{min} = 90\%$. Lines: components A (thick) and B (thin), Damköhler number, Da (dashed). Reaction-assisted regeneration taking place in zone I.

to the equations in Table 2.5, the minimum m^I value required to regenerate zone I can be easily calculated in the linear range for racemization reactions. Its value corresponds to the average of both Henry constants. Also, to ensure complete separation and pure product, the front of component A in zone II cannot reach the raffinate port. This limits m^{II} to lower values than H_A. Under these constraints, an overlap of the feasible regions can be found corresponding to the complete separation region, as indicated in Fig. 2.9, left. Thus, in theory, the production of pure less retained enantiomer is possible with an integrated 3-zone setup.

Analogously, for the production of A (right), complete regeneration of zone III is required. According to the equations in Table 2.5, the maximum m^{III} value required to regenerate zone III corresponds again to the average of both Henry constants. Further, to avoid product contamination, the front of component B in zone II cannot reach the extract port. This limits m^{II} to higher values than H_B. The overlap of the feasible domains indicates that a complete separation region can also be found, as shown in Fig. 2.9, right.
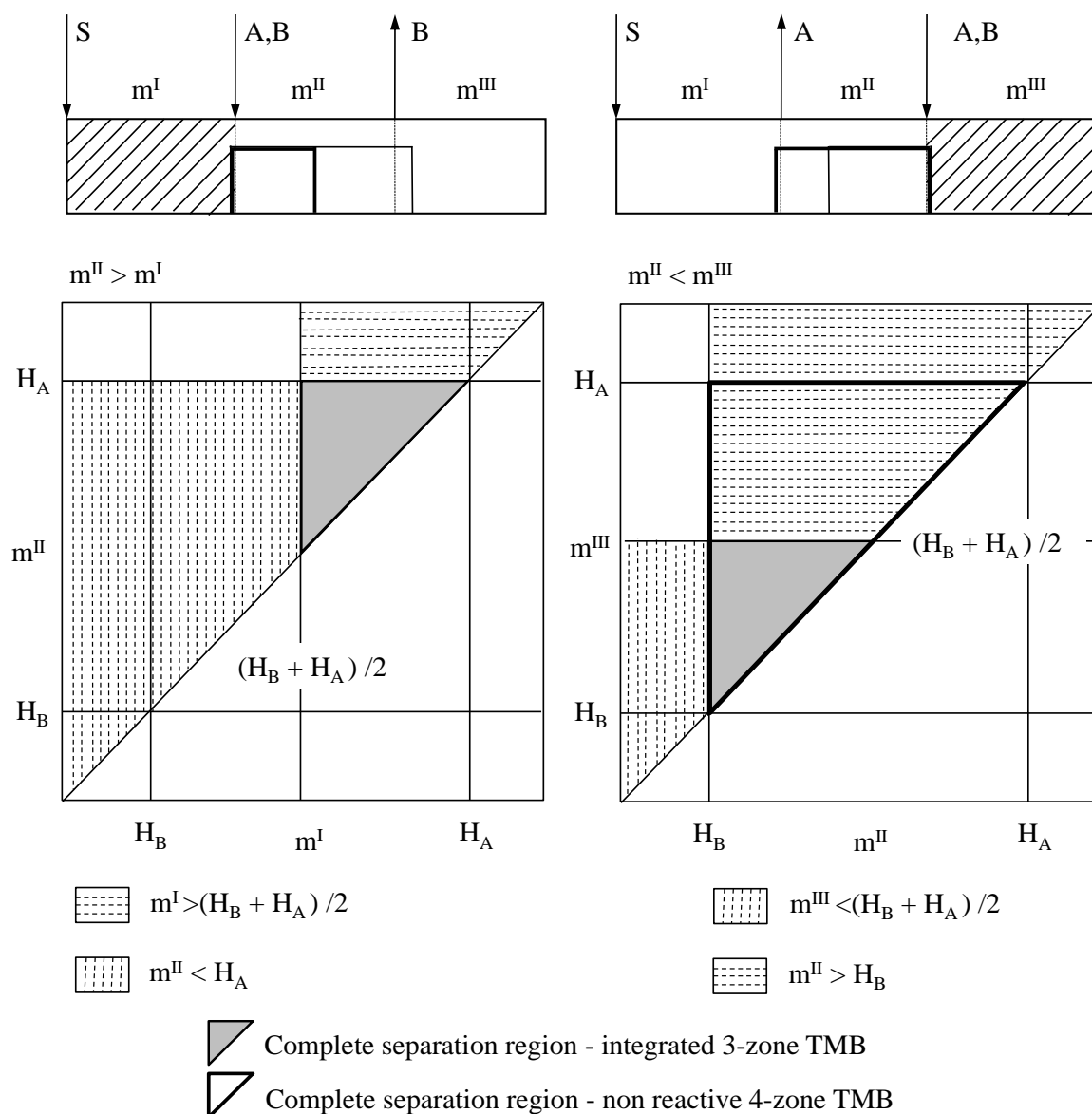
Figure 2.9. – Theoretical representation of the complete separation regions for process 5 in Figs. 2.1 and 2.2 with linear adsorption behavior. Left – for the production of the less retained component B on the m^I–m^{II} plane. Right – for the production of the more retained component A on the m^{II}–m^{III} plane. Regeneration in zones I and III, respectively, assisted by a homogeneously catalyzed racemization. The corresponding complete separation region for a non reactive 4-zone TMB, e.g. process 1 in Figs. 2.1 and 2.2, is also shown for comparison.

The corresponding complete separation region for a non reactive 4-zone TMB, e.g process 1 in Figs. 2.1 and 2.2, is also defined for comparison. Figure 2.9 indicates that the area of such region is significantly larger for the non reactive TMB. For purely separative TMB processes, the area of this region is proportional to the throughput of the system and therefore a straightforward indicator of the performance. However, for the processes studied here, the introduction of external recycle streams in the 4-zone TMB units does not allow a direct relation between throughput and performance. Therefore, no statement regarding performance can be made comparing the size of the regions for different process schemes.

2.3.4. Influence of other important parameters on optimal design

Now the investigations will be extended beyond the reference case. Enantiomeric systems are characterized by low separation factors, α, and a reaction equilibrium constant of $K_{eq} = 1$ (as studied above). Below, the two corresponding functionalities, "adsorption" and "reaction", will be adressed, as well as their optimal spatial distribution.

The results above indicate that the fully integrated process 3 is not suitable for isomerization problems. Furthermore, the Hashimoto concept (process 2) can be regarded as a special case of 3-zone systems with an internally distributed reaction (process 5). Therefore, in the following the focus is on the remaining processes 1, 4, and 5 shown in Fig. 2.1 for the production of the less retained component B.

2.3.4.1. Separation factor

The separation factor, α, plays a major role in any separation process. As it was demonstrated in Fig. 2.5, α also plays an important role with respect to the effectiveness of the reaction-assisted regeneration. The question to be answered here is whether different values for α will change the ranking of processes 1, 4 and 5 with respect to their performance.

It is difficult to vary the separation factor for the bi-Langmuir model in Eq. (2.9) in a useful manner without significantly affecting the nonlinear properties of the isotherms. The reason is the high number of parameters that determine α (see Eq. (2.12)). It can be expected, however, that similar trends will be obtained by using the Langmuir isotherms, Eq. (2.8), that were already used for the analysis in the previous section. Therefore, the parameters of the Langmuir model were adjusted such that the bi-Langmuir isotherms in Table 2.1 are matched closely ($q_s = 100$, $b_A = 0.20$, $b_B = 0.14$, and $\alpha = 1.43$).

Figure 2.10 shows the optimization results for the weaker adsorbing component B obtained at a purity of 90% (for other parameters than the isotherms, see Table 2.1). In the calculations, α was varied by increasing b_A and decreasing b_B in Eq. (2.11) by the same factor. As expected, the performance of all processes improves with increasing α. Process 4 has the best performance for the whole range studied. This is a consequence of the fact that process
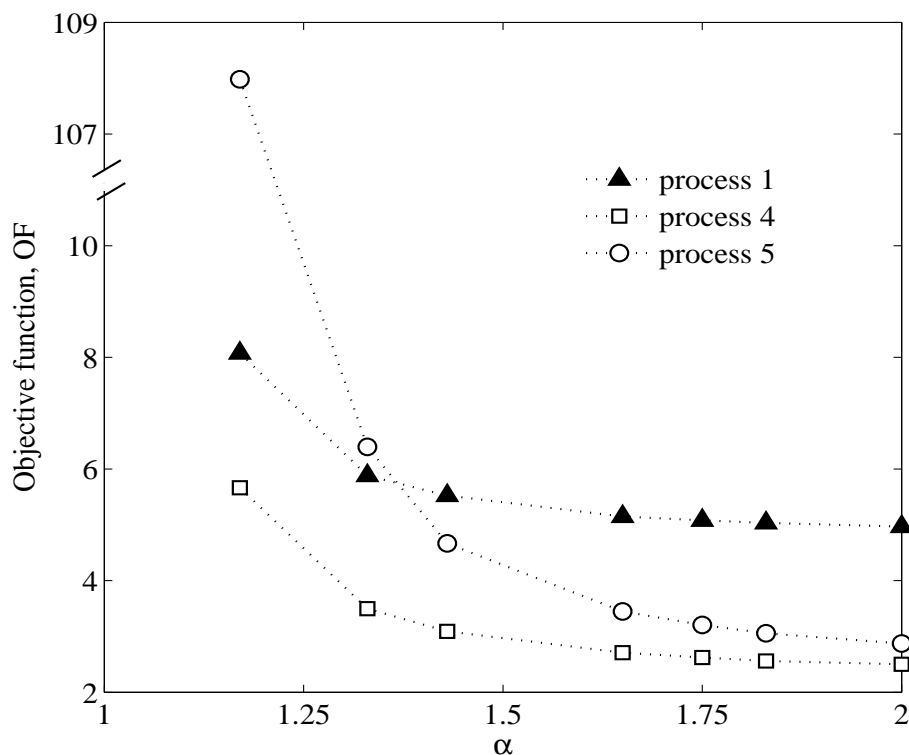
Figure 2.10. – Performance as a function of the separation factor α, Eq. (2.11) for Langmuir isotherms. The target product is the weaker adsorbed component B. $K_{eq} = 1.0$, $Pu_{min} = 90\%$. Lines are guide to the eye.

4 has four zones and, thus, the highest number of free variables. This superiority is more pronounced for easier separations (high α values). For $\alpha = 2.0$, the performance of process 4 is 200% of that of process 1. While for difficult separations, the conventional process 1 achieves an 'intermediate' value for the objective function, it is also outperformed by process 5 for easier separations. The latter achieves a similar performance as process 4 for sufficiently large values of α. This is a promising aspect, since the simple process 5 requires no additional external operations.

2.3.4.2. Reaction equilibrium

For racemization reactions $K_{eq} = 1$. However, the value of K_{eq} can be different for other isomerization reactions. Therefore, we will investigate the three processes 1, 4, 5 for different values of K_{eq}.

Figure 2.11 shows the results obtained for the objective function OF versus K_{eq}. Again, the weaker adsorbed component B was the target product, obtained at a purity of 90% (for the
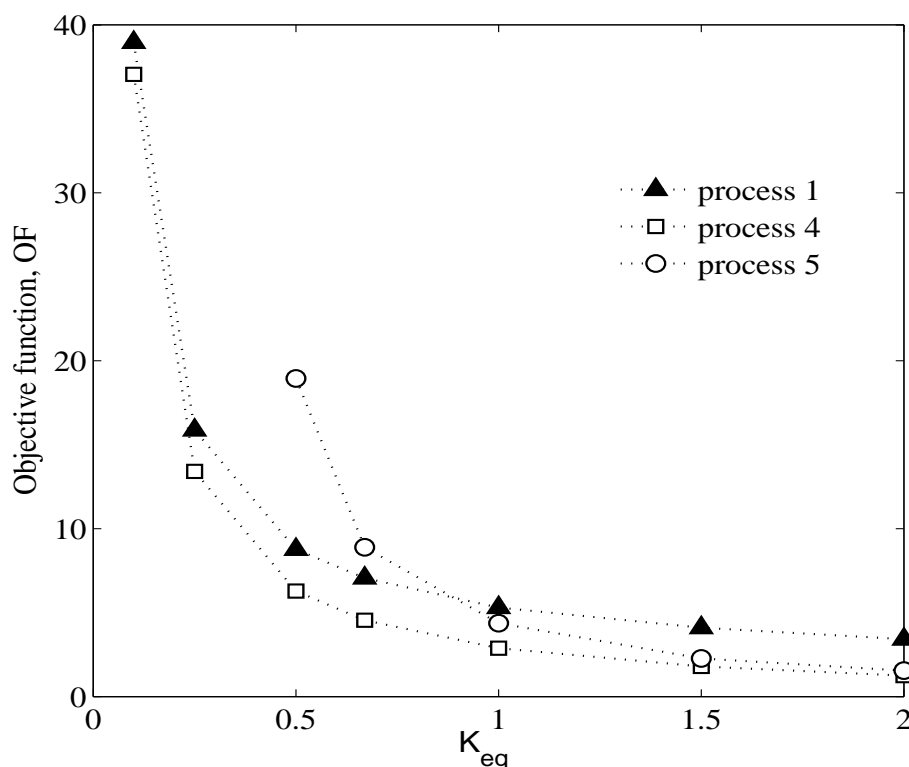
Figure 2.11. – Performance as a function of the reaction equilibrium constant K_{eq}, Eq. (2.2) (bi-Langmuir isotherms). The target product is the weaker adsorbed component B. $Pu_{min} = 90\%$. Lines are guide to the eye.

applied bi-Langmuir isotherms and other parameters, see Table 2.1). Here, the composition of the feed stock is assumed to be in chemical equilibrium, defined in each specific case by the value of the equilibrium constant assumed.

Similar trends are observed in comparison to the influence of α (see Fig. 2.10). Again, process 4 is the best performing setup. For low values of K_{eq}, which correspond to an unfavorable reaction equilibrium (see Eq. (2.2)), the performance of process 1 is lower than that for process 4. The objective function for process 5 improves significantly for favorable reaction equilibria and achieves a similar performance as process 4 for sufficiently large values of K_{eq}.

2.4. Conclusion

In this chapter, a systematic and fundamental theoretical study was performed with respect to the possibility of devising integrated reactive separations that combine continuous chro-

matography and isomerization reactions. A particularly important field of application for such processes is the production of single enantiomers.

Different process schemes were derived from the general options existing for process integration. The performance of the processes was compared using model-based optimization. A new process concept was suggested which utilizes an internal spatial distribution of the functionalities. It was assumed that a different Damköhler value can be adjusted for each specific zone of the TMB. In this case, the optimization results indicated that the reaction is optimally placed within the regeneration zone opposite to the product stream. Additional calculations allowing for a finer distribution of the reaction within the unit showed no significant effect on performance. Such a process could outperform conventional reactor-separator-recycle systems. It was found that the observed benefits were mainly originated from the easier regeneration of the corresponding zones of the chromatographic process. This effect, denoted as reaction-assisted regeneration, was analyzed on the basis of equilibrium theory. In this context, some of the limitations of existing process concepts could be explained.

Furthermore, the performance of the different schemes was evaluated in view of selected relevant aspects. It was found that the concept of internally distributing the functionalities could be an attractive option, in particular under favorable conditions with respect to reaction equilibrium and/or separation difficulty. In such cases, the performance of a simple 3-zone setup without any external unit operations is superior to that of more complex conventional process structures.

The next chapter will be devoted to the application of the results to practically feasible processes based on simulated moving bed systems.

CHAPTER *3*

Synthesis of Integrated SMB Processes

In the previous chapter it was shown that the integration of a racemization reaction into a continuous chromatographic unit can improve the production of single enantiomers. In a first step, the analysis in chapter 2 was based on a simplified process model assuming a true moving bed. In view of a practical implementation, the analysis is extended in this chapter to more realistic simulated moving bed processes. Here, the three different possible degrees of process integration are analyzed: flow-sheet, partial and total integration. The study is based on simultaneous optimization of the process structure and the operating conditions. The investigations indicate that a closed-loop 3-zone SMB with internal integration of the reaction is an interesting alternative. This idea combines good performance with relatively low complexity. The new process is investigated in detail to determine its capabilities and define its field of application.

> ❧ · ❧

3.1. Investigated processes

As in chapter 2, three different degrees of integration are considered: flow-sheet, partial and complete integration. A large number of structural possibilities arises from these combinations.

Five promising representatives of these concepts for obtaining the less retained enantiomer B are shown in Fig. 3.1. Process 1 is used as the reference case. It is a classical reactor-separator-recycle system (flow-sheet integration). Here, the SMB unit performs the separation of A and B. The undesired component A is recovered and reconverted into racemic mixture in an external reactor. An intermediate removal of solvent (SR) is included to counter-balance the typical dilution caused by the SMB system. Studies on process 1 have been reported for example in [8, 9] for enzymatically catalyzed isomerization reactions.
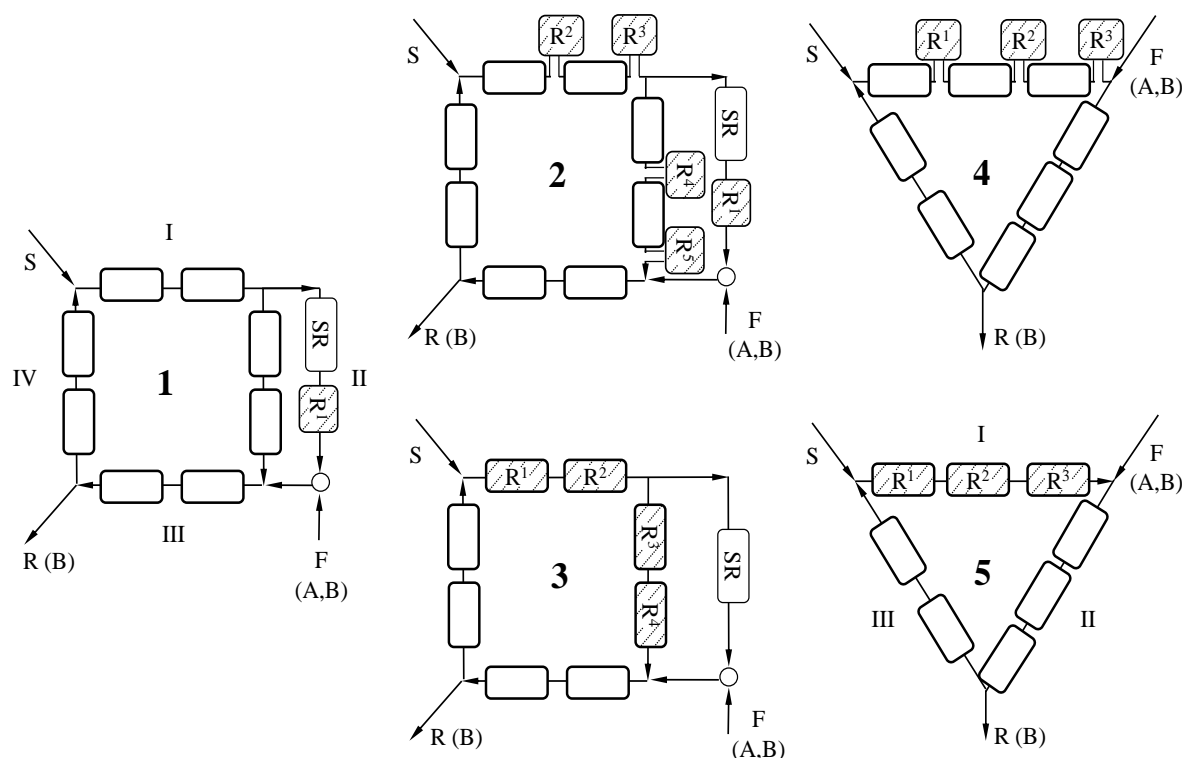

Figure 3.1. – Process schemes for producing the less retained enantiomer B by integrating SMB chromatography and isomerization reactions. 1 – conventional flowsheet-integrated SMB process (reactor-separator-recycle; fixed structure) with a solvent removal device (SR). Schemes 2 to 5 represent superstructures subject to optimization where R^1 to R^5 are used as decision variables determining if these positions should hold reaction: 2 – semi-integrated 4-zone SMB with side reactors. 3 – fully integrated 4-zone SMB. 4 – semi-integrated 3-zone SMB with side reactors (Hashimoto concept). 5 – fully integrated 3-zone SMB.

Scheme 2 in Fig. 3.1 is a superstructure containing attractive partially integrated candidates. Process 2 contains a 4-zone SMB with a solvent removal (SR) in the recycle stream. Further, the structure contains five degrees of freedom: a reactor in the recycle (R^1) and four reactors

more (R^2 to R^5) distributed along the zones I and II. Note that these five degrees of freedom generate 2^5 possible structural subsets.

In the previous chapter, the optimal location of the reaction was discussed. This can vary depending on the chemical system and the product purity requirement. However, in all cases studied, the reaction was placed optimally left of the feed point. Thus, only the five positions where the reactors can optimally be placed are considered here. This allows to reduce considerably the number of possible subsets. A similar partially integrated configuration was investigated in [15, 17] as a fixed structure for producing the more retained component. In that work, the suggested process contains only three reactors (equivalent to R^1, R^4 and R^5 positions). However, no evidence was given supporting that this corresponds to the optimal process scheme.
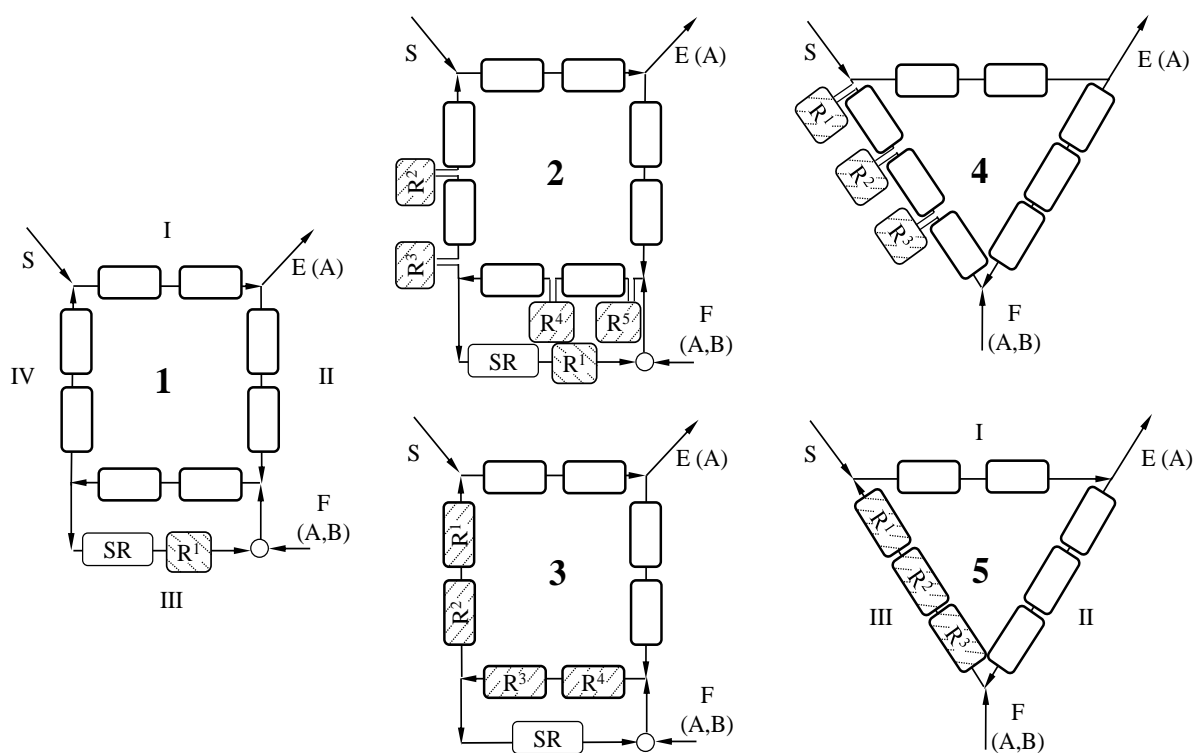

Figure 3.2. – Process schemes for producing the more retaining enantiomer A by integrating SMB chromatography and isomerization reactions. 1 – conventional flowsheet-integrated SMB process (reactor-separator-recycle; fixed structure). Schemes 2 to 5 represent superstructures subject to optimization where R^1 to R^5 are used as decision variables determining if these positions should hold reaction: 2 – semi-integrated 4-zone SMB with side reactors. 3 – fully integrated 4-zone SMB. 4 – semi-integrated 3-zone SMB with side reactors (Hashimoto concept). 5 – fully integrated 3-zone SMB.

Analogously, scheme 3 is a completely integrated device where the reaction takes place within the SMB unit. The structure contains four degrees of freedom (R^1 to R^4) corresponding to the four columns of the SMB where the reaction could take place. This generates 2^4 different structural subsets to be considered.

Further, schemes 4 and 5 represent the same concepts like processes 2 and 3 but containing a 3-zone SMB unit. These configurations benefit from a more simple setup avoiding recycle streams and solvent removal devices. Previous studies in process 4 concluded that its performance decreases rapidly for high purity demands [16, 52]. In those cases, process 5 appears as an attractive alternative to the use of side reactors as discussed in the previous chapter. Both structures contain three degrees of freedom considering a total of eight subsets in each case.

Analogous schemes are depicted in Fig. 3.2 for producing the more retained component A.

The defined sets of superstructures subsume in total 130 possible process setups. A fair comparison among all different structural possibilities requires simultaneous optimization of process structure and operating conditions. These cases fall into the category of Mixed Integer Non Linear Programming (MINLP), consisting of continuous and integer variables. Here, an optimization approach is applied consisting of dynamic process models combined with cyclic steady state detection and an external evolutionary algorithm.

3.2. Mathematical Model and Optimization

The MINLP optimization approach used in this study requires a flexible and numerically efficient mathematical model. As in chapter 2 an equilibrium stage model is used to describe the behavior of the chromatographic columns. The mass balances for the two components in the fluid and solid phases within each stage read as

$$\frac{\mathrm{d}c_i^{k,n}}{\mathrm{d}t} + F\frac{\mathrm{d}q_i^{k,n}}{\mathrm{d}t} = \frac{Q^z}{V\epsilon}\left(c_i^{k-1,n} - c_i^{k,n}\right) + R^j\,\nu_i\,r^{k,n} \tag{3.1}$$

where the indices $i = A, B$ denote the component, $k = 1 \ldots N_s$ the stage, $n = 1 \ldots N_c$ the column and $z = I \ldots N_z$ the corresponding zone of the SMB unit. c_i and q_i are the liquid and solid phase concentrations, V is the volume of a stage, ϵ the porosity and $F = (1 - \epsilon)/\epsilon$ is the phase ratio. Q is the volumetric flow rate of the fluid phase. The axial dispersion is adjusted by the number of stages, N_s [37].

The last term in Eq. (3.1) describes the chemical reaction. r is the reaction rate and ν_i is the stoichiometric coefficient. The decision variable $R^j \in \{0, 1\}$ describes whether chemical reaction is allowed in a chromatographic column at the position $j = 1 \ldots N_r$. N_r is the number of columns where the reaction can take place, depending on each particular

superstructure (see Figs. 3.1 and 3.2). A reversible racemization reaction $A \leftrightarrow B$ is assumed taking place exclusively in the fluid phase. Thus, the reaction equilibrium constant is given by Eq. (2.2). According to Eq. (2.2), the rate expression for an isomerization reaction taking place in the liquid phase is given by

$$r^{k,n} = k \left(c_A^{k,n} - \frac{c_B^{k,n}}{K_{eq}} \right) \tag{3.2}$$

The relation between the solid and the liquid phase concentrations in Eq. (3.1) is given by the adsorption equilibrium. We apply bi-Langmuir adsorption isotherms Eq. (2.9), which is frequently used for enantiomers.

The following mass balances define the connections among the columns in the 4-zone SMB units

$$
\begin{aligned}
\text{if } n = 8 \quad &: \quad Q^{IV} c_i^{N_s,n} + Q^S c_i^S = Q^I c_i^{0,1} \\
\text{if } n = 4 \quad &: \quad Q^{II} c_i^{N_s,n} + Q^{Rec} c_i^{Rec} + Q^F c_i^F = Q^{III} c_i^{0,n+1} \\
\forall n \neq \{4,8\} \quad &: \quad c_i^{N_s,n} = c_i^{0,n+1}
\end{aligned}
\tag{3.3}
$$

where the postitions 8 and 4 correspond to the columns previous to the desorbent and the feed points, respectively. $c_i^{0,n}$ is the concentration entering column n and Rec is the recycle stream present in all 4-zone systems (see Fig. 3.1 and Fig. 3.2).

For the case of the 3-zone systems, similar balances hold for the raffinate setups (see Fig. 3.1)

$$
\begin{aligned}
\text{if } n = 8 \quad &: \quad Q^{III} c_i^{N_s,n} + Q^S c_i^S = Q^I c_i^{0,1} \\
\text{if } n = 3 \quad &: \quad Q^{I} c_i^{N_s,n} + Q^F c_i^F = Q^{II} c_i^{0,n+1} \\
\forall n \neq \{3,8\} \quad &: \quad c_i^{N_s,n} = c_i^{0,n+1}
\end{aligned}
\tag{3.4}
$$

and for the extract schemes (see Fig. 3.2)

$$
\begin{aligned}
\text{if } n = 8 \quad &: \quad Q^{III} c_i^{N_s,n} + Q^S c_i^S = Q^I c_i^{0,1} \\
\text{if } n = 5 \quad &: \quad Q^{II} c_i^{N_s,n} + Q^F c_i^F = Q^{III} c_i^{0,n+1} \\
\forall n \neq \{5,8\} \quad &: \quad c_i^{N_s,n} = c_i^{0,n+1}
\end{aligned}
\tag{3.5}
$$

The continuous design variables to be optimized are the dimensionless zone flow rate ratios m^z for each zone z are defined as

$$m^z = \frac{Q^z t^* - \epsilon V_c}{(1 - \epsilon) V_c} \tag{3.6}$$

where V_c is the volume of a chromatographic column. t^* is the switching time of the SMB system.

The external devices connected to the SMB units shown in Figs. 3.1 and 3.2 were modeled as follows. The side reactors are described as continuously stirred tank reactors (CSTRs)

$$\frac{\mathrm{d}c_i^{0,n+1}}{\mathrm{d}t} = \frac{Q^z}{V_r\epsilon}\left(c_i^{N_s,n} - c_i^{o,n+1}\right) + R^j\,\nu_i\,r^j \tag{3.7}$$

where V_r is the volume of the side reactor.

The devices for solvent removal (SR) were assumed to instantaneously adjust the mixture concentrations such that the higher concentrated component has the same concentration as in the feed.

The specific solvent consumption was applied as the objective function in the optimizations to evaluate the different process schemes (see Eq. (2.13)).

The optimization problem can be summarized as

$$\begin{aligned}
&OF(m^z, R^j) \longrightarrow min \\
&s.t. \\
&Pu^{out} = \frac{c_i^{out}}{c_A^{out} + c_B^{out}} \geq Pu_{min}
\end{aligned} \tag{3.8}$$

where Pu^{out} denotes the product purity and Pu_{min} is the purity demand. Note that no additional constraint for the conversion is required because the processes in Fig. 3.1 and Fig. 3.2 have only a single outlet. For such processes, purity and conversion are related by simple global mass balance Eq. (4.6).

As in the previous chapter, the dynamic simulation of the SMB systems was done with DIVA [51, 58]. A Petri net routine was used to implement the periodic switching of the columns in opposite direction to the liquid flow. The routine defined the switching conditions as well as the related transitions.

The dynamic simulation reaches a cyclic steady state (CSS) after a certain number of cycles. This number varies strongly depending on the external devices and the operating parameters. Therefore, a stopping criterion based on a Poincaré map [54] was used to identify the CSS in each dynamic simulation. This routine identifies the values of the concentration of both components in each stage as a solution trajectory. These trajectories describe orbits for periodic systems which can intersect a hyperplane, the Poincaré map, once per cycle. The routine compares the values of the solution trajectories when they intersect the hyperplane from cycle to cycle. In the CSS, the trajectories intersect in a single point on the Poincaré map. The stopping criterion used here considers that the system has reached a CSS when the difference in the trajectories between two cycles is smaller than a tolerance.

Further, an evolutionary algorithm [83] is applied to optimize the CSS of the different superstructures. It applies an iterative mutation-selection principle which is based on the theory of evolutionary strategy (ES) of Rechenberg, Schwefel, Beyer et. al. [5, 11, 71].

At the start of the procedure only one individual is available, corresponding to the initial values. After mutation, taking into account the set bounds for the parameters to be optimized, a new individual is produced. The two mutants are recombined producing a set number of candidates, denoted frequently as children. The best two individual of the group of children are recombined and mutated again to produce a second generation. Recombination and mutation are performed using typical algorithms of ES, which include random value concerning techniques, based on routines in the NAG libraries of Fortran.

The described sequence is conducted in a loop until a fixed number of generations is reached. The number of generations should be high enough to ensure that the optimal solution is found. However, a high number of generations in combination with large numbers of model equations can be computationally expensive. Thus, a compromise in the number of generations needs to be met for each specific case based on previous experiences.

3.3. Results

The properties of an optimal process depend strongly on the specific requirements on the separation or production task. Besides fulfilling fundamental constraints on, for example, purity requirements, obvious objectives are high performance and low process complexity.

In the following section MINLP optimization is applied to find the optimal sub-processes of the superstructures depicted in Fig. 3.1 and Fig. 3.2 for different purity requirements. The identified process alternatives are compared with respect to their performance. They are critically analyzed accounting for their practical feasibility and complexity. To alleviate the analysis, in this first step reaction equilibrium corresponding to an infinitely fast reaction and negligible volume of the external devices is assumed. Afterwards, the effect of finite volumes of the external devices is investigated in section 3.3.2. Finally, the role of finite reaction kinetics is addressed for the most promising process candidate in section 3.3.3.

3.3.1. Process Synthesis and Optimization

For this chapter, the adsorption isotherm parameters of the chlorthalidone enantiomers are used as reported in [46]. The feed is considered to be racemic. Table 3.1 summarizes the parameter values and conditions used. Note that in the calculations a switching time of $t^* = 1$ min has been applied (cf. Table 3.1). In a real process, this arbitrary choice would be replaced, for example, by specifying an internal flow rate according to a pressure drop constraint. It is emphasized that t^* has no effect on the value of the objective function as long as the reaction

rate is infinite, since it is cancelled out when substituting the m-values into Eq. (3.8). An effect is observed only for systems with finite reaction kinetics as studied in section 3.3.3. In these cases the objective function is also rendered independent of t^* by using in the model a ratio of kinetic constants rather than individual rate constants.

Table 3.1. – System parameters and constant operating conditions. Properties of the model system CTD as taken from [46].

Parameter	Symbol		Values	
bi-Langmuir adsorption isotherms,	$q_{S,1}$	[g/l]	94.175	
Eq. (2.9)	$q_{S,2}$	[g/l]	0.244	
	$b_{i,1}$	[l/g]	0.207	0.141
	$b_{i,2}$	[l/g]	6.395	3.192
System parameters	L_c	[dm]	2.000	
	d_c	[dm]	0.040	
	ϵ	[−]	0.796	
Operating conditions	c_i^F	[g/l]	0.200	
	t^*	[min]	1.000	

The performance of the processes is evaluated in terms of their specific solvent consumption. The optimization problem minimizes this objective function under certain purity requirements (see Eq. (3.8)). The optimization variables are the m-values and the structural parameters R^j.

3.3.1.1. Moderate Purity Requirements

The production of pure enantiomers is generally carried out through successive separation stages. Often, chromatographic separation is followed by crystallization steps which increase the product quality. Moderate purity requirements for the SMB can result advantageous due to the existing interplay between productivity and purity. These relaxed purity demands may lead to an increase of the overall performance of the combined process [44]. Therefore, like in the previous chapter, also processes with moderate product purities are considered.

Table 3.2 contains the optimization results of the superstructures shown in Fig. 3.1 for the raffinate setups. The purity requirements correspond to moderate demands (90 and 95%). Low efficiency columns ($N_s = 25$) are used in this case for the SMB units.
The fixed structure 1 obtains an acceptable performance for both purity requirements. The performance of the conventional reactor-separator-recycle process 1 is used as a reference for the comparison with other optimized processes. Process 2 using side reactors clearly outperforms scheme 1. The optimal structure contains in this case five active side reactors (R^1 to R^5). The fully integrated scheme 3 using chromatographic reactors outperforms 1

Table 3.2. – Optimization results for the schemes depicted in Fig. 3.1 for the raffinate setup. Like in the previous chapter, the total number of stages was considered to be equal to 200 (25 stages per column).

Process	OF	Pu^R	m^I	m^{II}	m^{III}	m^{IV}	R^1	R^2	R^3	R^4	R^5
1	5.284	90.00	19.727	8.234	18.936	14.160	-	-	-	-	-
	6.026	95.00	19.941	10.731	18.404	13.196	-	-	-	-	-
2	3.607	90.00	17.838	8.632	19.031	13.479	1	1	1	1	1
	4.183	95.00	17.810	8.538	18.419	13.323	1	1	1	1	1
3	3.444	90.02	17.674	10.887	19.263	13.194	1	1	1	1	-
	3.941	95.00	17.633	9.401	18.226	13.432	1	1	1	0	-
4	3.465	90.00	16.569	19.062	13.461	-	1	1	1	-	-
	5.258	95.00	17.171	19.263	12.992	-	1	1	1	-	-
5	3.108	90.00	16.210	18.731	13.389	-	1	1	1	-	-
	4.115	95.00	16.731	19.033	13.131	-	1	1	1	-	-

and 2 for both purity requirements. In this case, the optimal structure changes from four ($Pu^R = 90\%$) to three ($Pu^R = 95\%$) reactive columns. This can be explained due to the trade-off between separation and reaction functionalities. This interaction makes preferable to reduce the reaction volume in favor of the separation for high purity requirements. The 3-zone system 4 using side reactors outperforms the classical approach 1, but cannot reach the performance of 2 and 3. Structure 5 obtains the best performance out of all options for $Pu^R = 90\%$ and the second best for $Pu^R = 95\%$. This is an encouraging finding since the structure corresponds to a rather simple 3-zone SMB system and supports the observations made in the previous chapter.

A closer look to the m-values in Table 3.2 allows us to identify the source of the difference on performance for the optimized processes. As already reported in chapter 2, the simultaneous reaction and separation can strongly benefit the regeneration of SMB units. Integrated systems require lower m^I values to regenerate zone I when the reaction is placed within this zone [64]. This decreases the solvent consumption and thus improves the overall performance.

Table 3.3 summarizes the optimization results for the setups as shown in Fig. 3.2. Similar trends can be observed compared to the schemes in Fig. 3.1. However, here both partial and complete integrated processes show greater benefits on performance compared to the classical

Table 3.3. – Optimization results for the schemes depicted in Fig. 3.2 for the extract setup. Like in the previous chapter, the total number of stages was considered to be equal to 200 (25 stages per column).

Process	OF	Pu^E	m^I	m^{II}	m^{III}	m^{IV}	R^1	R^2	R^3	R^4	R^5
1	4.982	90.00	17.939	12.301	19.684	12.940	-	-	-	-	-
	6.490	95.00	19.300	13.851	18.860	13.582	-	-	-	-	-
2	4.133	90.00	20.386	12.440	21.448	15.405	1	1	1	1	1
	4.949	95.00	20.033	12.987	20.209	14.863	1	1	1	1	1
3	3.955	90.00	20.435	12.445	21.070	15.682	1	1	1	1	-
	4.146	95.02	19.803	12.959	21.034	15.197	0	1	1	0	-
4	3.588	90.00	19.837	12.364	15.625	-	-	1	1	1	-	-
	4.838	95.00	21.020	12.749	15.663	-	-	1	1	1	-	-
5	3.577	90.00	19.898	12.457	15.709	-	-	1	1	1	-	-
	4.543	95.00	20.700	12.859	15.733	-	-	1	1	1	-	-

approach 1. Process 1 obtains the worst values out of all options. The best performance is obtained for process 5 followed by option 4 at $Pu^E = 90\%$. The 3-zone systems work considerably better for the production of the more retained component at reduced purity demands. Indeed, most of the studies related to process 4 focused specifically on the production of the most retained component [15, 28, 38]. At slightly higher purity demands $Pu^E = 95\%$ the totally integrated superstructure 3 obtains the best result. The optimal configuration constrains the reaction to the second and third columns within the SMB unit.

The better performance of the integrated schemes respect to process 1 is based on the effect of reaction-assisted regeneration. In these cases, the effect takes place in the last zone of the SMB in structures 2 to 5. There, we obtain higher optimal m-values when the reaction occurs (see Table 3.3). This high m-values permit a greater recycle of the solvent, reducing its consumption.

Summarizing, integrated processes offer an attractive alternative to the conventional reactor-separator-recycle 1 for reduced purity demands as already explained in chapter 2. Further, completely integrated schemes (3 and 5) outperformed the analogous partially integrated (2 and 4). The 3-zone fully integrated process 5 appears as a particularly attractive option, since it combines good performance with a simple setup.
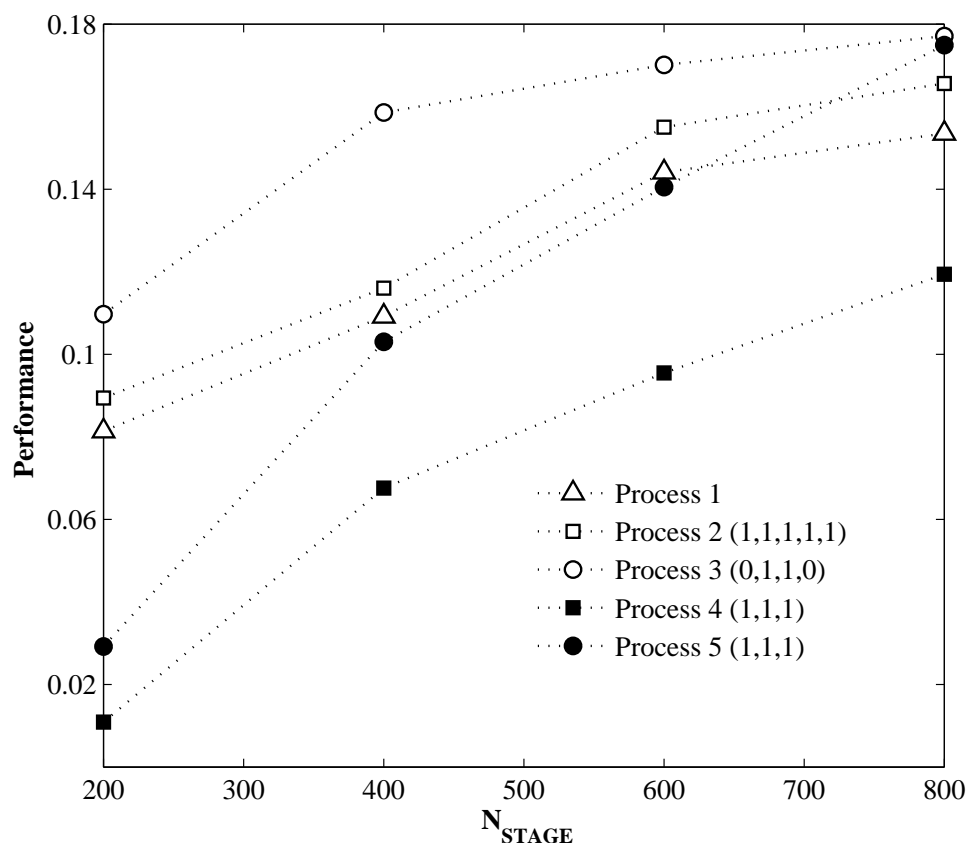
Figure 3.3. – Performance of the process schemes depicted in Fig. 3.1 for the raffinate setup vs. the total number of theoretical plates (NTP) of the SMB unit. For the superstructures 2 – 5 the optimal configuration (showed in brackets) was found to be independent of the NTP in the range studied.

3.3.1.2. High Purity Requirements

In this section, the production under high purity requirements is discussed. The purity requirement is set equal to $Pu^{out} = 99.9\%$, typical for pharmaceuticals products. Enantiomers are typically considered difficult separations. Therefore, more efficient columns are needed to perform this task.

The influence of the number of stages on the performance of the different systems defined as the reciprocal of the objective function in Eq. (2.13) is shown in Fig. 3.3. In all cases performance increases with increasing number of stages. This increase is more pronounced for the 3-zone schemes 4 and 5 in Fig. 3.3, since 3-zone schemes have only a single zone responsible for the separation. Hence, when comparing 4- with 3-zone schemes it is essential to use a sufficiently high number of theoretical stages. In the present case a total number of 800 stages was chosen corresponding to 100 stages per column.

Table 3.4. – Optimization results for the schemes depicted in Fig. 3.1 for the raffinate setup for $Pu^R = 99.9\%$ (100 stages per column)

Process	OF	Pu^R	m^I	m^{II}	m^{III}	m^{IV}	R^1	R^2	R^3	R^4	R^5
1	6.515	99.92	21.185	9.848	18.723	13.339	-	-	-	-	-
2	6.040	99.90	20.650	9.322	18.756	13.334	1	1	1	1	1
3	5.645	99.92	20.582	7.528	18.683	13.295	0	1	1	0	-
4	8.378	99.90	18.279	19.676	13.604	-	1	1	1	-	-
5	5.717	99.90	17.503	19.371	13.208	-	1	1	1	-	-

Detailed results for the production of pure B are reported in Table 3.4. The totally integrated process 3 obtains the best performance out of all the considered options. The optimal structure corresponds to the use of two reactive columns in the second and third positions. Between the 3-zone systems, large differences on the performance exist comparing the partially and the completely integrated superstructures. Both schemes require a lower m^I value than the purely separative SMB. However, the effect of the reaction-assisted regeneration in 5 is clearer, increasing its overall performance. This trend confirms the previous observations reported in chapter 2.

Analogously, Table 3.5 contains the optimization results obtained for the production of pure

Table 3.5. – Optimization results for the schemes depicted in Fig. 3.2 for the extract setup for $Pu^E = 99.9\%$ (100 stages per column)

Process	OF	Pu^E	m^I	m^{II}	m^{III}	m^{IV}	R^1	R^2	R^3	R^4	R^5
1	7.894	99.90	22.001	13.346	19.944	13.344	-	-	-	-	-
2	6.637	99.90	20.828	13.537	20.928	14.645	1	1	1	1	1
3	4.898	99.90	20.886	13.547	25.106	15.674	1	1	0	0	-
4	6.259	99.90	21.046	13.881	15.928	-	1	1	0	-	-
5	5.196	99.92	21.225	13.386	15.920	-	1	1	0	-	-

A. Here, similar trends are observed for the performance compared to the case with moderate purity demands (see Table 3.3). Process 1 is outperformed by all superstructures. The best performance corresponds to the completely integrated superstructure 3, followed by process 5, the 3-zone integrated SMB.
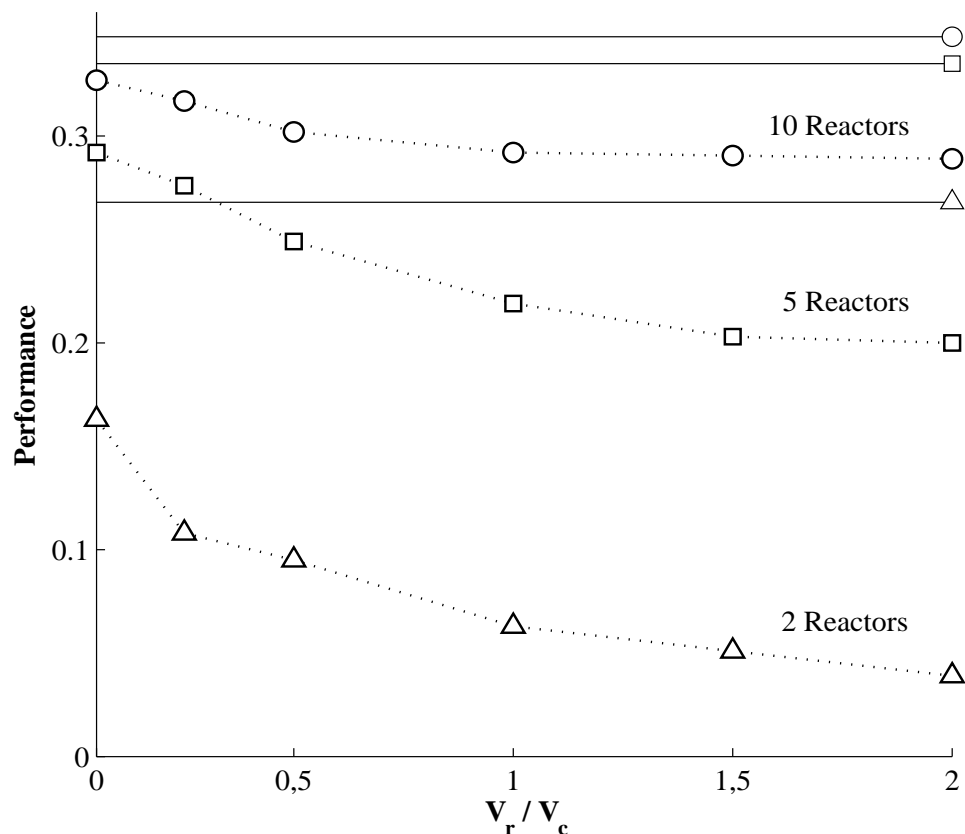

Figure 3.4. – Performance of process 4 (depicted in Fig. 3.1) under moderate purity requirements (90%) vs. the ratio between reactor and column volume ($\frac{V_r}{V_c}$). Low efficiency columns ($N_s = 25$). Structures with 2 ($\triangle$), 5 ($\square$) and 10 ($\circ$) side reactors in zone *I*. Lines serve for comparison to the performance of process 5 (also for 2, 5 and 10 reactive columns in zone *I*).

Summarizing, the integrated processes investigated in this section represent interesting alternatives to the conventional reactor-separator-recycle 1 for both cases, moderate and high purity demands. For the idealized scenario described here, assuming reaction equilibrium and negligible volume of side reactors, the results confirm the trends observed in the previous section based on TMB models.

The completely integrated schemes 3 and 5 outperform the analogous partially inte-

grated systems 2 and 4. The superiority of the completely integrated schemes is independent of the chosen product and particularly important for high purity requirements. This is due to the more pronounced effect of the reaction-assisted regeneration. Further, the fully integrated 3-zone process 5 appears as a particularly attractive option combining good performance and rather simple process setup.
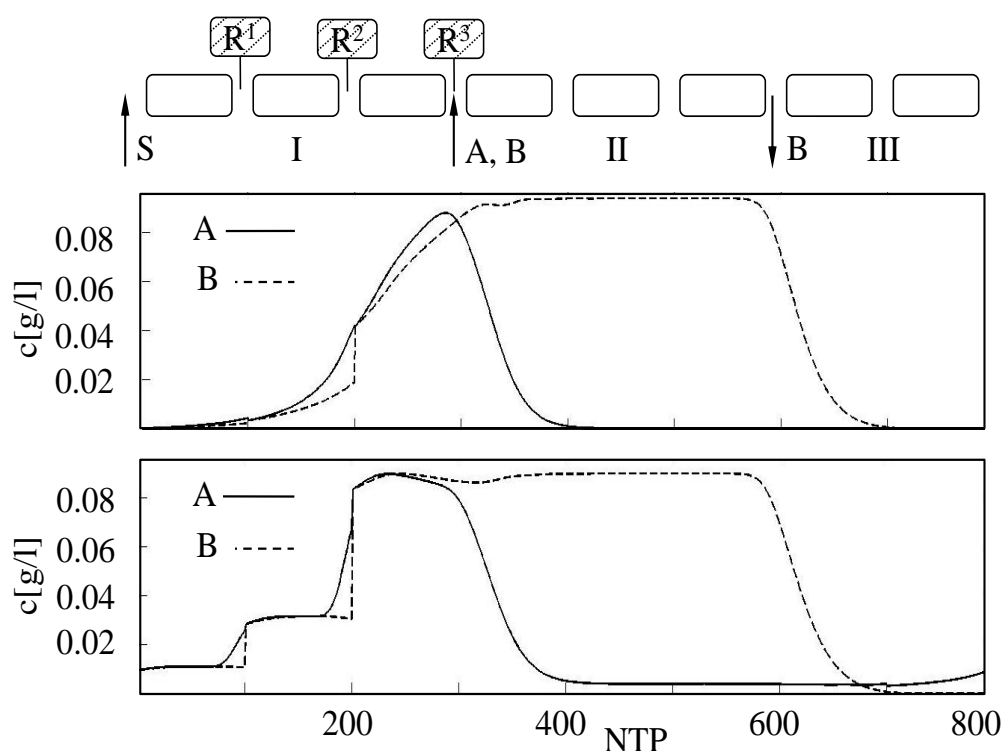
3.3.2. Side Reactors vs. Chromatographic Reactors

Figure 3.5. – Internal profiles for the raffinate setup of process 4 at the beginning of a switching interval. m-values corresponding to the optimal operating conditions given in Table 3.4 for process 4. Top – side reactors with negligible reactor volume; bottom – side reactors with a volume twice the empty volume of a chromatographic column.

The studies in the previous section have clearly shown that process integration is beneficial for the production of pure enantiomers. The 3-zone concepts seem the most promising. In a first step, focus was on a rather limited number of reactors with instantaneous reaction and negligible volume. The observed trends were along the results obtained in the previous chapter for TMB systems. However, these conditions do not fully reflect practical conditions. In particular there exists an interplay of the column switching in SMB processes with the

number and the size of the reactors, which could not be discussed in the previous section based on TMB models.

To further discriminate between partially and fully integrated 3-zone processes the influence of finite reactor volume and maximum number of reactors will be further elucidated in this section for the interesting case that the weaker adsorbing component is the desired product (i.e., raffinate setups).
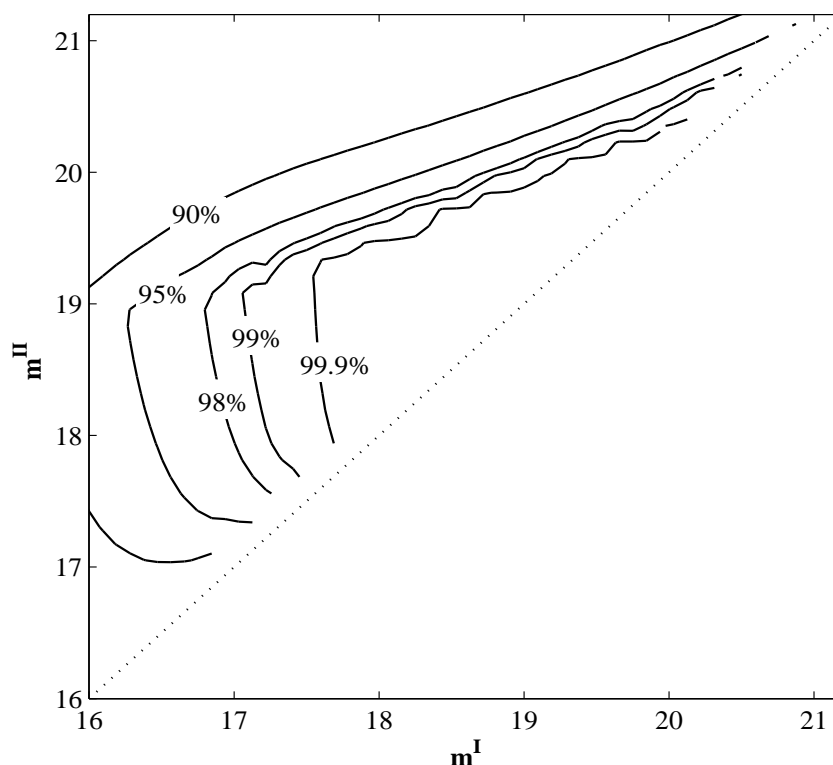

Figure 3.6. – Simulation results for process 5 at different product purities (90, 95, 98, 99 and 99.9%). The surfaces are depicted on the m^I-m^{II} plane for the raffinate setups in Fig. 3.1.

The results for process 4 are summarized in Fig. 3.4 as a function of the number and the volume of the side reactors. In the calculations, the number of columns and side reactors in the reactive zone was increased accordingly, while the non reactive zones remained unchanged. The results of a corresponding process 5, i.e. having the same number of columns in the reactive zone, are also included to establish a fair comparison.

In all cases the performance of the corresponding fully integrated process is better than for the partially integrated process. Comparing the idealized case of zero reactor volume, one observes that an efficient partially integrated scheme will require a relatively large number of side reactors. The gap between both processes is getting smaller with an increasing number of

reactors. Schemes 4 and 5 are equivalent only for an infinite number of side reactors. This is consistent with the earlier observations in chapter 2.

Further, the effect of reactor volume is also illustrated in Fig. 3.4. This was done by keeping the column volume constant, according to Table 3.1, and increasing only the reactor volume. It is observed that this volume plays a significant role for the performance. The differences on the performance of both processes increase for large reactors, independently of the number of side reactors.

This can be explained with the additional holdup of side reactors in SMB systems. In order to illustrate this effect, Fig. 3.5 shows the internal concentration profiles for process 4 in two different scenarios: with three side reactors with zero volume (top), in comparison to those obtained with side reactors with a two-fold column volume (bottom). In both cases the same m-values were applied (cf. Table 3.4). While the setup with ideal reactors (top) achieves the desired purity of 99.9%, the setup with finite reactor volume (bottom) reaches only 95.7%. The extra holdup of the large reactors provokes an accumulation of the undesired compound within zone I. Some of this component travels with the solid phase, contaminating the product stream. In order to achive a purity of 99.9%, the processs in the bottom would
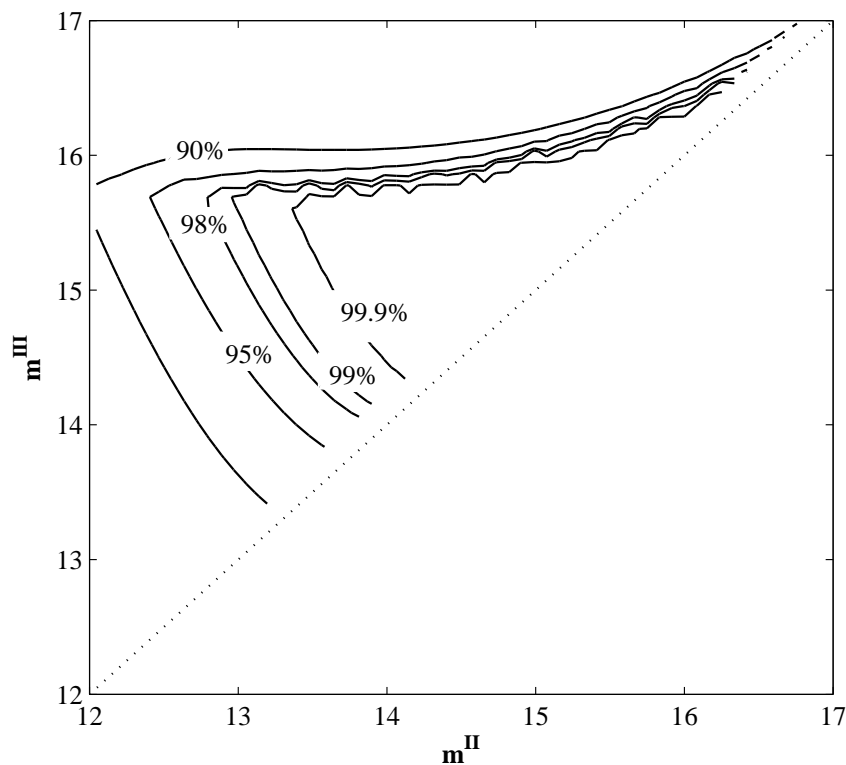

Figure 3.7. – Simulation results for process 5 at different product purities (90, 95, 98, 99 and 99.9%). The surfaces are depicted on the m^{II}-m^{III} plane for the extract configurations in Fig. 3.2.

require a higher m^I-value to regenerate zone I, decreasing the overall process performance.

Therefore, under realistic conditions where side reactors have a finite volume, partially integrated systems cannot reach the performance of fully integrated processes. This is a dynamic effect that cannot be observed based on TMB models.

Finally, it should be noted, that despite their lower performance, a main advantage of the side reactor concepts is increased flexibility. Therefore they are certainly a good alternative for cases where reaction and separation can not occur under similar operating conditions. This is often the case for enzymatic [38] or electrochemical [62] reactions.

3.3.3. The Integrated 3-zone SMB Reactor

In summary, process 5 (see Fig. 3.1) appears an interesting alternative to more conventional process alternatives. It combines good performance and relatively simple setup. This process
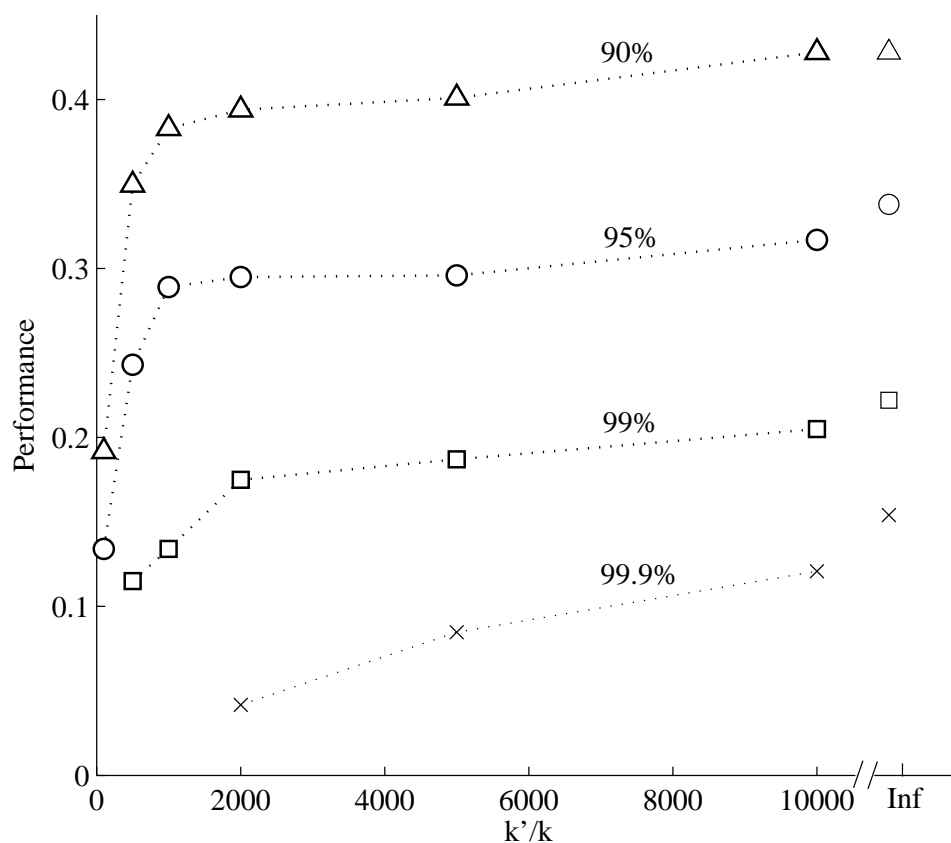

Figure 3.8. – Performance of process 5 (depicted in Fig. 3.1) with respect to the reaction gradient implemented ($\frac{k'}{k}$) for different purity requirements: 90%($\triangle$), 95%($\bigcirc$), 99%($\square$) and 99.9%($\times$). Lines are guide to eye.

consists of only three zones, and contains no external devices or recycle streams. No solvent removal is required. For these reasons, this new process concept deserves a more detailed analysis.
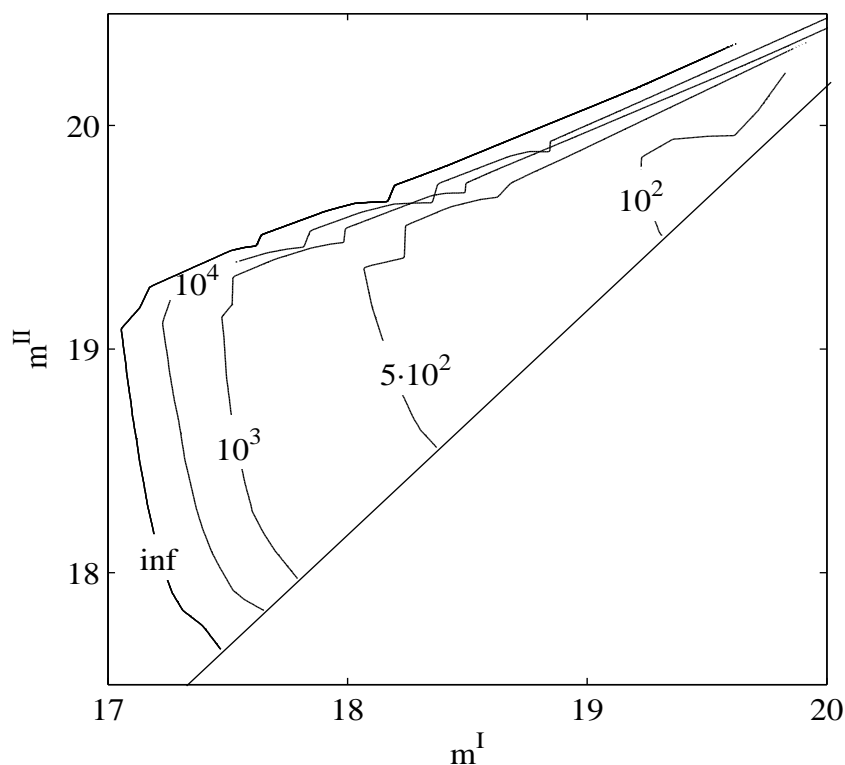

Figure 3.9. – Simulation results for process 5 under different reaction gradients ($\frac{k'}{k}$= 10^2, $5 \cdot 10^2$, 10^3, 10^4 and ∞) for $Pu_{min} = 99\%$. The surfaces are depicted on the m^I-m^{II} plane for the raffinate setups in Fig. 3.1.

For conventional 4-zone SMB systems triangle theory is used as a powerful design tool [61, 86]. Based on this theory, a region of complete separation can be plotted on the m^{II}–m^{III} plane. Usually, complete regeneration is assumed in zones I and IV. Analogously, the complete separation region can be shown for the 3-zone SMB reactor. In Figs. 3.6 and 3.7, the regions are plotted for different purity demands for the production of B and A, respectively (schemes 5 in Fig. 3.1 and Fig. 3.2). Complete regeneration is assumed to take place in zone III for the production of B. Similarly, complete regeneration is forced in zone I for the production of A. A large region of complete separation is obtained in both cases. These results further support the possibility to produce pure enantiomer with 100% yield and conversion.

In view of a practical realization, the spatial functionality distribution in this process deserves some remarks. Due to the periodic column switching, the desired internal distribution of the reaction can hardly be achieved by incorporating reactive columns into an SMB
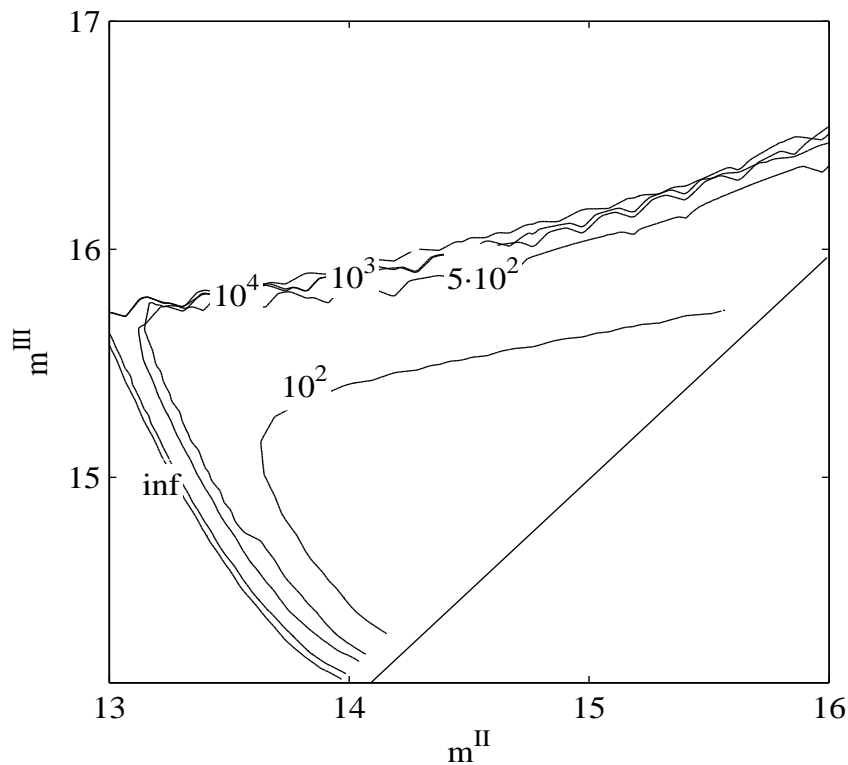
Figure 3.10. – Simulation results for process 5 under different reaction gradients ($\frac{k'}{k}= 10^2, 5 \cdot 10^2, 10^3, 10^4$ and ∞) for $Pu_{min} = 99\%$. The surfaces are depicted on the m^{II}-m^{III} plane for the extract configurations in Fig. 3.2.

process. Column switching in the SMB process requires on or off switching of the chemical reaction in the columns which enter or leave the reactive zone to exploit the full potential of this integrated process.

A useful alternative here is to introduce gradients of operating conditions, which is a well known approach in non reactive SMB processes. The most promising ideas in this context appear to be:

- The manipulation of adsorption behavior by gradients of solvent strength, salts, pH, etc. (see [2, 3, 42]) or temperature (see [76, 77]).
- The use of gradients of a homogeneous catalyst, for example of the pH value (see [33]). Note that racemization can be triggered for many enantiomers by changing the pH value.
- The use of gradients of inhibitors that suppress the reaction in some part of the unit, e.g. by reversibly adsorbing to an active center.
- Combinations of the above.

This list reveals that in general both functionalities (reaction and adsorption) could be spatially distributed. Up to now an ideal on and off switching of the chemical reaction in the columns of the fully integrated process was assumed. Triggering the reaction kinetics by the use of gradients introduces a limited change in the kinetic rate constants of the racemization reaction between different zones. The ratio of the kinetic constants in different zones (k'/k) will determine the efficiency of the system.

This more realistic scenario to investigate the capabilities of process 5 is addressed here. In Fig. 3.8 the performance of process 5 in Fig. 3.1 is plotted vs. the ratio of the kinetic constants for different purity requirements. For all cases studied, a critical value for the kinetic constant ratio exists. Below this critical number, the performance decreases rapidly. However, the critical ratio varies depending on the product purity required. Production of pure enantiomers demands an efficient tuning of the reaction kinetics. Nevertheless, with relatively low ratios of the kinetic constants, reasonable performance can be achieved under moderate purity requirements.

A more detailed example of this trend is shown in Figs. 3.9 and 3.10. There, the separation regions are plotted for $Pu^{out} = 99.0\%$ as a function of the ratio of the kinetic constants for raffinate and extract setups. In both cases, the areas decrease for lower kinetic ratios. However, the influence is greater for the production of the less retained component B. As observed in Fig. 3.8, for high purity requirements the performance can be strongly compromised by inefficient tuning of the reaction kinetics.

3.4. Conclusions

Towards practical implementation, an optimization study of processes combining continuous chromatography and racemization reactions was done in this chapter using a more detailed SMB model. The numerous process alternatives were represented by formulation of corresponding superstructures. Subsequently these superstructures were optimized using mixed integer optimization to identify the optimal process setup and operating conditions.

Trends observed in the previous chapter using a simplified TMB model were confirmed. They indicated that an integrated 3-zone SMB process is an interesting alternative to conventional reactor-separator-recycle schemes and the well known Hashimoto process using side reactors. The 3-zone integrated system combines good performance and a rather simple process structure.

Additionally, several effects coming into picture when looking at the transient SMB systems were investigated. The main finding was that an increasing volume of the side reactors for the Hashimoto setups causes decreasing performance. This detrimental effect cannot be fully compensated by increasing the number of side reactors. It is caused by the

extra holdup of the reactor volume. Such dynamic effect cannot be observed in studies based on TMB models.

Further, the effect of the reaction kinetics on the performance of the fully integrated 3-zone SMB was investigated. A sufficiently high ratio of the reaction rate constants between the different zones of the SMB unit was identified as an important design criterion for this concept.

CHAPTER *4*

Experimental Validation of a new Integrated SMB Process

In the previous chapter, several new integrated process concepts were investigated combining racemization reaction and continuous chromatography. Theoretically, these processes can produce single enantiomers with yield and conversion of 100%. In particular, a new integrated 3-zone simulated moving bed (SMB) concept with internal racemization reaction was suggested for the production of single enantiomers from racemic mixtures. Here, the concept is experimentally validated for the separation of a model system compound. The results demonstrate that the new concept is capable of producing a single enantiomer with purity, yield and conversion of 100%.

ഔ · ക

4.1. Introduction

After evaluating theoretically a high number of process alternatives in the previous chapter, the integrated closed-loop 3-zone SMB concept, shown in Fig. 3.1 (5) and Fig. 3.2 (5), was identified as an interesting process candidate. This scheme combines good performance with a relatively simple setup. It contains no external solvent removal devices or recycle streams. The racemization reaction is optimally performed within the regeneration zone. Figure 4.1 shows schematically the 3-zone process for the production of the more (A) and less adsorbed
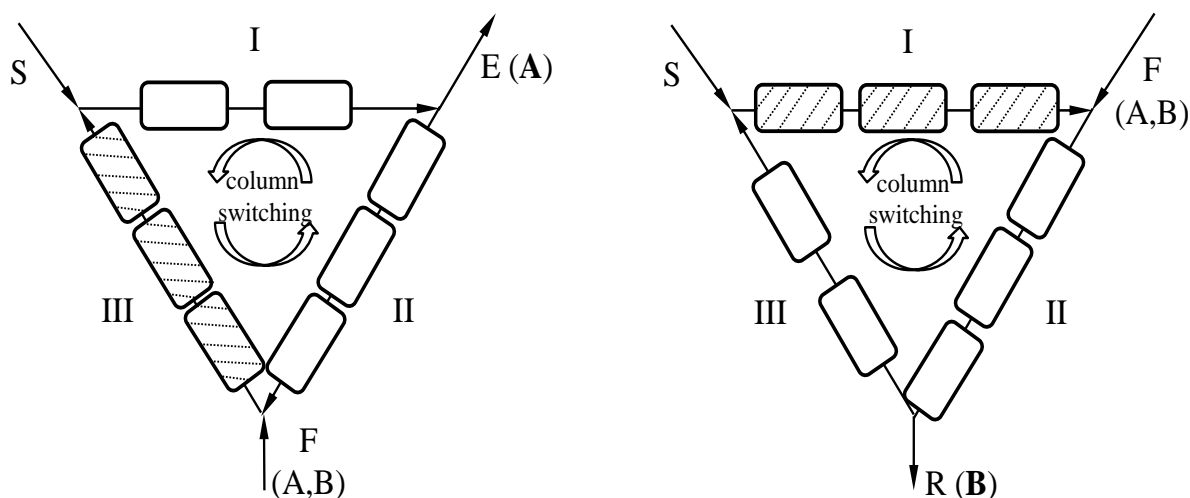
component (B), respectively.

Figure 4.1. – Integrated 3-zone SMB processes combining chromatographic sep-
aration and racemization reaction, as reported in [65]. Hatched
columns denote chromatographic columns in which the racemiza-
tion reaction is triggered. Left – setup for the production of the
strongly retained component A (extract setup). Reaction takes
place within zone III; right – setup for the production of the
weakly retained component B (raffinate setup). Reaction takes
place within zone I. F – feed, S – solvent, E – extract, R – raf-
finate.

In order to fully exploit the potential of the scheme the racemization reaction needs to be
performed only in a single specific zone of the SMB. This corresponds to zone III for the
production of the stronger retained component A, and zone I for the production of the weakly
adsorbing enantiomer B (see Fig. 4.1). In practice, the reaction could be controlled and placed
specifically in the desired zones by using gradients. As discussed in the previous chapter,
temperature, pH, modifiers or additives can trigger strongly the reaction kinetics depending
on the specific chemical system under consideration.

In this chapter, this process concept is validated experimentally for the raffinate setup
(see Fig. 4.1, right). It should be noticed that this is a particularly interesting case. In the
previous chapter, the production of the weak adsorbing B using a raffinate setup appeared
to be the most challenging scenario for the conventional Hashimoto process. Note that the
focus of the experimental investigations concerning the Hashimoto concept has been mainly
on the production of the more retained component [16, 38, 52]. Hashimoto processes or
similar concepts have never been applied to interconvert an isomeric mixture into the weaker

adsorbing component only. As demonstrated in the previous chapter, this would in principle be possible, but requires a large number of columns and reactors.

Here, for the experimental validation the enantiomers of chlorthalidone (CTD) will serve as experimental model system. In this particular example, an internal gradient of the pH value is used to control the reaction. Therefore at first, the effect of the pH on the racemization kinetics and on the adsorption behavior is investigated. The obtained parameters are applied in a detailed mathematical process model used for designing the process. A semi-preparative SMB unit is used under pH-gradient operation to produce the less retained enantiomer in validation experiments.

4.2. Theory

A conventional equilibrium stage model is applied to simulate the integrated SMB process. Analogous to Eq. (3.1), the mass balances for the two components in the fluid and solid phases within each stage read as

$$\frac{\mathrm{d}c_i^{k,n}}{\mathrm{d}t} + F\frac{\mathrm{d}q_i^{k,n}}{\mathrm{d}t} = \frac{Q^z}{V\epsilon}\left(c_i^{k-1,n} - c_i^{k,n}\right) + \nu_i\, r^{k,n} \tag{4.1}$$

The chemical reaction is taking place in the liquid phase. For the reaction rate in Eq. (4.1) now holds:

$$r^{k,n} = k(pH)\left[c_A^{k,\,n} - c_B^{k,\,n}\right] \tag{4.2}$$

with $k(pH)$ the rate constant of the reaction as a function of pH.

The adsorption behavior of CTD can be described as before with a bi-Langmuir adsorption isotherm model

$$q_i = \frac{q_{s,1}(pH)\,b_1 c_i}{1 + b_1(c_A + c_B)} + \frac{q_{s,i,2}\,b_{i,2}c_i}{1 + b_{A,2}c_A + b_{B,2}c_B}\ ,\quad i = (A,\, B) \tag{4.3}$$

According to the Pasteur principle, Eq. (4.3) describes competitive adsorption of the two solutes $(A,\, B)$ on two different types of adsorption sites of the solid: type 1 (achiral) and type 2 (chiral); $q_{s,1}$ and $q_{s,i,2}$ are the saturation capacities for the corresponding sites, respectively. Note that here the saturation capacities of the chiral adsorption sites 2 are no longer considered to be equal for both enantiomers.

Here, the integrated SMB unit is operated using pH gradients. For the model system CTD it was found useful to describe the dependency of the adsorption behavior on the pH value in the term $q_{s,1}(pH)$. This corresponds to cases where the capacity of the achiral sites depends most strongly on the pH [27].
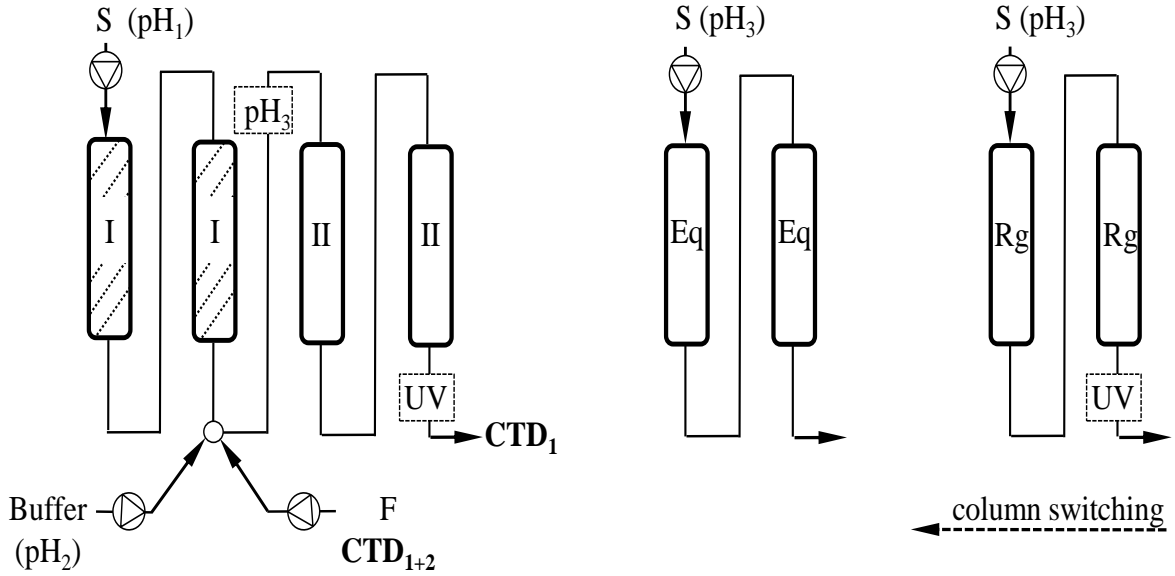
Figure 4.2. – Open-loop experimental setup of the 2-zone integrated SMB for producing the less retained enantiomer CTD_1. Zone I, at pH_1 performs simultaneous reaction and separation benefiting from the effect of reaction-assisted regeneration [64]. Zone II, is responsible for the chiral separation at pH_3. Additional zones are implemented to equilibrate (Eq) and regenerate (Rg) the columns before re-entering zone II.

The SMB configuration used for the validation experiments is a four column 2-zone open-loop system for the production of the weakly retained enantiomer (see Fig. 4.2). Zone I performs the solid phase regeneration and the racemization reaction, while zone II is responsible for the separation. The regeneration of the liquid phase is carried out in two external zones as shown in Fig. 4.2. In contrast to a 3-zone system with closed loop, in this setup the third zone and the recycle stream are omitted for the sake of simplicity. Furthermore, analyzing the effluents of the external zones allows to identify possible issues such as incomplete regeneration or side product formation.

For this system, the corresponding boundary conditions are:

$$
\begin{array}{llll}
\text{if n} = 1 & : & Q^S c_i^S = Q^I c_i^{0,1} \\
\text{if n} = 3 & : & Q^I c_i^{N_s,n-1} + Q^F c_i^F = Q^{II} c_i^{0,n} & \quad (4.4) \\
\text{if n} = 2,4 & : & c_i^{N_s,n-1} = c_i^{0,n}
\end{array}
$$

where $c_i^{0,n}$ corresponds to the concentration of component i entering column n.

The dimensionless zone flow rate ratios m^z are used as design variables for each zone

z of the SMB as shown in Eq. (3.6).

The performance parameters product purity Pu^R, conversion X and recovery yield Y are defined as follows:

$$Pu^R = \frac{c_B^R}{c_A^R + c_B^R} \cdot 100 \,, \tag{4.5}$$

$$X_A = \frac{c_A^F Q^F - c_A^R Q^R}{c_A^F Q^F} \cdot 100 \,, \tag{4.6}$$

$$Y = \frac{(c_B^F + c_A^F) Q^F}{(c_B^R + c_A^R) Q^R} \cdot 100 \,. \tag{4.7}$$

As explained in section 3.2, the dynamic simulations of the batch and SMB systems were performed using the simulation enviroment DIVA [51, 58]. The periodic switching of the columns was implemented with a Petri net routine. A Poincaré map [54] based stopping criterion was used to identify the CSS in each dynamic simulation.

4.3. Experimental

4.3.1. Chemicals

The enantiomers of chlorthalidone (CTD), (*RS*)-2-chloro-5-(1-hydroxy-3-oxo-2,3-dihydro-1*H*-isoindol-1-yl)benzene-1-sulfonamide, were used as model system for the experimental validation of the integrated SMB process. They were purchased from Sigma-Aldrich (Steinheim, Germany) and from Molekula (Gillingham, Dorset, UK).

Two buffer systems were used for the different ranges of the pH value applied: Bis-Tris propane (BTP) (Sigma-Aldrich, Munich, Germany) and Triethylammonium acetate (TEAA), 1 mol/L (Merck, Darmstadt, Germany).

Further, acetic acid (AA), 100%, triethylamine (TEA), and HCl, 32%(v/v) (all from Merck, Germany) were required to prepare solutions at different pH values. Methanol (MeOH) at gradient grade LiChrosolv® Reag. Ph Eur (Merck, Darmstadt, Germany) was used as a non-retained tracer compound. All aqueous solutions were prepared with ultrapure water prepared in-house using a Millipore Milli-Q® gradient system (Molsheim, France).

4.3.2. Sample analysis by HPLC

The analysis of samples was carried out by HPLC using a Ultimate 3000 series chromatograph from Dionex (Idstein, Germany) controlled by the software Chromeleon. UV detection was set to 260 nm. A 200 x 4 mm Nucelodex-β-OH (Macherey-Nagel, Düren, Germany) column with an average particle size of 5 μm was used for the analysis, which was performed at 10°C, a flow

rate of 0.75 mL/min and an injection volume of 100 μL using TEAA at pH 5.0. MeOH/TEAA (aq.) (40/60 v/v) was used as solvent.

4.3.3. Racemization kinetics

To determine the racemization kinetic constant k as a function of the pH (cf. Eq. (4.2)), samples of pure CTD enantiomer were required. For this purpose, a chromatographic column Nucelodex-β-OH, with 10 mm diameter and 125 mm length, was connected to the HPLC. Relatively large injections (2000μL) of racemic CTD 0.4 g/L were injected and the fractions of highly purified S-enantiomeric form of CTD ($Pu > 98\%$) were recovered.

The previously obtained S-enantiomer solutions were diluted in two different buffer systems (50mM) to cover the whole pH-range of interest. TEAA was used for solutions at pH = 3.00, 4.05, 5.00, and 5.80, while BTP was used for mixtures at pH = 5.30, 5.95, 6.90, 8.10, and 9.00. Afterwards, these solutions were prepared to racemize at ambient temperature.

The experiments were performed in batch mode, using vials of approximately 15 mL volume. Samples were taken at different times and immediately frozen and stored at -18°C. Each sample was analyzed later by HPLC to determine the extent of the racemization reaction. The time during which the samples were handled in liquid form was minimized in order to minimize possible errors due to spontaneous racemization. This attempt was successful, as indicated by negligible deviations between the purities of the fractionated original solutions and the samples taken at the beginning of the racemization experiments.

4.3.4. Adsorption behavior

Semi-preparative columns (16 x 65 mm) were used for the isotherm parameter determination as well as for the SMB experiments. The columns provided from Macherey-Nagel are packed with the same chiral stationary phase as the analytical column (same batch).

Classical methods to determine isotherm parameters experimentally are not suitable under reactive conditions. Therefore, an inverse method ('peak fitting') was applied accounting also for the injection profile [24].

Column porosity was determined by a 20 μL injection of MeOH as a non-retained tracer compound. The flow rate was 2 mL/min. The column void volume was determined equal to 8.9 mL and the porosity $\epsilon = 0.681$. The number of theoretical stages N_s in Eq. (4.1) was determined at a flow rate of 6 mL/min. From 20 μL injections of racemic CTD with a concentration of 0.05 g/L (rac.) an average value of $N_s = 750$ was obtained calculating the first and the second moments of the peaks. No significant influence of pH on N_s was observed.

For the isotherm determination MeOH/BTP (aq.) 50 mmol/L (40/60 v/v) was used as

solvent. 2000 μL samples of racemic CTD in the aqueous BTP solution were injected at five different pH values (5.3, 6.0, 7.0, 8.0 and 9.0) adjusted using HCl. The flow rate was adjusted to 6 mL/min and the temperature was set to 25°C. The concentration of racemic CTD was equal to 0.5 g/L corresponding to the maximum solubility in the used mobile phase composition.

4.3.5. SMB experiments

For the experimental validation of the new concept, the setup in Fig. 4.2 was equipped with eight columns. The SMB unit used is a CSEP® C916 64 port SMB unit (Knauer, Berlin, Germany). This valve is designed for up to 16 column slots. Thus, the number of columns needs to be a divisor of 16 to perform symmetric switching conditions. It should be noted that, in principle, only three columns would be sufficient for the implementation of this process: one for the separation, one for the reaction and one for the equilibration/regeneration.

Five HPLC pumps (Knauer, Berlin) equipped with two 10 mL and three 50 mL pump heads, were used. Further, two UV detectors, model K-2600 (Knauer) were used at 1 Hz and 260 nm. The data from the UV detectors were monitored using the software EuroChrom2000 (Knauer). An Amersham Biosciences (now GE Healthcare, Freiburg, Germany) UPC-900 pH detector was used for inline pH measurement.

The experiments were carried out at ambient temperature (25°C). The product samples collected were cooled down rapidly by collecting them in an ice bath to stop racemization and analyzed inmediately by HPLC.

Table 4.1. – System parameters of the reactive 2-zone SMB process.

L	d_c	ϵ	c^F	t^*	T
[mm]	[mm]	[-]	[g/L]	[min]	[°C]
65	16	0.681	0.5	7.0	25

4.4. Results and discussion

4.4.1. Model parameters

In this section, the racemization kinetics and the adsorption isotherms are investigated as functions of the pH value. Appropiate simple models are suggested to describe the corresponding parameter dependencies.

4.4.1.1. Racemization mechanism and kinetics

As it was shown in the previous chapter, insufficient tuning of the reaction kinetics would compromise the performance and even the feasibility of this process (see Fig. 3.9). Here, the reaction rate of the racemization of CTD enantiomers is influenced strongly by the temperature [46]. Thus, in principle, the integrated SMB process could be realized by temperature gradient since the kinetic constant changes by approximately a factor of 500 between $10°C$ and $60°C$. However, for CTD, pH gradients are more attractive since they can provide an even stronger modulation of the racemization rate constant.

In Fig. 4.3, based on [13, 53, 85], a reaction mechanism for the racemization of CTD is suggested in acidic ambience. There, a planar coordinated carbenium ion is generated after the protonation of the OH groups and the release of water. Afterwards, the OH groups in solution can attack the achiral intermediate from both sides equiprobably, due to the planar geometry. This chemical mechanism can also promote the formation of chiral methyl ether side products of CTD in the presence of MeOH (denoted as SP1 and SP2 in Fig. 4.3). Further, an achiral dehydration side product SP3 could also be formed. These side reactions can challenge the production of pure CTD enantiomers. This issue will be addressed later and several possible solutions will be discussed.

In Fig. 4.4, the reaction mechanism of the racemization of CTD enantiomers in basic ambience is suggested based on [13, 53]. Here, a ring opening through dissociation of the OH group's leads to an achiral intermediate. A double bound is established between the carbon atom, marking the former chiral center, and the oxygen, while the bound to the nitrogen is broken. This leads to the formation of an achiral benzophenone derivative as a planar intermediate stage. In presence of water, OH groups can be released and the bounds can now strike back forming CTD enantiomers equiprobably. A priori, no side product formation is expected via this chemical mechanism.

Note, that the mechanism via ring opening at high pH can be seen as energetically more favorable than the formation of a carbenium ion at low pH. This can translate into a faster racemization reaction in basic ambience than in acidic solutions.

Lamparter et al. [53] investigated the influence of pH on the racemization kinetics of CTD between pH= 2 and pH= 6. They observed a minimum of the kinetic constant at pH= 3. This is along the expectations based on the different racemization mechanisms discussed above.

Here, a larger range of the pH value, between pH= 3.0 and pH= 9.0 was investigated to analyze the full potential of a pH gradient. Several experiments were carried out at different pH values as explained in section 4.3. The concentration of the enantiomers in the solution was measured periodically to determine the extent of the racemization reaction. Figure 4.5 contains the data recovered in five experiments where only the pH value of the solution was
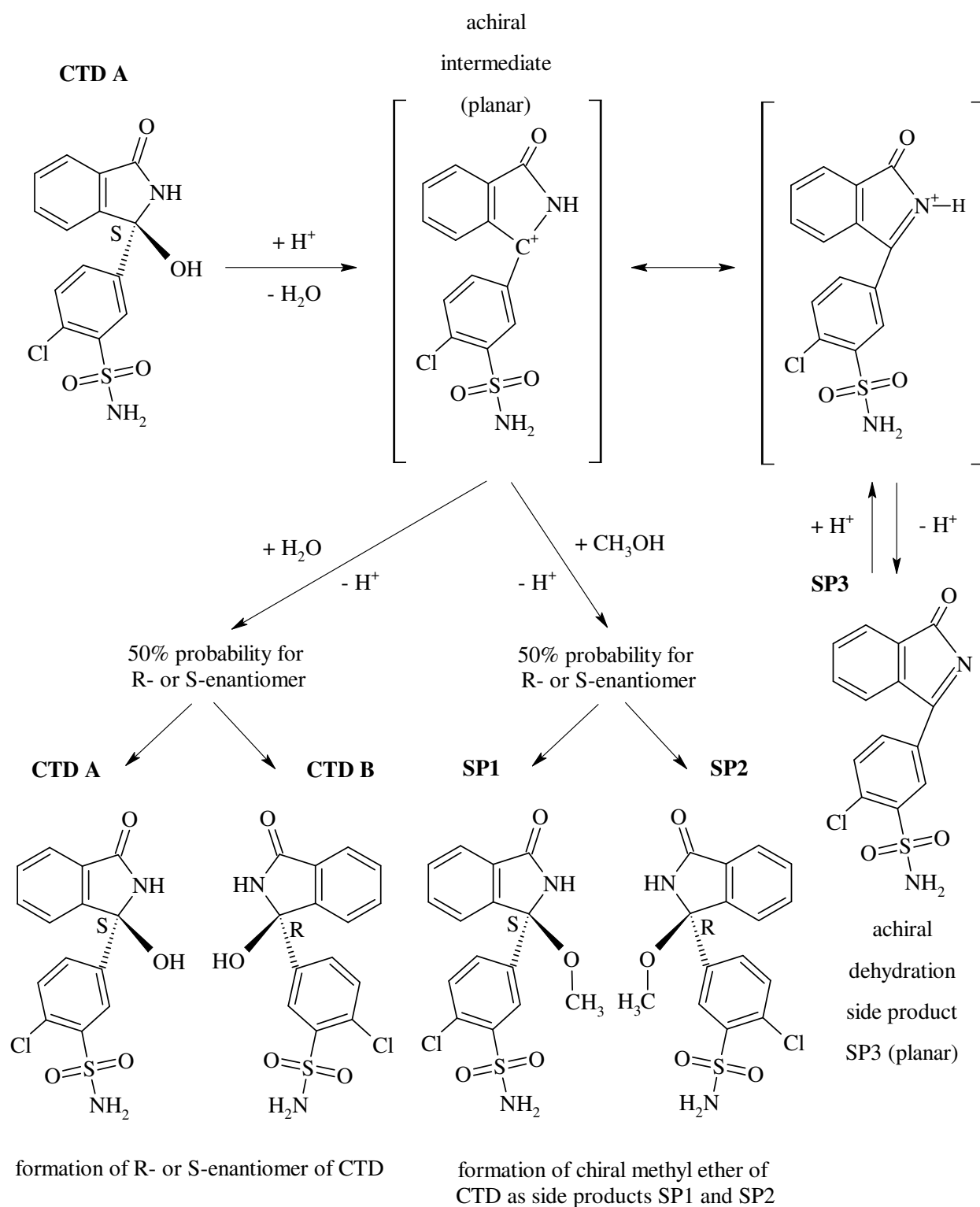
Figure 4.3. – Racemization mechanism of CTD in acidic ambience according to [13, 53, 85], shown for the S-enantiomer. Additionally the scheme illustrates the formation of the chiral methyl ether of CTD, side products SP1 and SP2, and the achiral side product SP3.
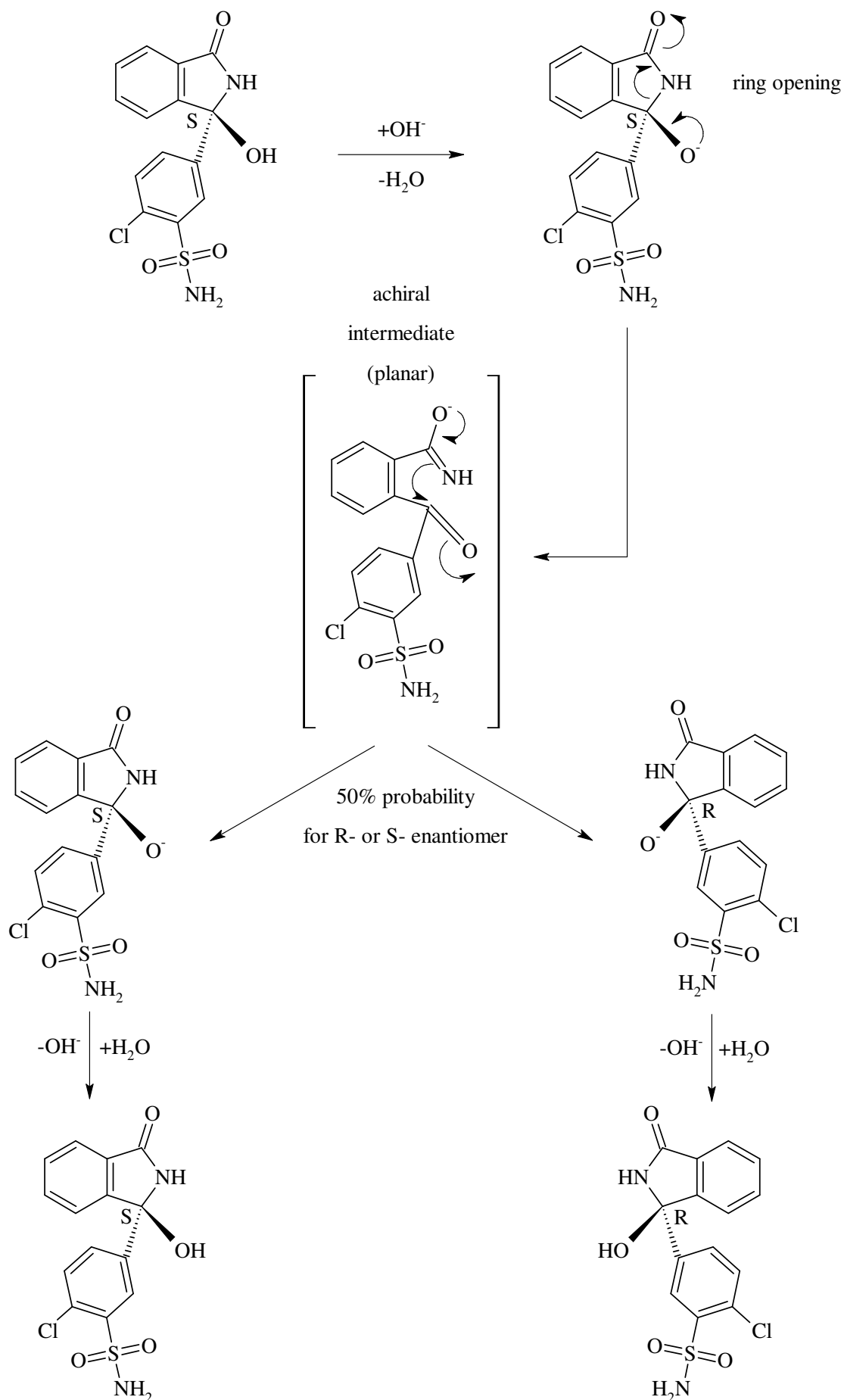
Figure 4.4. – Racemization mechanism of CTD in basic ambience according to
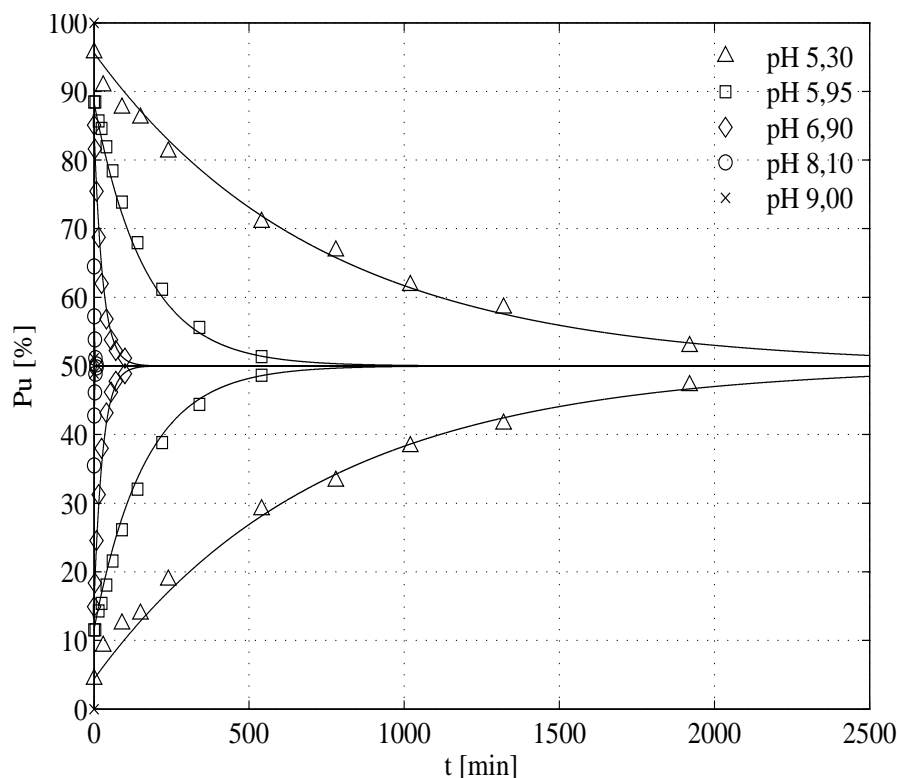[13, 53], shown for the S-enantiomer.

Figure 4.5. – Course of the concentration of both CTD enantiomers during the time of racemization at different pH values.

modified. Using this information, the values of the kinetic constant were obtained based on the material balance for the batch reactor

$$\frac{dc_{CTD_1}}{dt} = k(pH) \left[c_{CTD_1} - c_{CTD_2} \right] = 2k(pH)c_{CTD_1} - k(pH)c^{ini} \tag{4.8}$$

where the indices 1 and 2 mark the S- and the R-enantiomer of CTD, and c^{ini} is the initial concentration of racemic CTD in the mixture.

After integration and re-arrangement we obtain the linear relation

$$k(pH) = \frac{1}{2\,t} \, Ln \frac{c^{ini} - 2\,c_{CTD_1}^{ini}}{c^{ini} - 2\,c_{CTD_1}(t)} \tag{4.9}$$

Figure 4.6 shows the corresponding concentration profiles obtained by racemizing S-CTD solutions at five different pH values (5.30, 5.95, 6.90, 8.10, and 9.00) plotted according to the terms in Eq. (4.10). $k(pH)$ is obtained as the slope of the linear regression in the figure.

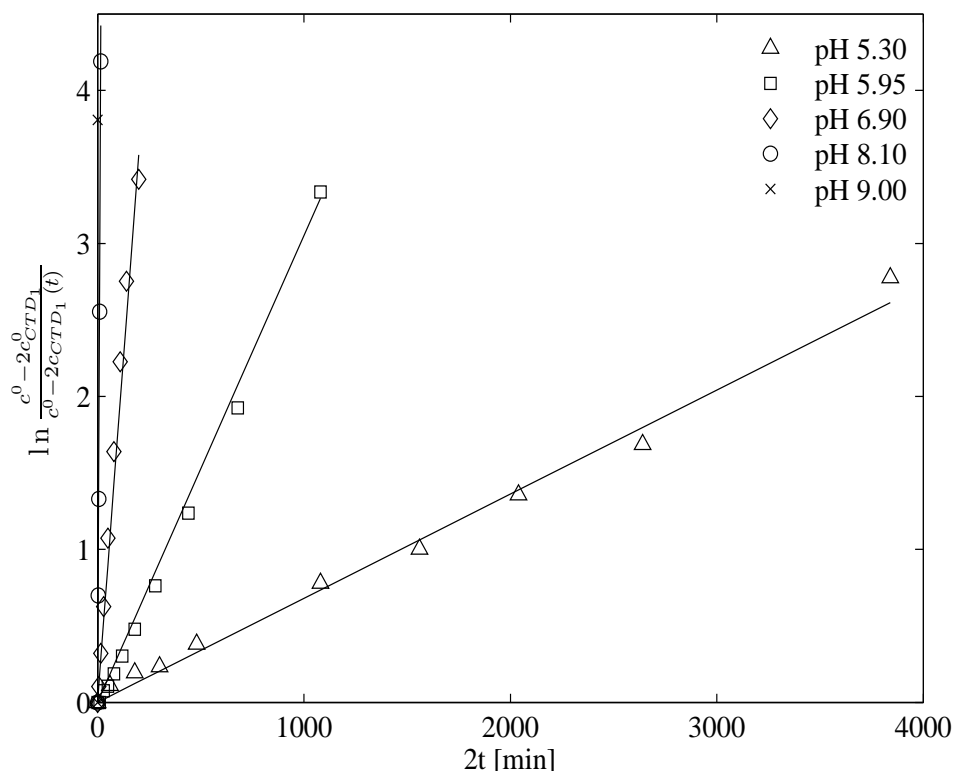Figure 4.7 contains all experimental results obtained for the kinetic constant k as a

Figure 4.6. – Experimental results for the racemization kinetics of CTD_1 at different pH values. Lines are the results according to Eq. (4.9) for the experimental data shown in Fig. 4.5.

function of the pH value for the two different buffer systems. In analogy to [53], the logarithm of k (which has units s^{-1}) is plotted in order to cope with the scale of the values. Also, the results at different temperatures as reported in [46] are plotted for comparison. The influence of the pH on the reaction kinetics is greater than that of the temperature. Changes in the kinetic constant of factor 5600 are possible in the pH range between 5.3 and 9.0. Therefore, a pH gradient between 5.3 and 9.0 can provide an 'on and off' switching behavior of the reaction within the SMB unit. For this range, only BTP as buffer compound is required.

An exponential function can be used to describe $k(pH)$ in Eq. (4.2) within this pH range:

$$k(pH) = k_0 \cdot e^{C_1 \cdot pH} \tag{4.10}$$

where $k_0 = 5.67 \cdot 10^{-11} s^{-1}$ and $C_1 = 2.28$. The coefficient of correlation was $R_c = 0.997$.

It should be emphasized that the strong influence of the pH on the racemization rate of CTD enantiomers is not an isolated scenario. More examples can be found where the pH influences significantly the kinetics of racemization [22], epimerization [55] or isomerization
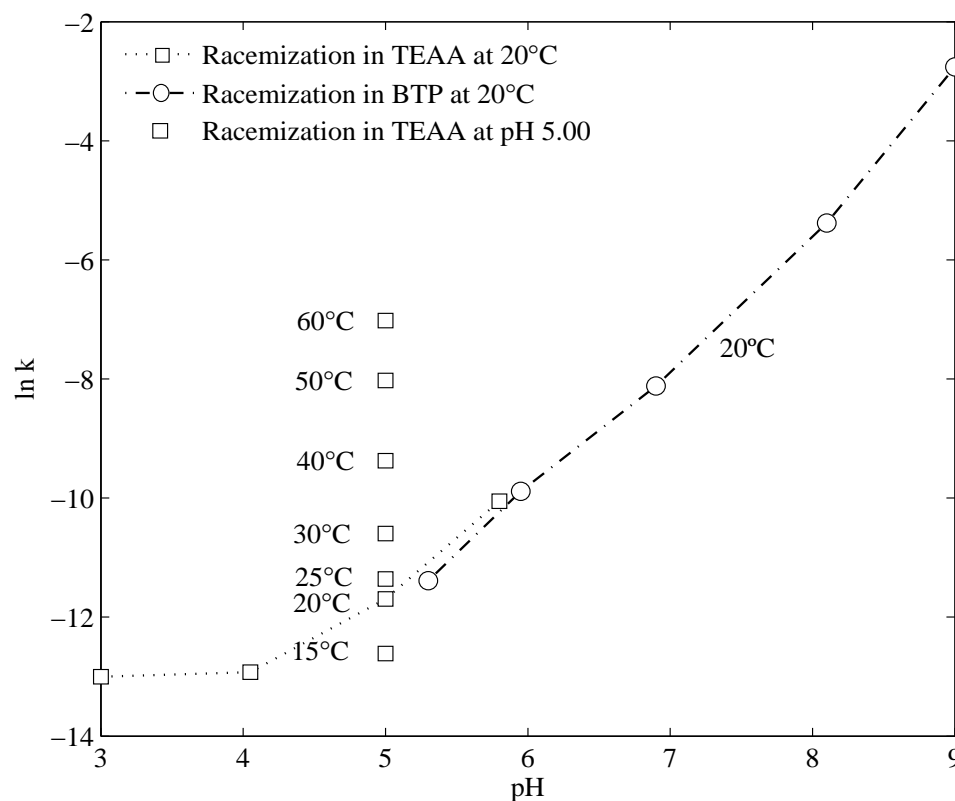
Figure 4.7. – Racemization kinetics for the model system chlorthalidone (CTD). Results for the thermal and pH-dependent racemization are depicted for two different buffer systems: triethylammonium acetate (□) and bis-tris propane (◦). Lines are guide to the eye.

[41].

4.4.1.2. Adsorption behavior

The adsorption isotherm model in Eq. (4.3) contains six parameters that need to be determined experimentally. Further, the saturation capacity of the achiral sites $q_{s,1}(pH)$ is considered a function of the pH value. Since classical methods for isotherm determination are not applicable under reactive conditions, the isotherm parameters were estimated numerically by applying the inverse method (for details see, e.g., [84]).

First, the injection profile obtained using the HPLC pump needs to be characterized to increase the accuracy of the simulation results. Often, the injection profile is ideally assumed to describe a rectangular pulse. However, here, as frequently observed in real applications, this is not the case.

The real injection profile can be modelled accurately using a set of three sigmoidal

functions. The total concentration of the model substance injected c_t can be defined as

$$
c_t = \begin{cases}
c_{ip,1} & if \ \ t < t_1 \\
c_{ip,2} & if \ \ t_1 < t < t_2 \\
c_{ip,3} & if \ \ t_2 < t < t_{end}
\end{cases}
\tag{4.11}
$$

where the three contributions for the calculated injection profile $c_{ip,d}$ are defined as

$$
c_{ip,d} = \frac{p_{1,d} \cdot c_{inj,d}}{1 + e^{\frac{t - p_{2,d}}{p_{3,d}}}}
\tag{4.12}
$$

t_1, t_2, and t_{end} define the corresponding domain for each sigmoidal function. These times were adjusted manually to the values 0.23, 0.32, and 1.5 min, respectively. $d = 1, 2, 3$ represent each of the three parts into which the injection profile was divided. c_{inj} is the injection concentration, and p_1, p_2, p_3 are model parameters for the fit.

Table 4.2. – Parameters from fit for injection profile at V_{inj} = 2000 µL, c_{inj} = 0.05 g/L, Q = 6 mL/min and T = 20°C.

Parameters	d		
	1	2	3
p_1 [-]	1.0	2.0	0.985
p_2 [min]	0.020	0.228	0.315
p_3 [min]	-0.003	0.078	0.1060

An additional equation was implemented to assure mass conservation:

$$
Q \int_0^{t_{end}} c_t(t)dt = Q \cdot c_{inj} \cdot t_{inj}
\tag{4.13}
$$

where for ideal rectangular injection profiles t_{end} equals t_{inj}.

The objective function to minimize reads as:

$$
OF = \sum_1^P \left(c_t - c_{exp} \right)^2
\tag{4.14}
$$

with c_{exp} the experimental determined concentration and P equal to the number of data points.

The optimization was performed using an evolutionary algorithm available in DIVA. Figure 4.8 shows that the calculated profile fits satisfactorily the real case. The results for the fitting are summarized in Table 4.2.
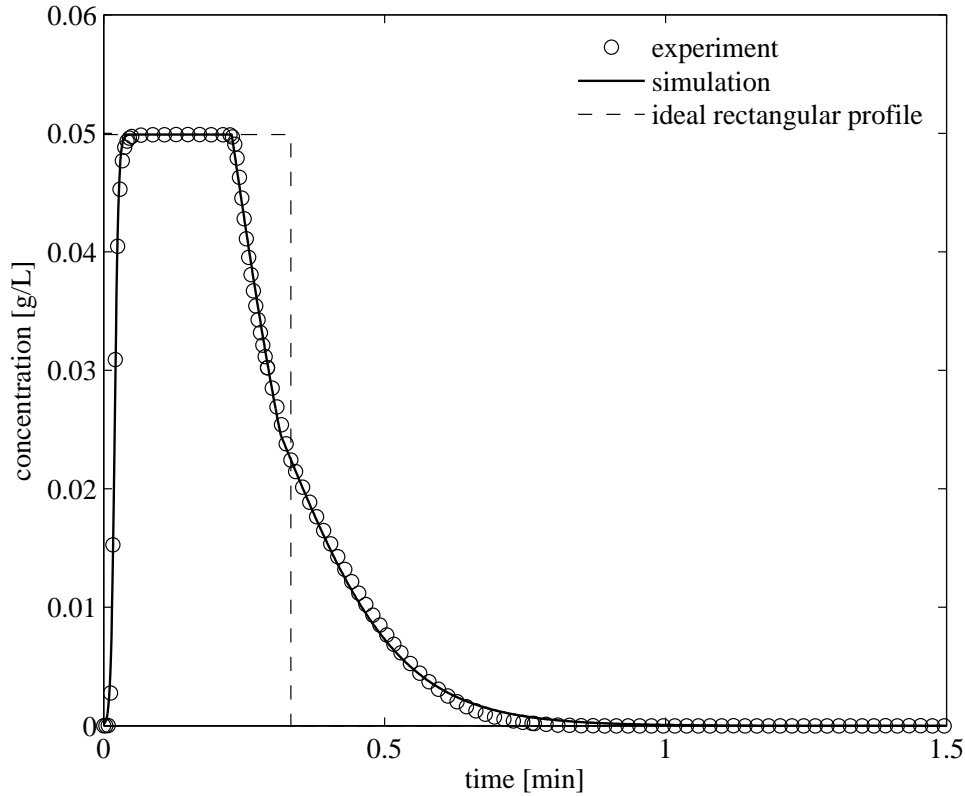
Figure 4.8. – Injection profile obtained experimentally (symbols) and fitting results (line). Ideal rectangular profile (- -) plotted for comparison.

Afterwards, five samples of racemic CTD were injected at pH values equal to 5.3, 6.0, 7.0, 8.0 and 9.0. The column model was solved using the previously obtained function for the kinetic constant in Eq. (4.10) and the injection profile as boundary condition. The evolutionary algorithm in DIVA was used to estimate the isotherm parameters minimizing the differences between calculated and experimental chromatograms as in Eq. (4.14). The following sigmoidal function was assumed for $q_{s,1}(pH)$:

$$q_{s,1}(pH) = \frac{q_{s,1}(pH = 5.3)}{1 + e^{\frac{pH - C_2}{C_3}}} \qquad (4.15)$$

with the two additional free parameters C_2 and C_3.

A total of seven free parameters in Eq. (4.3) and Eq. (4.15) are used to describe the adsorption behavior. The experimentally determined isotherm parameters reported in [46] were used here as initial guess. The results of the parameter estimation are summarized in Table 4.3.

Figure 4.9 shows the obtained adsorption isotherms for both components at the five pH values of interest (5.3, 6.0, 7.0, 8.0 and 9.0). The slope of the isotherms decreases significantly
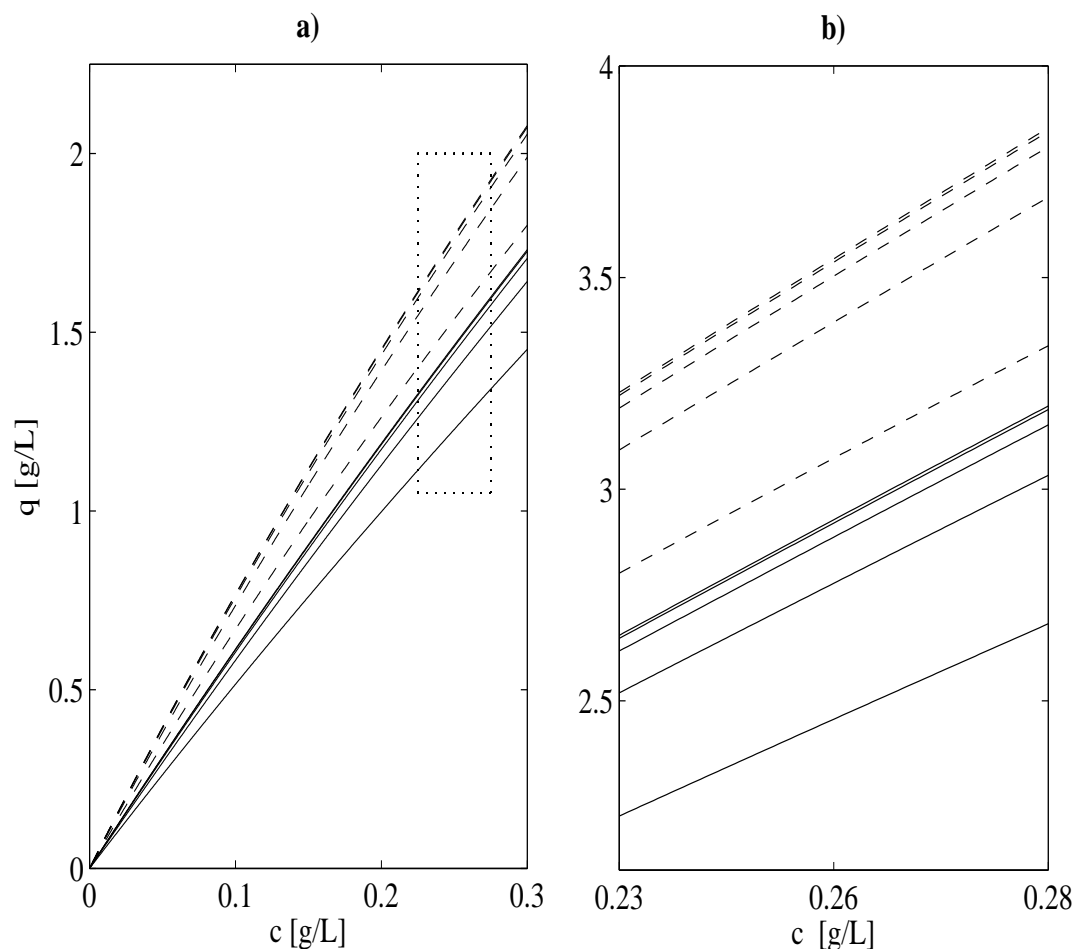
Figure 4.9. – Resulting adsorption isotherms for component A (dashed lines) and
B (solid lines) for the five different pH values of interest (5.3, 6.0,
7.0, 8.0 and 9.0). For each component, reading from bottom to top
corresponds to changing from the highest to the lowest pH value.
The dotted rectangle marks the region zoomed in the subplot b).

for increasing pH value, indicating that stronger adsorption in acidic than in basic ambience
takes place. Note that a simpler isotherm model might be applied requiring less parameters to
be fitted. However, the bi-Langmuir model is most frequently used for enantiomers and it was
suggested in the specific case of CTD in [46].

Figure 4.10 shows the experimental chromatograms together with the numerical results.
A good agreement is observed between them. However, larger areas are observed for the
simulated results compared to the experiments. As explained earlier, side reactions can be
expected based on the racemization mechanism. The formation of side products reduces
the total amount of CTD enantiomers in the mixture, decreasing the area of the CTD peaks
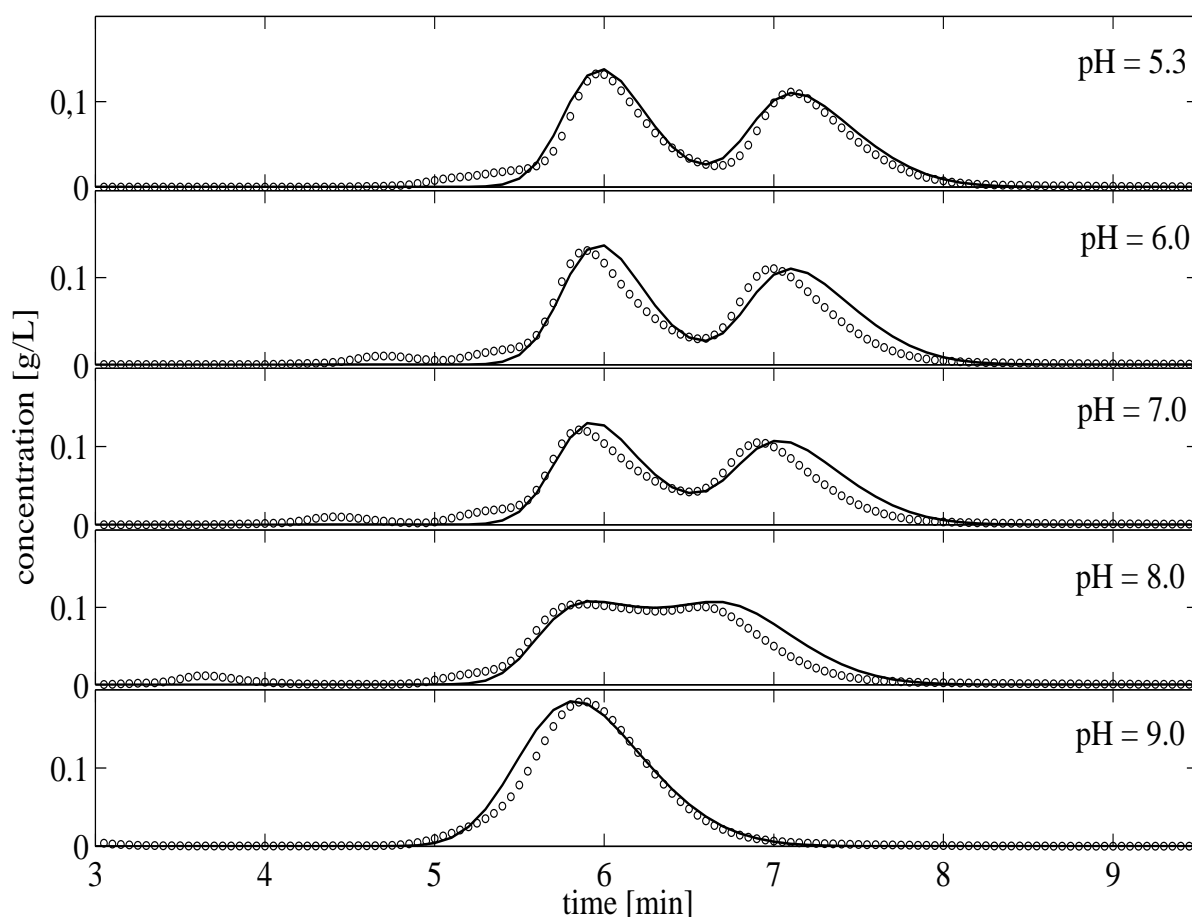
Figure 4.10. – Experimental chromatograms (symbols) and fitting results (lines) of CTD enantiomers at different pH values.

Table 4.3. – Adsorption isotherm parameters for the enantiomers of CTD as a function of pH (cf. Eqs. (4.3) and (4.15)).

$q_1^s(pH = 5.3)$	C_2	C_3	b_1	$q_{A,2}^s$	$q_{B,2}^s$	$b_{A,2}$	$b_{B,2}$
[g/L]	[-]	[-]	[L/g]	[g/L]	[g/L]	[L/g]	[L/g]
82.289	10.300	0.803	0.075	0.434	3.209	0.355	0.620

observed in the experimental chromatograms.

Almost baseline separation can be observed at pH=5.3. At pH=8.0, an intermediate plateau is formed. Further, at pH=9.0 a single peak is obtained due to the fast racemization kinetics. These are typical effects observed in 'on column' racemization [20, 93, 94]. The retention time decreases with increasing pH value. This is not only an effect of the reaction-assisted regeneration but also due to a change of the adsorption strength. The effect of the pH on the retention time increases if the pH is in the proximity of the pK$_a$ value of

CTD, $pK_a = 11, 1$ [87]. This effect has been observed also for other compounds [10, 59, 74].
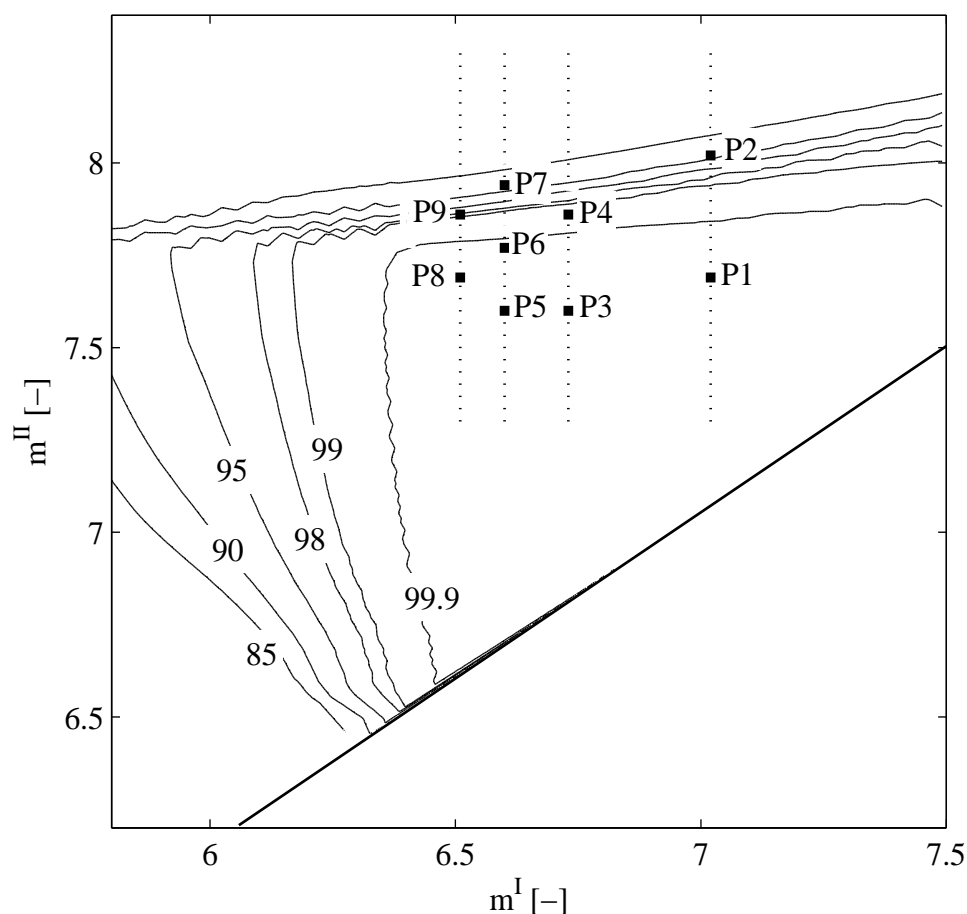

Figure 4.11. – Simulation results corresponding to the scanning of the m^I vs. m^{II} region for the model substance CTD. Surfaces denote the achievable product purity. Points P1 to P9 represent the operating conditions for the 9 experimental runs.

4.4.2. Experimental validation of the process concept

For conventional non-reactive SMB processes triangle theory is used as a powerful design tool [61, 86]. Based on this method, a region of complete separation can be plotted on the m^{II}–m^{III} plane as explained in chapter 2. Analogously, such complete separation region was shown for the new integrated SMB system in chapter 3 (see Fig. 3.6). In the case considered here, where the weaker adsorbed enantiomer is produced, the corresponding region is defined in the parameter space m^I–m^{II} in order to determine the operating diagram. The mathematical model was solved until the cyclic steady state using the determined kinetic constant of the racemization and the adsorption isotherm parameters. A step gradient of the pH was assumed that gives maximum performance in the frame of the investigated parameter range. In the

reactive zone I pH was set to 9.0, while in the non reactive zone II a pH of 5.3 was used. Figure 4.11 shows the simulation results where triangular regions are plotted for different purity requirements.

To validate the process experimentally, nine operating points are selected inside and outside of the region of complete separation ($P1$ to $P9$). No points are chosen left from the boundary of the 99.9% purity region since we are interested in achieving complete regeneration. These nine points were applied in nine different experimental runs using the setup in Fig. 4.2. The eluent used was methanol/50 mM BTP (40/60 v/v). The same pH gradient was used as in the simulations above. For this purpose, the pH of the desorbent S (pure eluent) was adjusted to
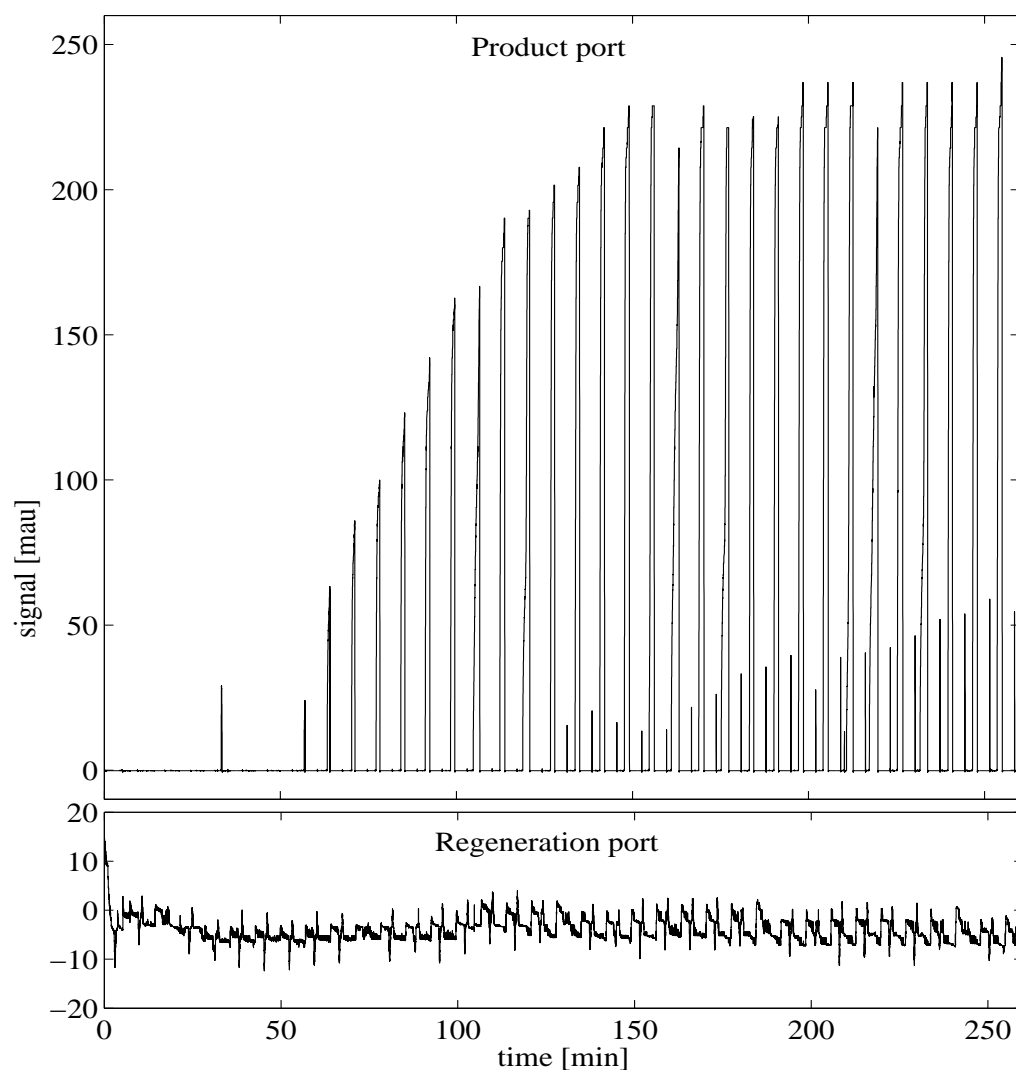

Figure 4.12. – Start-up behaviour of the 2-zone SMB unit obtained for $P8$ (see Fig. 4.11). Signals of the UV online measurements for the product and the regeneration ports (see Fig. 4.2).
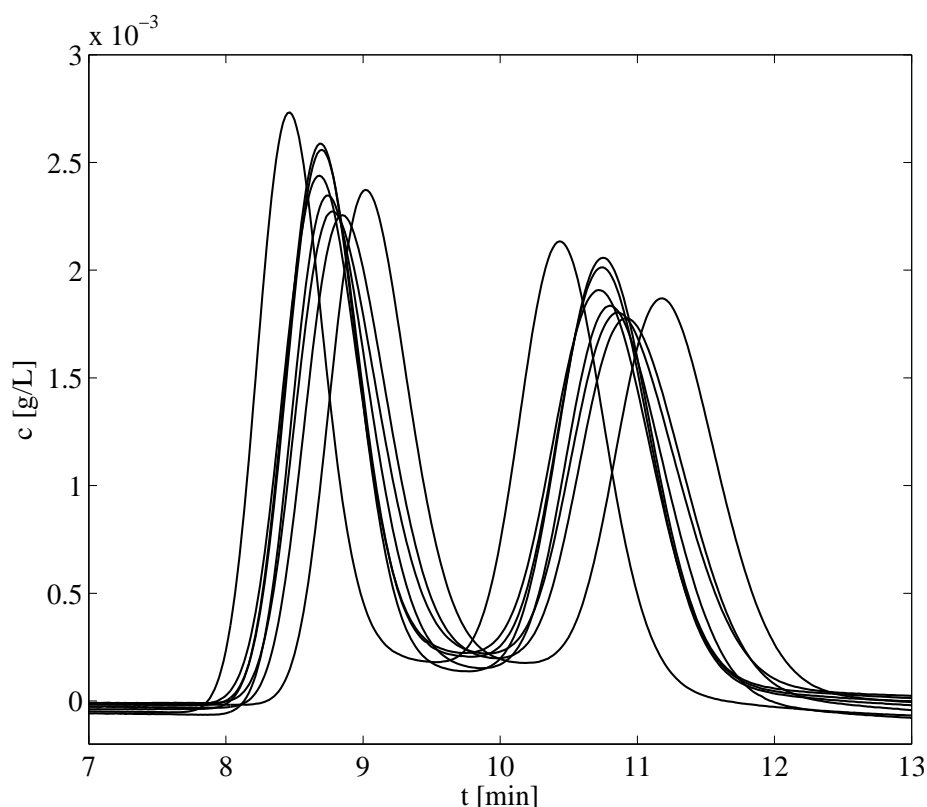
Figure 4.13. – Reproducibility test for the eight semi-preparative columns used
in the SMB setup. Same operating conditions deliver different
results due to differences in packing quality.

$pH_1 = 9.0$, for the regeneration streams (pure eluent) to $pH_3 = 5.3$, and that of the additional buffer to $pH_2 = 1.0$ (cf. Fig. 4.2). The latter was in each case prepared such that, after mixing it with the effluent of zone I and the actual feed (0.5 g/L racemic CTD in pure methanol), the fluid entering zone II had the desired composition (methanol/50 mM BTP, 40/60 v/v) and pH value of 5.3. The switching time of $t^* = 7$ min was chosen as a compromise between throughput and pressure drop. All individual flow rates can be calculated from the parameters given in Table 4.1 and the m-values in Table 4.4.

For the sake of brevity, only the results for one operating point, $P8$, will be discussed in detail. $P8$ corresponds to the highest throughput among the operating points contained in the complete separation region.

As indicated in Fig. 4.2, during the experiments online measurement was carried out with two UV detectors: one at the product outlet of the 2-zone SMB, and the other at the outlet stream of the regeneration zone.
In Fig. 4.12 the UV-signal is shown for the start-up of the experimental run of $P8$. The CSS

is reached approximately after 150 minutes. This corresponds to 21 column switches, i.e. 5 cycles of the 2-zone SMB. After the CSS is reached, deviations from peak to peak can be observed for the product port. This is due to the different packing quality observed among the columns as the reproducibility tests indicate in Fig. 4.13. However, this is a minor problem since SMB units can be operated successfully with columns giving significantly different retention times for the two compounds involved [63]. Further, perturbations are observed in the product port after every switching event. These perturbations can be observed in Fig. 4.12 after approximately 125 minutes. The peaks reach a considerable height in the cyclic steady state. However, their peak area is negligible and they are categorized as system peaks, since a detrimental effect on product quality was not observed.

Figure 4.14 shows the online pH-measurent carried out after the feed port (see Fig. 4.2). The results indicated that during the operation in CSS regime lower pH values than adjusted in the buffer solutions occured temporarily in zone II. These lower pH values were observed immediately after the switching of the columns (every 3.5 minutes). At this point in time, the pH of the liquid contained in the void volume of the column left to the feed port (coming from
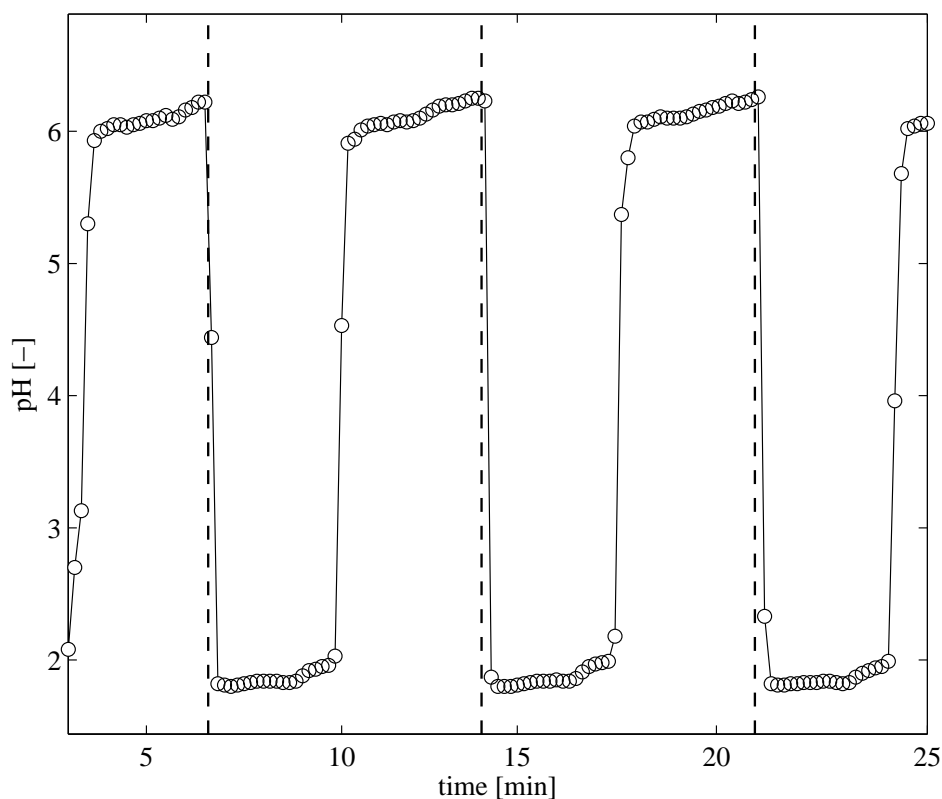

Figure 4.14. – pH value vs. time from the online measurement after the feed port (see Fig. 4.2). Vertical dashed lines indicate the moment of a switching event.

zone *II*) is equal to 5.3. Mixing this liquid with the feed stock and the acidic buffer leads to momentary low pH values (between 1.5 and 3.0).

In the present case, this transient effect causes the formation of side products. This observation is in full agreement with the chemical mechanism discussed in Fig. 4.3 for acidic ambience. However, during the operation of the SMB setup, only small amounts of the undesired side products are observed (always $< 5\%$ of the total feed), causing almost no detrimental effect on the product purity. For cases where side product formation is an issue, advanced feeding strategies could be implemented modulating the pH of the buffer periodically to compensate this behavior and overcome the problem.
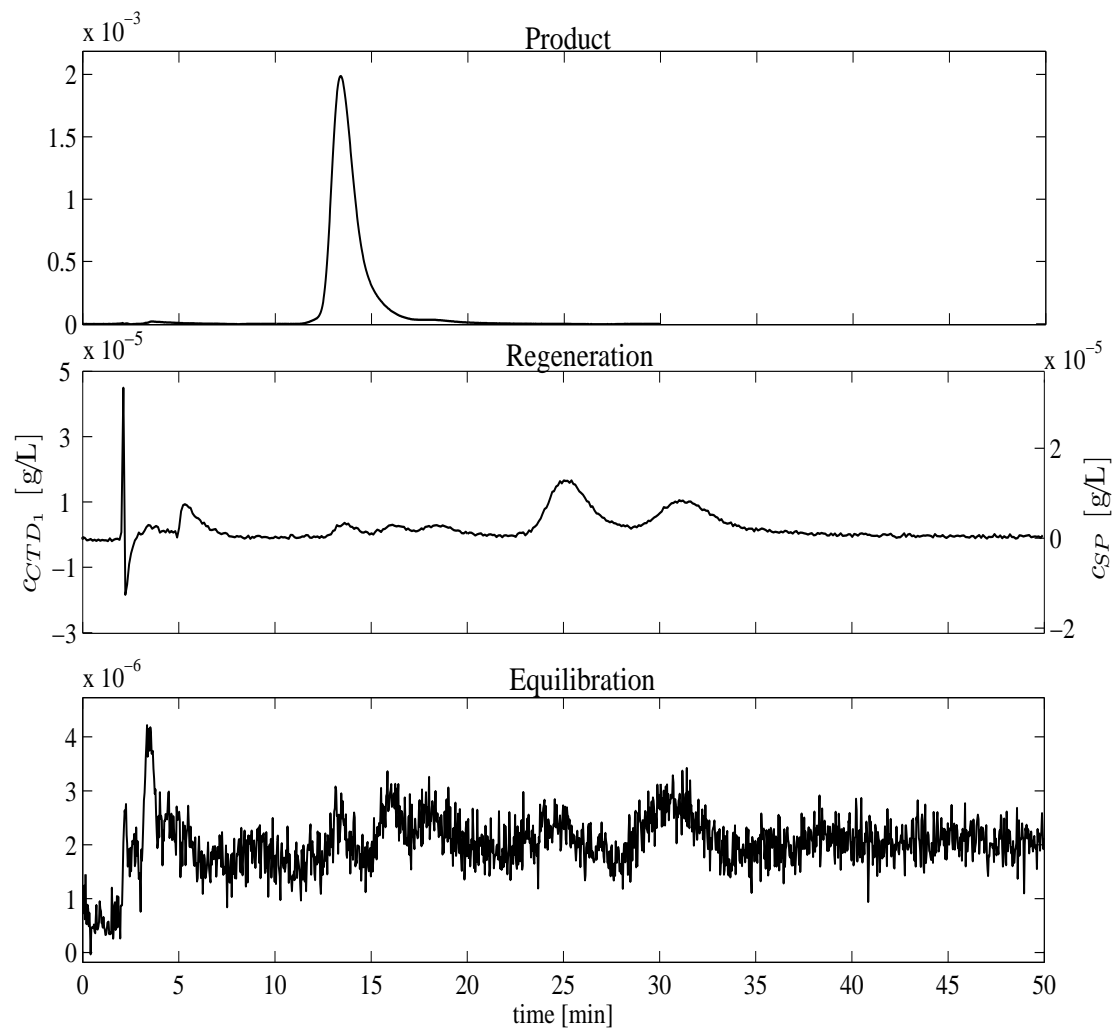

Figure 4.15. – Experimental results obtained for $P8$ (see Fig. 4.11). HPLC analysis of the product stream, regeneration and equilibration streams after reaching the cyclic steady state. c_{sp} denotes the concentration of the side products.

Once the unit reached the CSS, the product, regeneration and equilibration streams were collected and analyzed by HPLC. In Fig. 4.15, the analysis results are plotted for the three outlet streams. The analysis of the product stream shows a single peak eluting at the retention time of the less retained enantiomer CTD_1. The purity of CTD_1 is close to 100%. Note that the detection limit of HPLC analysis with respect to enantiomeric purity was estimated to be 98% because a baseline separation could not be achieved. It could not be clarified whether this is due to on-column racemization or other separation difficulty.

The analysis of the regeneration stream indicates that four different components are present in the mixture. CTD_1 and CTD_2, as well as the two side products SP_1 and SP_2. These were expected based on the reaction mechanism at low pH values suggested in Fig. 4.3. Note that the scale of this plot is two orders of magnitude lower than the one for the product stream. This makes the amounts of CTD in the regeneration a 0.8% of the total throughput, while the side product formation makes up only a 1.2%. Note that for cases where the side product formation extent is significant an open-loop concept like here might be preferred over a 3-zone closed-loop.

In the analysis of the equilibration stream only noise can be observed.

Table 4.4. – Simulated and experimental results of the SMB experiments. $P1$ to $P9$ correspond to the nine different operating points on the $m^I - m^{II}$ plane as shown in Fig. 4.11.

Operating point	m^I [-]	m^{II} [-]	Simulation		Experiment		
			Pu^R [%]	X_{CTD_2} [%]	Pu^R [%]	X_{CTD_2} [%]	Y [%]
$P1$	7.02	7.69	99.9	99.9	> 98	95.1	95.3
$P2$	7.02	8.02	87.6	75.3	71.2	42.1	94.3
$P3$	6.73	7.60	99.9	99.9	> 98	95.1	98.7
$P4$	6.73	7.86	99.7	99.4	97.1	93.3	98.0
$P5$	6.60	7.60	99.9	99.9	> 98	95.6	95.4
$P6$	6.60	7.77	99.9	99.9	> 98	96.8	98.1
$P7$	6.60	7.94	86.9	73.8	91.1	79.5	97.0
$P8$	6.51	7.69	99.9	99.9	> 98	96.1	98.0
$P9$	6.51	7.86	99.1	98.0	92.9	85.1	97.1

Note that in this work the 2-zone open loop concept was implemented for the sake of easier process monitoring and guaranteeing the proper functioning of the regeneration zone. Apart from that, in cases where the side product formation is significant and an accumulation of

side products is expected due to their adsorption behavior, an open-loop concept like here might be preferred over a 3-zone closed-loop. An important aspect of 3-zone closed loop processes is related to the pH gradient. In order to maintain the magnitude of this gradient, the pH of the desorbent and feed streams will have to be adjusted to more 'extreme' values.

The numerical and experimental results for the nine operating points are summarized in Table 4.4. Five operating points were chosen inside the complete separation region: $P1$, $P3$, $P5$, $P6$ and $P8$, where 100% purity, conversion and yield were expected. The other four operating points were chosen outside this triangle to determine the limits of the complete separation region. A good agreement is obtained between experiments and theoretical predictions. For the five operating points inside the complete separation region the detection limit for the product purity of 98% is reached. Conversions and yields above 95% are obtained in these cases from the overall material balances. Also, for the experimental runs corresponding to $P2$, $P4$, $P7$, and $P9$ a good agreement is obtained between the experimental results and the calculated purity regions obtained from the simulations.

High product purity and negligible amounts of CTD enantiomers in the regeneration stream were observed in the experiments designed to produce pure product. This demonstrates that the new integrated SMB concept is capable of producing single enantiomers with purity, conversion and yield close to 100%.

4.5. Conclusions

A new integrated 3-zone SMB process was identified in previous chapter 3 as an attractive concept to produce single enantiomers. In this chapter, the concept was experimentally validated for the model system chlorthalidone (CTD).

First, the racemization kinetics of CTD were determined as a function of the pH value. Afterwards, the adsorption isotherms were determined applying the inverse method in the pH range of interest. To design the process, a mathematical model was implemented accounting for the experimentally investigated reaction rate and adsorption isotherms.

For the sake of better controllability, the experimental validation was performed using a 2-zone open-loop configuration. A 3-zone implementation is straightforward if side product formation is negligible. Such side product formation can also be reduced by a modified feeding strategy.

In a semi-preparative SMB setup several experimental runs were carried out corresponding to different operating points. The results confirm that pure single enantiomers can be produced with the new integrated process achieving conversion and yield values very close to 100% [67].

The new integrated process can be applied to enantiomeric systems where the racem-

ization kinetics can be tuned significantly by means of the pH value. The dependency of the racemization kinetics on the pH is reported for other species (e.g., in [22]), as well as for epimerization [55] and isomerization kinetics [41]. Alternatively, other gradients of, for example, temperature, modifiers, additives, homogeneous catalysts or inhibitors could also modulate sufficiently the reaction kinetics, enabling a broader application of this concept.

CHAPTER 5

Conclusions

The thesis was concerned with the selective continuous production of single enantiomers from racemic mixtures, i.e. 50/50 mixtures of both enantiomers. Several process alternatives combining continuous chromatography and racemization reactions were suggested able to deliver pure enantiomeric forms with 100% purity, yield, and conversion. This problem has been hardly considered in literature in a systematic way despite its practical importance.

A comprehensive evaluation of these process alternatives was performed applying mathematical model-based optimization. Different degrees of integration were considered: flowsheet integration, partially integrated systems using side reactors, and completely integrated schemes. Belonging to the last case, a new completely integrated process idea was suggested. In this new process the reaction functionalities are spatially distributed within the chromatographic unit.

The novel process idea was identified as a promissing alternative. Based on this idea, a 3-zone system performing racemization within the regeneration zone obtained very good performance results in the optimization study. Despite its rather simple setup, this process was able to outperform more complex 4-zone systems containing external recycles or/and side reactors. Further, the beneficial effect of the racemization reaction on the regeneration of the chromatographic unit was analyzed theoretically on the basis of equilibrium theory.

A practical implementation of the new process idea was suggested in the frame of SMB processes. The spatial distribution of the reaction within the unit was performed by tuning

the reaction kinetics using specific gradients. Different gradients were considered able to modulate the racemization kinetics based on, for example, pH, temperature, modifiers, salts, homogeneous catalysts or inhibitors, to name some.

The experimental validation of the new process was carried out in a preparative scale for a model compound. A pH gradient was used to modulate the racemization kinetics within the SMB unit. The results supported that single enantiomers can be produced with the new integrated process achieving conversion and yield values close to 100%.

APPENDIX $\mathcal{A}$

Analysis of reaction-assisted regeneration in TMB

In chapter 2 the benefits of performing a reversible isomerization reaction $A \leftrightarrow B$ within specific zones of a true moving bed (TMB) unit were discussed. The source of this benefit lies in the fact that the reaction itself leads to significantly easier regeneration of the solid and liquid phases in the TMB unit. This effect is denoted as reaction-assisted regeneration.

Here, simple formulas are derived assuming adsorption and reaction equilibria in order to quantify and to further understand this effect.

For non reactive countercurrent chromatographic processes, equilibrium theory can be applied to derive analytical solutions under linear and nonlinear conditions for Riemann problems (i.e. piecewise constant boundary and initial conditions).

The mass balances for a single zone are given by the following system of first-order partial differential equations

$$\frac{\partial}{\partial \tau} \left[\mathbf{c} + F\mathbf{q}(\mathbf{c}) \right] + \frac{\partial}{\partial x} \left[\mathbf{c} - \mu\mathbf{q}(\mathbf{c}) \right] = \mathbf{0}$$

$$\text{with } x = \tfrac{z}{L}, \ \tau = \tfrac{t \cdot v}{L}, \ \mu = \tfrac{1-\epsilon}{\epsilon} \tfrac{v_s}{v} = \tfrac{1}{m}$$

(A-1)

where v and v_s are the liquid and solid phase velocity, respectively. v and v_s are assumed to be constant. $F = (1 - \epsilon)/\epsilon$ is the phase ratio, m the flow rate ratio, z the spatial coordinate, and L the total length.

(A-1) is a homogeneous system of quasilinear equations which describes wave phenomena. Analytical solutions for the Riemann problem can be obtained with the method of characteristics [73].

In order to design continuous chromatographic processes, the propagation velocity of the 'j' front, λ_j, can be calculated for simple waves in non reactive systems by

$$\lambda_j = \frac{1 - \mu\sigma_j}{1 + F\sigma_j} \tag{A-2}$$

where σ_j are the eigenvalues of the Jacobian matrix of the adsorption isotherm. This holds for favorable isotherms, like Langmuir-type, in desorption fronts. These fronts correspond to spreading waves in which each point propagates with a different velocity. Thus, σ_j are concentration dependent.

A different scenario is observed in the adsorption waves for Langmuir-type behavior. These fronts correspond to self sharpening fronts, which steep up until they form, eventually, a discontinuity. In this case, all points move at the same velocity, which is defined by an overall mass balance. Thus, in Eq. (A-2), σ_j has to be replaced by the concentration difference across the shock discontinuity Σ_j

$$\Sigma_j = \Delta q_j / \Delta c_j \tag{A-3}$$

Of main interest here are the first and last zones of the TMB unit. These zones are responsible for the regeneration of the solid (zone I) and the liquid phase (zone III or IV), respectively (see Fig. 1.2).

For a complete regeneration of zone I in the non reactive case, the corresponding front has to be stabilized avoiding its propagation towards zone IV through the recycle stream. This implies that $\lambda_j = 0$ in Eq. (A-2). The following conditions for the required flow rate ratios m can be derived from Eq. (A-2):

$$m^I = \frac{1}{\mu} = \left.\frac{\partial q_A(c_A, c_B)}{\partial c_A}\right|_{c_A=0,\ c_B=0} \tag{A-4}$$

Similarly, to completely regenerate the last zone N_z, the corresponding shock front within this zone must not propagate towards zone I through the recycle stream. Thus, to immobilize this shock in non reactive systems, the following condition holds for the flow rate ratio

$$m^{N_z} = \frac{q_B(0, c_B) - q_B(0, 0)}{c_B - 0} = \frac{q_B(0, c_B)}{c_B} \tag{A-5}$$

For reactive systems, it is more difficult to obtain explicit solutions, because the underlying

mass balances (one for each component) are no longer homogeneous

$$\frac{\partial}{\partial \tau} \left[\mathbf{c} + F\mathbf{q}\left(\mathbf{c}\right) \right] + \frac{\partial}{\partial x} \left[\mathbf{c} - \mu \mathbf{q}(\mathbf{c}) \right] = \boldsymbol{\nu}\mathbf{r}$$

$$\text{with } \mathbf{r} = \left\{ \begin{array}{ll} \mathbf{r(c)} & : \quad \text{homogeneous reaction} \\ \mathbf{r(q)} & : \quad \text{heterogeneous reaction} \end{array} \right.$$

(A-6)

To determine the m-values required for complete regeneration of these reactive zones, we apply transformed concentration variables that take into account simultaneous reaction and adsorption equilibrium [26, 36]. For the reversible isomerization reaction $A \leftrightarrow B$, we define for the fluid and the solid phase, respectively,

$$C = c_A + c_B \,,$$

(A-7)

$$Q = q_A + q_B \,.$$

(A-8)

Substituting these transformed variables into the mass balances in Eq. (A-6) a scalar partial differential equation is obtained

$$\frac{\partial}{\partial \tau} \left[C + FQ(C) \right] + \frac{\partial}{\partial x} \left[C - \mu Q(C) \right] = 0$$

(A-9)

Thus, we can apply the same solution strategies of equilibrium theory that Eq. (A-4) and Eq. (A-5) are based upon. On this basis, we can derive analogous expressions for the optimal flow rates for regeneration:

$$m^I = \left. \frac{\partial Q(C)}{\partial C} \right|_{C=0} ,$$

(A-10)

and

$$m^{N_z} = \frac{Q(C)}{C}$$

(A-11)

In order to solve Eq. (A-10) and Eq. (A-11), an explicit form of the transformed equilibrium function $Q\left(C\right)$ is required. This can be found from the equilibrium constant of the isomerization reaction.

For a homogeneously catalyzed reaction holds

$$K_{eq} = \frac{c_B}{c_A}$$

(A-12)

Analogously, for heterogeneously catalyzed isomerization

$$K'_{eq} = \frac{q_B}{q_A}$$

(A-13)

Assuming reaction equilibrium for a *homogeneous* chemical reaction in the fluid phase Eq. (A-

12), we find from Eq. (A-7)

$$c_A = \frac{1}{1 + K_{eq}}C \,, \tag{A-14a}$$

$$c_B = \frac{K_{eq}}{1 + K_{eq}}C. \tag{A-14b}$$

Substituting these c_i in the adsorption isotherms Eq. (2.9) and further substituting the obtained loadings q_i into Eq. (A-8) gives an explicit equilibrium function $Q(C)$. From this, we can evaluate the derivative and the fraction in Eq. (A-10) and Eq. (A-11).

For a *heterogeneous* reaction, the reaction equilibrium is given by Eq. (A-13). For this case, it is more involved to derive an explicit relation between c_i and C (as given by eqs. (A-14) for the homogeneous reaction). In the following, in a joint work with Prof. Dr. D. Flockerzi at Max-Planck-Institut, Magdeburg, the derivation for the bi-Langmuir adsorption isotherm model is summarized. Note that the corresponding Langmuir solutions are included for the specific case of $H_{i,2} = 0$.

From

$$K'_{eq}\, q_A \overset{!}{=} q_B \qquad (c_A \geq 0, \ c_B \geq 0) \tag{A-15}$$

and the adsorption isotherms, Eq. (2.9),

$$q_A = c_A \left[\frac{H_{A,1}}{L_1} + \frac{H_{A,2}}{L_2}\right] , \qquad q_B = c_B \left[\frac{H_{B,1}}{L_1} + \frac{H_{B,2}}{L_2}\right] ,$$
$$L_1 = 1 + b_{A,1}c_A + b_{B,1}c_B \,, \qquad L_2 = 1 + b_{A,2}c_A + b_{B,2}c_B \,,$$

we find the following quadratic relation between c_A and C:

$$A_2 c_A^2 - 2A_1(C)c_A + A_0(C) \overset{!}{=} 0 \tag{A-16}$$

with

$$A_2 = K'_{eq}(a_{12} - a_{11}) + (a_{22} - a_{21}) \,,$$
$$A_1 = \frac{1}{2}\left[\left(K'_{eq}\gamma_1 + \gamma_2\right) + \left(K'_{eq}a_{12} - a_{21} + 2a_{22}\right)C\right] \,,$$
$$A_0 = C\left(\gamma_2 + a_{22}C\right) \,,$$

$$\gamma_1 = H_{A,1} + H_{A,2} \,, \qquad \gamma_2 = H_{B,1} + H_{B,2} \,,$$
$$a_{11} = H_{A,1}b_{A,2} + H_{A,2}b_{A,1} \,, \qquad a_{12} = H_{A,1}b_{B,2} + H_{A,2}b_{B,1} \,,$$
$$a_{21} = H_{B,1}b_{A,2} + H_{B,2}b_{A,1} \,, \qquad a_{22} = H_{B,1}b_{B,2} + H_{B,2}b_{B,1} \,.$$

It can be shown that independently from the sign of A_2, this leads to

$$c_A = \Psi_A(C) := \frac{A_0(C)}{A_1(C) + \sqrt{[A_1^2(C) - A_2 A_0(C)]}} \qquad with \ \Psi_A(0) = 0 \qquad (A\text{-}17)$$

where the radicant can be shown to be nonnegative so that $\Psi_A(C) : \mathbb{R}_+ \to \mathbb{R}_+$ is a bijection. Since for the computation of $\frac{\partial Q(0)}{\partial C}$ in Eq. (A-10) only linear terms are needed, we can employ the Taylor expansion

$$c_A = \frac{\gamma_2}{K'_{eq} \gamma_1 + \gamma_2} C + \mathcal{O}(C^2) \qquad (A\text{-}18)$$

to obtain the minimum m^I for complete regeneration

$$m^I = \left. \frac{\partial Q}{\partial C} \right|_{C=0} = \frac{(K'_{eq} + 1)\gamma_1 \gamma_2}{K'_{eq} \gamma_1 + \gamma_2} \ . \qquad (A\text{-}19)$$

The condition for regeneration of the last zone z reads as follows:

$$m^{N_z} = \frac{Q(C)}{C} = \frac{1}{C} \frac{1 + K'_{eq}}{2 K'_{eq}} \left[K'_{eq} q_A(c_A, c_B) + q_B(c_A, c_B) \right] \qquad (A\text{-}20)$$

$$\text{with } c_A = \Psi(C), \ c_B = C - \Psi(C) \, .$$

The resulting expressions for the minimun m^I and maximum m^{N_z} for the three cases studied: non reactive, homogeneous reaction and heterogeneous reaction, are reported in Table 2.5 for the Langmuir model and in Table 2.6 for the bi-Langmuir case.

Bibliography

[1] A. Abate, E. Brenna, C. Fuganti, F. G. Gatti, and S. Serra. Lipase-catalysed preparation of enantiomerically enriched odorants. *Journal of molecular catalysis B : Enzymatic*, 32:33, 2004.

[2] S. Abel, M. Mazzotti, and M. Morbidelli. Solvent gradient operation of simulated moving beds: 2. Langmuir isotherms. *Journal of Chromatogaphy A*, 1026:47, 2004.

[3] D. Antos and A. Seidel-Morgenstern. Application of gradients in the simulated moving bed process. *Chemical Engineering Science*, 56:6667, 2001.

[4] E. J. Ariëns. Stereochemistry, a basis for sophisticated nonsense in pharmacokinetics and clinical pharmacology. *European Journal of Clinical Pharmacology*, 26:663, 1984.

[5] D. V. Arnold and H.-G. Beyer. Performance analysis of evolution strategies with multi-recombination in high-dimensional R^N search spaces disturbed by noise. *Theoretical Computer Science*, 289:629, 2002.

[6] L. Aumann and M. Morbidelli. A continuous multicolumn countercurrent solvent gradient purification (MCSGP) process. *Biotechnology & Bioengineering*, 98:1043, 2007.

[7] D. C. S. Azevedo and A. E. Rodrigues. Fructose-glucose separation in a SMB pilot unit: Modeling, simulation, design and operation. *AIChE Journal*, 47:2042, 2001.

[8] M. Bechtold, M. Füreder, N. Wagner, and S. Panke. Potenzial von Prozessintegration mit Adsorbern zur Herstellung seltener Monosaccharide – eine modellbasierte Untersuchung. *Chemie Ingenieur Technik*, 82:65, 2010.

[9] M. Bechtold, S. Makart, M. Heinemann, and S. Panke. Integrated operation of continuous chromatography and biotransformations for the generic high yield production of fine chemicals. *Journal of Biotechnology*, 124:146, 2006.

[10] R. Bergés, V. Sanz-Nebot, and J. Barbosa. Modelling retention in liquid chromatography as a function of solvent composition and pH of the mobile phase. *Journal of Chromatography A*, 869:27, 2000.

[11] H.-G. Beyer and H.-P. Schwefel. Evolution strategies – A comprehensive introduction. *Natural Computing*, 1:3, 2002.

[12] M. C. Bjorklund and R. W. Carr. The simulated countercurrent moving bed chromatographic reactor: a catalytic and separative reactor. *Catalysis Today*, 25:159, 1995.

[13] G. Blaschke and H. Markgraf. Chromatographische Racemattrennungen, IX. Chlortalidon-, Chlortalidon-methylether- und Oxazepam-Enantiomere. *Chemische Berichte*, 113:2031, 1980.

[14] E. A. Borges da Silva, D. P. Souza, A. A. Ulson de Souza, S. M. A. Guelli U. Souza, and A. E. Rodrigues. *Chemical Engineering Journal*, 118:167, 2006.

[15] T. Borren. *Untersuchungen zu chromatographischen Reaktoren mit verteilten Funktionalitäten*. PhD thesis, Universität Dortmund, 2006.

[16] T. Borren and J. Fricke. *Preparative Chromatography of Fine Chemicals and Pharmaceutical Agents*, chapter Chromatographic Reactors. Wiley-VCH, Weinheim, 2005.

[17] T. Borren and H. Schmidt-Traub. Vergleich chromatographischer Reaktorkonzepte. *Chemie Ingenieur Technik*, 76:805, 2004.

[18] E. Breitmeier and G. Jung. *Organische Chemie*. Georg Thieme Verlag Stuttgart, New York, 1994.

[19] D. Broughton and C. Gerhold. Continuous sorption process employing fixed bed of sorbent and moving inlets and outlets, US patent 2 985 589, 1961.

[20] K. Cabrera, M. Jung, M. Fluck, and V. Schurig. Determination of enantiomerization barriers by computer simulation of experimental elution profiles obtained by high-performance liquid chromatography on a chiral stationary phase. *Journal of Chromatogaphy A*, 731:315, 1996.

[21] B. Cho, R. Aris, and R. Carr. The mathematical theory of a countercurrent catalytic reactor. *Proceedings of the Royal Society A*, 383:147, 1982.

[22] H. Diab, P. Hendry, A. Ludi, K. B. Reddy, and R. van Eldik. Labilization by steric crowding. hydrolysis and racemization kinetics of co(tmen)$_3^{3+}$, TMEN = 2,3-diamino-2,3-dimethylbutane. *Inorganica Chimica Acta*, 175:83, 1990.

[23] E. Eliel, S. Wilen, and M. Doyle. *Basic Organic Stereochemistry*. Wiley-Interscience, New York, 2001.

[24] A. Felinger, D. Zhou, and G. Guiochon. Determination of the single component and competitive adsorption isotherms of the 1-indanol enantiomers by the inverse method. *Journal of Chromatography A*, 1005:35, 2003.

[25] E. Fischer. Über die Configuration des Traubenzuckers und seiner Isomeren. *II. Berichte der Deutschen Chemischen Gesellschaft*, 24:2683, 1891.

[26] D. Flockerzi, A. Bohmann, and A. Kienle. On the existence and computation of reactive invariants. *Chemical Engineering Science*, 62:4811, 2007.

[27] T. Fornstedt, G. Gotmar, M. Andersson, and G. Guiochon. Dependence on the mobile-phase pH of the adsorption behavior of propranolol enantiomers on a cellulase protein used as the chiral selector. *Journal of the American Chemical Society*, 121:1164, 1999.

[28] J. Fricke. *Entwicklung einer Auslegungsmethode für chromatographische SMB-Reaktoren*. PhD thesis, Universität Dortmund, 2005.

[29] G. K. Gandi, V. M. Silva, and A. E. Rodrigues. Acetaldehyde dimethylacetal synthesis with Smopex 101 fibres as catalyst/adsorbent. *Chemical Engineering Science*, 62:907, 2007.

[30] J. Gangadwala. *Optimal Design of Combined Reaction Distillation Processes*. PhD thesis, Universität Magdeburg, 2007.

[31] D. Gelosa, M. Ramaioli, G. Valente, and M. Morbidelli. Chromatographic reactors: Esterification of glycerol with acetic acid using acidic polymeric resins. *Industrial & Engineering Chemistry Research*, 42:6536, 2003.

[32] D. Gelosa, A. Sliepcevich, and M. Morbidelli. Chromatographic reactors with reactive desorbents. *Industrial & Engineering Chemistry Research*, 45:3922, 2006.

[33] N. Gottschlich, S. Weidgen, and V. Kasche. Continuous biospecific affinity purification of enzymes by simulated moving bed chromatography. Theoretical description and experimental results. *Journal of Chromatography A*, 719:267, 1996.

[34] A. Grandeury., L. Renou, F. Dufour, S. Petit, G. Gouhier, and G. Coquerel. Chiral resolution by crystallization of host-guest supramolecular complexes. *Journal of Thermal Analysis and Calorimetry*, 77:377, 2004.

[35] C. M. Grill, L. Miller, and T. Q. Yan. Resolution of a racemic pharmaceutical intermediate. A comparison of preparative HPLC, steady state recycling, and simulated moving bed. *Journal of Chromatography A*, 1026:101, 2004.

[36] S. Grüner and A. Kienle. Equilibrium theory and nonlinear waves for reactive distillation columns and chromatographic reactors. *Chemical Engineering Science*, 59:901, 2004.

[37] G. Guiochon, S. Shirazi, and A. Katti. *Fundamentals of Preparative and Nonlinear Chromatography*. Academic Press, London, 1994.

[38] K. Hashimoto, S. Adachi, H. Noujima, and Y. Ueda. A new process combining adsorption and enzyme reaction for producing higher-fructose syrup. *Biotechnology & Bioengineering*, XXV:2371, 1983.

[39] K. Hashimoto, S. Adachi, and Y. Shirai. *Preparative and Production Scale Chromatography*, chapter Development of New Bioreactors of a Simulated Moving Bed Type. Marcel Dekker, New York, 1993.

[40] K.-H. Hellwich. *Stereochemie. Grundbegriffe*. Springer, Berlin, 2002.

[41] J. Jacobson, W. Melander, G. Vaisnys, and C. Horvath. Kinetic study on cis-trans proline isomerization by high-performance liquid chromatography. *The Journal of Physical Chemistry*, 88:4536, 1984.

[42] T. B. Jensen, T. G. P. Reijns, H. A. H. Billiet, and L. A. M. van der Wielen. Novel simulated moving-bed method for reduced solvent consumption. *Journal of Chromatography A*, 873:149, 2000.

[43] M. Juza, M. Mazzotti, and M. Morbidelli. Simulated moving-bed chromatography and its application to chirotechnology. *Trends in Biotechnology*, 18:108, 2000.

[44] M. Kaspereit, K. Gedicke, V. Zahn, A. W. Mahoney, and A. Seidel-Morgenstern. Shortcut method for evaluation and design of a hybrid process for enantioseparations. *Journal of Chromatography A*, 1092:43, 2005.

[45] M. Kaspereit, P. Jandera, M. Skavrada, and A. Seidel-Morgenstern. Impact of adsorption isotherm parameters on the performance of enantioseparation using simulated moving bed chromatography. *Journal of Chromatography A*, 944:249, 2002.

[46] M. Kaspereit, J. G. Palacios, T. M. Fernández, and A. Kienle. Systematic design of production processes for enantiomers with integration of chromatography and racemisation reactions. In *18th European Symposium on Computer Aided Process Engineering*, volume 25 of *Computer-Aided Chemical Engineering*, page 97, 2008.

[47] M. Kaspereit, A. Seidel-Morgenstern, and A. Kienle. Design of simulated moving bed processes under reduced purity requirements. *Journal of Chromatogaphy A*, 1162:2, 2007.

[48] M. Kawase, Y. Inoue, T. Araki, and K. Hashimoto. The simulated moving bed reactor for production of bisphenol A. *Catalysis Today*, 48:199, 1999.

[49] M. Kawase, A. Pilgrim, T. Araki, and K. Hashimoto. Lactosucrose production using a simulated moving-bed reactor. *Chemical Engineering Science*, 56:453, 2001.

[50] M. Kawase, T. B. Suzuki, K. Inoue, K. Yoshimoto, and K. Hashimoto. Increased esterification conversion by application of the simulated moving-bed reactor. *Chemical Engineering Science*, 51:2971, 1996.

[51] R. Köhler, K. Mohl, H. Schramm, M. Zeitz, A. Kienle, M. Mangold, E. Stein, and E. Gilles. *Adaptative Method of Lines*, chapter Method of Lines within the Simulation Environment DIVA for Chemical Processes, page 371. Chapman & Hall/CRC, London, 2001.

[52] A. Küpper and S. Engell. Optimierungsbasierte Regelung des Hashimoto-SMB-Prozesses. *at - Automatisierungstechnik*, 57:360, 2009.

[53] E. Lamparter, G. Blaschke, and J. Schlueter. Racemisation of Chlorthalidone in the presence of liposomes. *Chirality*, 5:370, 1993.

[54] R. Leven, B. Koch, and B. Pompe. *Chaos in dissipativen Systemen*. Akademie Verlag, Berlin, 1994.

[55] L. Li, R. Thompson, J. J. R. Sowa, A. Clausen, and T. Dowling. Kinetic study on the epimerization of trityloxymethyl butyrolactol by liquid chromatography. *Journal of Chromatogaphy A*, 1043:171, 2004.

[56] O. Ludemann-Hombourger, G. Pigorini, R. M. Nicoud, D. S. Ross, and G. Terfloth. Application of the VARICOL process to the separation of the isomers of the SB-553261 racemate. *Journal of Chromatography A*, 947:59, 2002.

[57] N. M. Maier, P. Franco, and W. Lindner. Separation of enantiomers: needs, challenges, perspectives. *Journal of Chromatography A*, 906:3, 2001.

[58] M. Mangold, A. Kienle, K. D. Mohl, and E. D. Gilles. Nonlinear computation using DIVA – Methods and applications. *Chemical Engineering Science*, 55:441, 2000.

[59] R. M. L. Marques and P. J. Schoenmakers. Modelling retention in reversed-phase liquid chromatography as a function of pH and solvent composition. *Journal of Chromatography A*, 592:157, 1992.

[60] T. Masuda, T. Sonobe, F. Matsuda, and M. Horie. Process for fractional separation of multi-component fluid mixture, US patent 5 198 120, 1993.

[61] M. Mazzotti, G. Storti, and M. Morbidelli. Optimal operation of simulated moving bed units for nonlinear chromatographic separations. *Journal of Chromatogaphy A*, 769:3, 1997.

[62] M. Michel, H. Schmidt-Traub, R. Ditz, M. Schulte, J. Kinkel, W. Stark, M. Kuepper, and M. Vorbrodt. Development of an integrated process for electrochemical reaction and chromatographic SMB-separation. *Journal of Applied Electrochemistry*, 33:939, 2003.

[63] K. Mihlbachler, J. Fricke, T. Yun, A. Seidel-Morgenstern, H. Schmidt-Traub, and G. Guiochon. Effect of the homogeneity of the column set on the performance of a simulated moving bed unit: I. Theory. *Journal of Chromatography A*, 908:49, 2001.

[64] J. G. Palacios, M. Kaspereit, and A. Kienle. Conceptual design of integrated chromatographic processes for the production of single (stereo-)isomers. *Chemical Engineering & Technology*, 32:1392, 2009.

[65] J. G. Palacios, M. Kaspereit, and A. Kienle. Integrated simulated moving bed processes for the production of single enantiomers. *Chemical Engineering & Technology*, 34:688, 2011.

[66] J. G. Palacios, M. Kaspereit, G. Ziomek, D. antos, and A. Seidel-Morgenstern. Optimization and analysis of possible column arrangements for multicomponent separations by preparative chromatography. *Industrial & Engineering Chemistry Research*, 48:11148, 2009.

[67] J. G. Palacios, B. Kramer, A. Kienle, and M. Kaspereit. An integrated reactive simulated moving bed for production of single enantiomers. *Journal of Chromatography A*, 1218:2232, 2011.

[68] T. Petroulas, R. Aris, and J. R.W. Carr. Analysis and performance of a countercurrent moving-bed chromatographic reactor. *Chemical Engineering Science*, 20:2233, 1985.

[69] A. K. Ray and R. W. Carr. Numerical simulation of a simulated countercurrent moving bed chromatographic reactor. *Chemical Engineering Science*, 50:3033, 1995.

[70] A. K. Ray, R. W. Carr, and R. Aris. The simulated countercurrent moving bed chromatographic reactor – a novel reactor-separator. *Chemical Engineering Science*, 49:469, 1994.

[71] I. Rechenberg. *Evolutionsstrategie '94*. Frommann-Holzboog, Stuttgart, 1994.

[72] M. Reist, B. Testa, P. A. Carrupt, M. Jung, and V. Schurig. Racemization, enantiomerization, diastereomerization and epimerization: their meaning and pharmacological significance. *Chirality*, 7:396, 1995.

[73] H.-K. Rhee, R. Aris, and N. Amundson. *First-Order Partial Differential Equations. Vol. II. Theory and Application of Hyperbolic Systems of Equations*. Prentice-Hall, Englewood Cliffs, New Jersey, 1989.

[74] M. Rosés and E. Bosch. Influence of mobile phase acid-base equilibria on the chromatographic behaviour of protolytic compounds. *Journal of Chromatography A*, 982:1, 2002.

[75] A. M. Rouhi. Chiral Chemistry. *Chemical & Engineering News*, 82:47, 2004.

[76] D. M. Ruthven and C. Ching. Counter-current and simulated counter-current adsorption separation processes. *Chemical Engineering Science*, 44:1011, 1989.

[77] T. Sainio, M. Kaspereit, A. Kienle, and A. Seidel-Morgenstern. Thermal effects in reactive liquid chromatography. *Chemical Engineering Science*, 62:5674, 2007.

[78] M. Sardin, D. Schweich, and J. Villermaux. *Preparative and Production Scale Chromatography*, volume 61, chapter Preparative fixed-bed chromatographic reactor, page 477. Marcel Dekker, New York, 1993.

[79] M. Sardin and J. Villermaux. Synthese de l'acetate de menthyle par chromatographie reactive. *The Chemical Engineering Journal*, 30:91, 1985.

[80] H. Schmidt-Traub, editor. *Preparative Chromatography of Fine Chemicals and Pharmaceutical Agents*. Wiley-VCH, Weinheim, 2005.

[81] H. Schramm, M. Kapereit, A. Kienle, and A. Seidel-Morgenstern. Simulated moving bed process with cyclic modulation of the feed concentration. *Journal of Chromatography A*, 1006:77, 2003.

[82] H. Schramm, A. Kienle, M. Kaspereit, and A. Seidel-Morgenstern. Improved operation of simulated moving bed processes through cyclic modulation of feed flow and feed concentration. *Chemical Engineering Science*, 58:5217, 2003.

[83] H. P. Schwefel. *Evolution and Optimum Seeking*. Wiley, New York, 1995.

[84] A. Seidel-Morgenstern. Review. Experimental determination of single solute and competitive adsorption isotherms. *Journal of Chromatography A*, 1037:255, 2004.

[85] G. Severin. Spontaneous racemization of chlorthalidone: kinetics and activation parameters. *Chirality*, 4:222, 1992.

[86] G. Storti, M. Mazzotti, M. Morbidelli, and S. Carrà. Robust design of binary counter-current adsorption separation processes. *AIChE J.*, 39:471, 1993.

[87] O. Stålberg, M. Kruusmägi, M. A. Svensson, U. Norinder, and C. Pettersson. Structure-interaction relationships between the bile acid GCA and pharmaceuticals using multivariate data analysis and capillary electrophoresis. *Journal of Pharmaceutical Science*, 96:2057, 2007.

[88] G. Ströhlein, Y. Assuncao, N. Dube, A. Bardow, M. Mazzotti, and M. Morbidelli. Esterification of acrylic acid with methanol by reactive chromatography: Experiments and simulations. *Chemical Engineering Science*, 61:5296, 2006.

[89] G. Ströhlein, M. Mazzotti, and M. Morbidelli. Optimal operation of simulated moving bed reactors for nonlinear adsorption isotherms and equilibrium reactions. *Chemical Engineering Science*, 60:1525, 2005.

[90] K. Sundmacher, A. Kienle, and A. Seidel-Morgenstern, editors. *Integrated Chemical Processes*. Wiley-VCH, Weinheim, 2005.

[91] H. Teff and C. R. Munro. *Thalidomide: the legal aftermath*. Saxon House, Westmead, UK, 1976.

[92] A. Toumi and S. Engell. Optimization-based control of a reactive simulated moving bed process for glucose isomerization. *Chemical Engineering Science*, 59:3777, 2004.

[93] O. Trapp, G. Schoetz, and V. Shurig. Determination of enantiomerization barriers by dynamic and stopped-flow chromatograophic methods. *Chirality*, 13:403, 2001.

[94] O. Trapp and V. Schurig. Approximation function for the direct calculation of rate constants and Gibbs activation energies of enantiomerization of racemic mixtures from chromatographic parameters in dynamic chromatography. *Journal of chromatography A*, 911:167, 2001.

[95] M. Tylko. *Funktionalitätenverteilung und Produktbereiche für die Prozesssynthese integrierter reaktiver Trennverfahren*. PhD thesis, Universität Dortmund, 2008.

[96] F. Vögtle. Grundlagen der organischen Stereochemie. *Angewandte Chemie*, 96:169, 1983.

[97] P. Vollhardt and N. Schore. *Organische Chemie*. WILEY-VCH GmbH & Co. KGaA, Weinheim, 2005.

[98] T. D. Vu, A. Seidel-Morgenstern, S. Grüner, and A. Kienle. Analysis of ester hydrolysis reactions in a chromatographic reactor using equilibrium theory and a rate model. *Industrial & Engineering Chemistry Research*, 44:9565, 2005.

[99] Y. Zhang, K. Hidajat, and A. Ray. Optimal design and operation of SMB bioreactor: production of high fructose syrup by isomerization of glucose. *Biochemical Engineering Journal*, 21:111, 2004.

[100] Z. Zhang, M. Mazzotti, and M. Morbidelli. PowerFeed operation of simulated moving bed units: changing flow-rates during the switching interval. *Journal of Chromatography A*, 1006:87, 2003.

[101] Z. Zhang, M. Mazzotti, and M. Morbidelli. Continuous chromatographic processes with a small number of columns : comparison of simulated moving bed with Varicol, PowerFeed, and ModiCon. *Korean Journal of Chemical Engineering*, 21:454, 2004.